(12)

AD

SIMULATION EXPERIMENTS OF REACTING TWO-PHASE FLOW

Final Technical Report

by

Guenter Klingenberg

April 6, 1987

United States Army

EUROPEAN RESEARCH OFFICE OF THE U.S. ARMY

London England

CONTRACT NUMBER DAJA 45-84-C-0013

CONTRACTOR: Fraunhofer-Gesellschaft zur Förderung der
Angewandten Forschung e. V.
Leonrodstrasse 54, 8000 Munich, F.R.G.

Approved for Public Release; distribution unlimited

Unclassified
SECURITY CLASSIFICATION OF THIS PAGE

AD-A181 760

REPORT DOCUMENTATION PAGE

Form Approved
OMB No 0704-0188
Exp. Date Jun 30, 1986

1a. REPORT SECURITY CLASSIFICATION Unclassified	1b. RESTRICTIVE MARKINGS
2a. SECURITY CLASSIFICATION AUTHORITY	3. DISTRIBUTION / AVAILABILITY OF REPORT Approved for public release; distribution unlimited
2b. DECLASSIFICATION / DOWNGRADING SCHEDULE	
4. PERFORMING ORGANIZATION REPORT NUMBER(S)	5. MONITORING ORGANIZATION REPORT NUMBER(S) R&D 4387-R-AN
6a. NAME OF PERFORMING ORGANIZATION Fraunhofer-Institut für Kurzzeitdynamik - EMI-AFB 6b. OFFICE SYMBOL (If applicable)	7a. NAME OF MONITORING ORGANIZATION USARDSG(UK)
6c. ADDRESS (City, State, and ZIP Code) Hauptstrasse 18, 7858 Weil am Rhein Germany	7b. ADDRESS (City, State, and ZIP Code) Box 65 FPO New York 09510-1500
8a. NAME OF FUNDING / SPONSORING ORGANIZATION USARDSG(UK) 8b. OFFICE SYMBOL (If applicable) AMXSN-UK-RA	9. PROCUREMENT INSTRUMENT IDENTIFICATION NUMBER DAJA45-84-C-0013
8c. ADDRESS (City, State, and ZIP Code) Box 65 FPO New York 09510-1500	10. SOURCE OF FUNDING NUMBERS PROGRAM ELEMENT NO. 61102A; PROJECT NO. 1L161102BH57; TASK NO. 06; WORK UNIT ACCESSION NO.
11. TITLE (Include Security Classification) (U) Simulation Experiments of Reacting Two-Phase Flow	
12. PERSONAL AUTHOR(S) G. Klingenberg	
13a. TYPE OF REPORT Final Technical 13b. TIME COVERED FROM Feb. 84 TO Apr. 87	14. DATE OF REPORT (Year, Month, Day) 1987, April, 6 15. PAGE COUNT 115
16. SUPPLEMENTARY NOTATION	

17. COSATI CODES		
FIELD	GROUP	SUB-GROUP
20	04	
20	06	

18. SUBJECT TERMS (Continue on reverse if necessary and identify by block number)
Ballistics Simulators, Interior Ballistics, Transitional Ballistics, Combustion of Hydrogen, Validation Experiments, Muzzle Flash, In-bore Parameters, Two-phase Flow

19. ABSTRACT (Continue on reverse if necessary and identify by block number)

A gas gun simulator that permits the generation of relatively clean, two-phase, reacting flows with realistic ballistic gas pressures and temperatures has been developed. This gas gun is driven by the combustion of the gas mixture $3H_2^1 + O_2^1 + 8He$. With this gas propellant mixture, the gas gun is capable of simulating both the interior and transitional ballistic flows of medium caliber weapons. In the experiments, emphasis has been given to the study of reacting muzzle flows. The reason for this was to investigate, in accordance with the contract officer, primarily the basic muzzle flash phenomena. It is shown for the first time that hydrogen/oxygen reactions alone can be suppressed by the addition of conventional gun muzzle flash suppressants, i.e., by alkali salts which are added to the propellant gases. These results support the supposition used by the modelling community that only the hydrogen (and possibly the CO) chemistry are needed to describe the kinetics pertinent to gun muzzle flash and its chemical suppression by inhibiting alkali salts. Because of the importance of the simulation experiments, a further three years program is envisaged.

20. DISTRIBUTION / AVAILABILITY OF ABSTRACT XX UNCLASSIFIED/UNLIMITED XX SAME AS RPT. XX DTIC USERS	21 ABSTRACT SECURITY CLASSIFICATION Unclassified
22a. NAME OF RESPONSIBLE INDIVIDUAL Dr. Fritz H. Oertel, Jr.	22b TELEPHONE (Include Area Code) 01-409 4423 22c OFFICE SYMBOL AMXSN-UK-RA

DD FORM 1473, 84 MAR

83 APR edition may be used until exhausted
All other editions are obsolete

SECURITY CLASSIFICATION OF THIS PAGE
Unclassified

TABLE OF CONTENTS

LIST OF ILLUSTRATIONS

LIST OF TABLES

1. INTRODUCTION

The research objective of the present study is to test and improve procedures for investigating unsteady two-phase (gas/solid) chemically reacting flows. Two-phase gasdynamic numerical and computer programs exist; but they need augmentation by realistic laws governing processes such as turbulent mixing, interphase friction and heat transfer, and friction and heat transfer between the flowing media. Also to construct plausible chemical mechanisms that can explain the complex reacting flow phenomena occurring in-bore and within the unsteady expanding muzzle exhaust flows of guns we must know the (a) identity of the kinetically important chemical species, (b) the reaction network that describes how these species interact, and (c) the rate coefficients. However, the kinetic even of basic combustion reactions is not known in detail.

A thorough understanding of these reacting flows is limited by the harsh environment encountered in actual gun firings, because the probing as well as the prediction of such complex phenomena is very difficult. On the other hand, these are the very same data that are required to elucidate the basic physical and chemical processes needed in the development of predictive models. The result is that existing present-day models of both the interior and transitional ballistics rely on idealizations of the flow. The solutions obtained from these models and hence their underlying assumptions are often inadequately verified by experimentation, if at all. To overcome these difficulties validation experiments using a simulator have been recommended by Klingenberg and Banks [1] at the Sixth International Symposium on Ballistics in October 1981. The simulator considered was aimed at the generation of well-defined, well-controlled, simplified flows beginning with single-phase, inert flows and progressing in a step-wise fashion to more complex two-phase, reacting flows. These efforts should permit one to isolate, identify and understand the important flow phenomena and thereby enhance the chances of successfully modelling the physical and chemical events that occur in actual ballistic flows.

These recommendations had led to the fundamental research work described here. A gas gun facility, based on the studies of Lord [2] and Wilkins and Carros [3] was built at EMI-AFB. With this gas gun simulator we generated single-phase and two-phase, chemically reacting flows at temperatures and pressures typical of an actual gun. The gas propellant used was a suitably diluted mixture of hydrogen and oxygen. Thus, the interior ballistic flow and subsequent muzzle flow dynamics were simulated with a particularly simple chemistry.

The development of the gas gun and the experiments performed have been made possible through the support and sponsorship of both the Ministry of Defence of the Federal Republic of

Germany and the U.S. Government through its European Research Office of the U.S. Army (U.S. Army Research, Development and Standardization Group (UK), London). A three years contract (Contract Number DAJA 45-84-C-0013) was awarded by the European Research Office which expires April 5, 1987. The scientific research performed hereunder is summarized in the present Final Report.

Dr. J.M. Heimerl of the U.S. Army Ballistic Research Laboratory (BRL), Aberdeen Proving Ground, Maryland, USA, came as an Exchange Scientist with EMI-AFB to Weil am Rhein from January 1985 to April 1986. As the BRL Contract Monitor of this contract, he bore part of the responsibility for the conduct of the research work and participated in the theory and experiments done under this contract. Since his primary commission was to investigate basically the fundamentals of blast and flash and the chemical suppression of secondary flash, we obtained the Contracting Officer's approval to address primarily the simulation and probing of the transitional or intermediate ballistic flow. The conduct of the research was aimed at attaining these stated objectives within the limits of contract's terms and conditions. Prior to description of the experiment, the background of simulation research is briefly discussed. Then, the gas gun simulator is described. Next, the results of thermodynamic (BLAKE) code calculations for the closed bomb mode of the EMI-AFB gas gun simulator are presented. Then, we report on experiments of simulating and probing primarily the reacting gun muzzle exhaust flow.

2. BACKGROUND

2.1 Interior Ballistics Requirements

The development of high-performance propelling charges has been marked by damaging overpressures and breechblows, nearly always in gun systems for which the interior ballistic environments were characterized by the presence of large pressure waves. Multiphase interior ballistic models responded to the need for a quantitative predictive and diagnostic tool for assessing the causes and cures for these problems. Codes developed in the USA and Europe have identified the causes for numerous problems experienced in both howitzers and tank guns and have provided design guidelines for the igniter/propellant interface and packaging configurations for many new propelling charges. Moreover, experimental studies essential to the formulation and validation of these codes have also resulted in new techniques capable of providing detailed characterization of particular attributes of new charge configurations in order to solve critical problems which jeopardized program success [4,5].

Charge designers today are facing ever-increasing performance demands and are investigating the use of more energetic propellants at higher loading densities, operating at even higher pressures than those currently used. Such conditions exacerbate problems with the formation of pressure waves and their influence on maximum chamber pressures and with heat transfer to an erosion of the bore surface. Further, efforts to develop low-vulnerability propellants are being hampered by lack of full understanding of the role of ignition dynamics and low-pressure combustion kinetics associated with these formulations. In addition, advanced payloads often pose new launch constraints, requiring considerable fine-tuning of the launch signature to assure survivability and reliability. And finally, new projectile configurations sometimes extend well back into the space normally occupied by the propelling charge, again impacting ignition and subsequent hydrodynamics [4].

2.2 Transitional Ballistics Requirements

The effluent from a weapon that uses H-C-H-O based solid propellant charges is known to consist of a fuel-rich mixture containing H_2 and CO. Upon mixing with the surrounding air, which is entrained turbulently, a combustion process can take place that results in a high intensity flash, called muzzle flash [6].

Three main luminous regions exist in the muzzle effluent that are separated in space and time [7]. The first region, located at the muzzle, is of small spatial extent and low luminosity. The radiation from this region is commonly called the primary flash. Farther downstream from the muzzle is a more extensive region of greater luminosity. It is separated from the primary flash by a dark zone and is called the intermediate flash. Still farther downstream from the muzzle and adjacent to the intermediate flash is an extensive and very luminous region called the secondary flash [7,8].

The operational importance of suppressing the muzzle flash especially of large artillery or tank cannons lies in three areas. In the field the brilliant flash is easily detected and so reveals gun positions. The muzzle flash can also cause temporary loss of vision of the gun crew, especially at night. Since the amount of energy released nearly instantaneously in the secondary muzzle flash is comparable to that released at the muzzle exit as the projectile uncorks the gun tube, the concomittant blast wave of present-day high performance weapons can lead to overpressures that exceed those due to the primary blast wave. For large caliber gun systems these combined overpressures can be so great as to cause physical damage to the gun system and non-auditory physiological damage to a nearby gun crew [6].

2.3 Generation of Muzzle Flash

That oxygen needs to be entrained and mixed with the fuel-rich muzzle effluents in order to obtain muzzle flash has been established by Klingenberg and Heimerl [8,9,10]. By firing rounds that were known to produce muzzle flash into surrounding atmospheres of nitrogen and oxygen they found that, relative to firings into air, the secondary flash was completely suppressed with nitrogen and was sensibly enhanced with oxygen. They [10,11,12] also confirmed that oxygen is entrained, and combustion reactions take place in the intermediate flash region. These combustion reactions control the ignition sequence leading to the secondary flash, and they are inhibited by alkali salts as flash suppressants.

2.4 Flash Suppression by Mechanical Devices

Shock formation has also been shown to be a necessary process in the generation of flash. There are two types of mechanical flash suppressors effective for small caliber weapons [13]. The first is a cone shaped hider that is attached to the muzzle. It allows the expanding muzzle gases to approach atmospheric pressure before mixing with the surrounding air takes place. The second mechanical suppressor consists of two or more bars that are arranged symmetrically about the gun axis and extend beyond the muzzle. In the former case, the expansion ratio of the emerging gases is lower so that the strength of the inner shock disk is considerably reduced. In the latter case, the bars reduce the shock formation. The opposite experiment has also been performed. Schmidt [14] has placed baffles (muzzle brakes) in the exhaust gases of a gun firing conventional ammunition with chemical flash suppressant. He observed a progressive and substantial increase in luminosity with increasing number of baffles; i.e., hardly any luminosity is observed with no baffle but with two baffles the observed luminosity envelopes the entire exhaust field. Shock formation on the baffle surfaces overcame the chemical suppression including secondary flash. And so for secondary muzzle flash, the necessity of processing the exhaust gases through a strong shock structure is indicated.

As just discussed, mechanical attachments to the muzzles of small caliber guns have proved effective in helping to reduce muzzle flash; but, for large caliber guns such mechanical devices would prohibitively increase the cost and weight of the gun system and the devices themselves would be susceptible to damage during handling [13,15]. Thus we neglect any further discussion of flash suppression in large caliber guns by mechanical means.

2.5 Suppression of Muzzle Flash by Chemical Means

The suppression of muzzle flash by chemical means leads to two distinct approaches. Since muzzle flash requires, among other things, a fuel-rich effluent, use of a propellant that is stoichiometrically balanced would preclude secondary muzzle flash. Some liquid propellant formulations offer this potential benefit. However, at the present time liquid propellants have not been fielded and are at the stage of a research and development project [16].

For solid propellants such attempts have already been reported [17]. Nitroglycerine flake powder was rolled into tubes which were filled with ammonium nitrate so that a stoichiometrically balanced mixture was obtained. For comparison there existed another nitroglycerine-based charge that had about the same energy content and weight. When fired from a 40 caliber experimental gun with a short length tube, these two different charges produced about the same maximum gas pressure in the gun. High speed photography showed that the emission produced by the stoichiometrically balanced charge was much less intense and was of shorter duration than that of the comparison charge. The former could be attributed to the primary and intermediate flashes while the latter was obviously secondary muzzle flash. However, because such stoichiometrically balanced solid propellants erode a gun tube very rapidly, they are not practical to use in the field.

The other chemical approach has been the addition of suppressant compounds to solid propellants. This approach has been largely empirical because a fundamental understanding of the underlying suppressant mechanism has been lacking. Many compounds, most of them alkali salts, have been reported to suppress muzzle flash [6]. For example, Table 1 shows results in Germany covering the period 1914 - 1945 that have been reviewed by Kesslau [18,19]. Observations were made by eye. Kesslau reports on test firings in 8.8 cm and 10 cm fielded guns. Results in Japan up to 1945 are also shown in Table 1 [6]. The empirical work continues even today. For example, in a relatively recent paper, Bracuti, Bottei and Davis [20] employed a closed bomb vented by a short barrel (22.86 cm) and found the ranking of compounds seen in Table 1. Unpublished results of Klingenberg at EMI-AFB had shown that to suppress the flash in a 7.62 mm rifle the amount of KNO_3 that must be added is twice that of either $NaHCO_3$ or $Na_2H_2O_4$.

In Table 1 we see that only a few percent (by weight) alkali salt addition have been found to be effective in suppressing flash in these (and other) gun systems. This is a strong

Table 1. Compounds reported to suppress muzzle flash [6]

Flash Suppressants Ranked According to Effectiveness				
Kesslau [a]	Bracuti et al. [b]	Klingenberg [c]	Most Effective Japanese Compounds	Others Mentioned by Kesslau
K_2SO_4	$KHCO_3$	$NaHCO_3$	CsI [d]	K
KNO_3	NH_4HCO_3	$Na_2C_2O_4$	KI [e]	$NaHCO_3$ [f]
$KHC_4H_2O_6$	$(NH_4)_2CO_3$	KNO_3	KBr [e]	$Na_2C_2O_4$ [f]
KCl	K_2CO_3		$K_2C_2O_4 \cdot H_2O$	$NCH_2(CO)NH_2$
	KNO_3		$KHC_2O_4 \cdot 1/2\ H_2O$	$NHCN(HCN)NH_2$
	K_2SO_4		K_2SO_4	

Notes:

a: (0.5 - 5) % added by weight

b: (8 - 9) % added by weight

c: 0.5 % of the sodium salts and 1 % of the potassium salt required to suppress flash

d: most effective alkali-halide

e: other alkali-halide compounds alluded to but not specified

f: other sodium compounds alluded to but not specified

support that the suppressant mechanism is chemical rather than physical in nature. However, since there exists no fundamental understanding of the chemical mechanism of flash suppression, it is difficult, of not impossible, to correlate the results of one test with those of another. By pursuing a trial-and-error approach one can develop a chemical flash suppressor for a particular weapon without any particular knowledge of the origin or mechanisms by which flash occurs and is suppressed. This approach is time-consuming and uncertain since there is no way to define an optimum amount of suppressant; nor are the results necessarily transferable to another weapon system.

The fact that a great number of alkali compounds are effective as flash suppressants suggests that some alkali reaction network is active during the ballistic cycle and that this network is approximately the same regardless of which alkali compound has been added to the propellant.

One might think that continued simple addition of, say K_2SO_4, to the propellant would suffice to suppress secondary flash. However, such additions lead to an undesirable change in ballistic performance. Also, the continued addition of these salts, particularly K_2SO_4, causes progressively larger increases

in smoke formation [21,22], so that in some cases the increased smoke can be more objectionable than the flash. Thus the continued simple addition of more salt turns out not to be a viable solution to suppress muzzle flash in high-performance, large-caliber, gun systems.

One can ask: how efficient is alkali salt in weapon systems as a flash suppressant? And: are there reasonable grounds to expect that some other more efficient substance might exist? If the suppressant mechanism were understood, these questions could be addressed. Then both charge and suppressant could be tailored to achieve a desired ballistic performance early in the design stages of a new weapon or weapon subsystem. This procedure could lead to substantial cost saving over the current practice or treating each case empirically after the fact.

2.6 Objective

The need to solve problems such as interior ballistic flows or gun muzzle blast and flash requires a more detailed understanding of the processes involved. The objective of this research is to perform benchmark validation experiments in the gas gun simulator in order to understand the basic gasdynamic and associated chemical processes occurring during the interior and transitional ballistic cycles of gun systems.

According to the recommendations of Klingenberg and Banks [1] simulation experiments are conducted in the European Community which are thought to address the fundamentals of gun ballistic flows.

2.7 European Simulation Experiments

As mentioned, simulation experiments are currently under way within the European Community [23,24,25]. Table 2 shows a list of such simulation experiments.

These simulators address flow problems with increasing complexity. The compression chamber at Imperial College [26] can consider two-phase flows but is limited to inert gases or particles, and to low pressures and low temperatures. The shock tube facility at the German-French Research Institute (ISL) [24] is used to simulate single-phase, inert flows at temperatures characteristic of ballistic environments, but at pressures that are a factor of six or more lower than those encountered in ballistic flows. The goal is to study two-phase (gas/solid) reacting flows. The light gas gun facility, also at ISL [24], is being used to simulate single-phase, inert flows at pressure and at temperatures that are characteristic of ballistic flows. The goal

Table 2. Simulation experiments within the European Community

Institute Country	Facility	Maximum Pressure (MPa)	Maximum Temp. (K)	Flow Status	Flow Goal
Imperial College * (UK)	Compression Chamber	1 - 10	---	Inert Two Phase	
I S L (FR/GR)	Shock Tube	15 - 50	3000	Inert One Phase	Reacting Two Phase
I S L (FR/GR)	Light Gas Gun	350 - 400	3000	Inert One Phase	Inert Two Phase
EMI-AFB* (GR)	Gas Gun	350 - 450	3000	Reacting One Phase	Reacting Two Phase

* Supported by the U.S. Army through its European Research Office

here is to investigate particle-laden flows. The limitation is that only inert gases and particles can be used. Comparatively, the gas gun facility used at EMI-AFB simulates single-phase, reacting flows at temperatures and pressures typical of an actual gun.

While each of these simulators is necessary to provide the stepwise increase in complexity required for the complete understanding of multiphase, high temperature, high pressure, reacting flows, only the gas gun simulator at EMI-AFB permits the simulation of controllable reactive flows with characteristics similar to those of medium caliber gun systems [23,24,25].

2.8 Lord's Work Done in the 1960's

The feasibility of a gas gun driven by the combustion of a prepressurized mixture of hydrogen and oxygen diluted with helium to prevent detonative reactions has already been demonstrated during the early 1960's. For example, Lord [2] investigated the performance of a 40-mm combustion heated light gas gun launcher achieving controlled combustion with a gas mixture of three moles hydrogen, one mole oxygen, and eight moles helium, i.e., $3H_2 + O_2 + 8He$. The objective of his study was to attain high launch velocity of the projectile by using low molecular

weight propellant gas. The gases were prepressurized and subsequently filled into the gun chamber. Ignition of the gas mixture was performed by the discharge of a small capacitor bank through fuze wires positioned at three locations along the axis of the gun chamber. A maximum final chamber pressure of about 350 MPa was attained in these firings [2]. Also, Lord [2] used a rather rudimentary thermodynamic code to compute achievable final pressures, p_F, as a function of the pre-pressure or charge pressure, p_I.

For example, Figure 1 presents his computed results for the complete combustion of the gas mixture $3H_2 + O_2 + 8He$ at a temperature of T = 2700 K. Since the final chamber pressure, p_F, is dependent upon the charge density, i.e., the charge pressure, p_I,* high chamber pressures of more than 400 MPa are theoretically obtained for charge pressures exceeding 60 MPa. However, in practice, the attained maximum pressures must stay below the

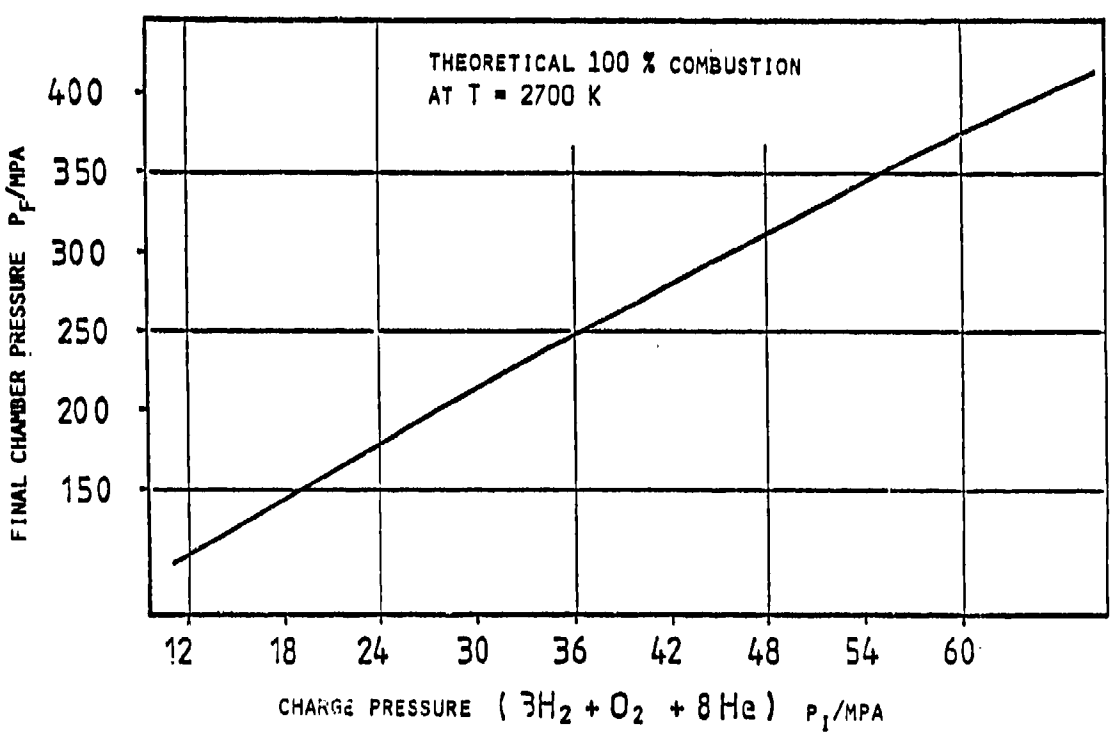

Fig. 1. Final chamber pressure, p_F, versus charge pressure, p_I, at T = 2700 K according to the computation of Lord [2]

---

* The charge pressure, p_I, is also called initial chamber pressure, initial loading pressure, or prepressure of the propellant gases, introduced into the chamber of the gas gun before ignition (see references 2 and 3).

theoretical level due to unavoidable heat losses that occur during the combustion of the gas mixture. Nevertheless, it was demonstrated by Lord [2] that chamber pressures approaching real interior gun conditions could be realized with this particular gas mixture. Note, however, that BLAKE calculations, performed more recently, show that the calculations of Lord [2] are in error (see Section 4.).

2.9 Investigations Performed by Wilkins and Carros in the 1960's

Wilkins and Carros [3] reported in 1963 on combustion tests performed with stoichiometric gas mixtures of oxygen, hydrogen, and helium as well as with gas mixtures of oxygen and hydrogen. Two chambers were used. The small chamber had an inner diameter of about 3.81 cm (1 1/2 inches) and an inside length of about 38.7 cm (15 1/4 inches), i.e., the volume was approximately 0.5 liter. The parameters varied in these small chamber tests were the

(a) mixing procedure,

(b) mixing time,

(c) method of ignition

(d) flame path-length,

(e) composition of the gas mixture, and

(f) charge pressure.

Charge pressures up to about 55 MPa (8000 pounds per square inch) were tested.

Some tests were also made in a larger chamber with an inside diameter of about 15.9 cm (6 1/4 inches) and an inside length of approximately 1.22 m (40 feet), i.e., a volume of about 242 liters. Maximum charge pressures of about 5 MPa (815 pounds per square inch) were used in these large chamber tests [3].

Adequate mixing of the gases was found to be very important in determining whether or not the burning was smooth The order and rate of introducing the gases affected the mixing and hence the burning. For example, in the small chamber adequate mixing depended upon the order in which the three gases hydrogen, oxygen, and helium were introduced. Pressure-time history recordings indicated that mixing of the gases was adequate for the following orders of introduction:

(a) Hydrogen, followed by helium, then followed by oxygen, or

(b) oxygen, followed by premixed helium and hydrogen.

In the large chamber, the order of introducing the gases and particularly the flow rate thereof was important in promoting mixing [3].

Four different ignition sources were tried in the small chamber. Three of these igniter devices were found to be satisfactory, i.e.,

(a) a 1.27 cm (1/2 inch) long exploding wire,

(b) a chemically reacting wire, and

(c) a heated tungsten wire.

In the large chamber, the tungsten wire, which was heated electrically, was the most satisfactory ignition source tested.

In addition, Wilkins and Carros [3] showed that the type of ignition device used affects whether combustion or detonation of the gas mixture occurs in the gun chamber. For our experiments, both the exploding wire and the heated tungsten wire technique were used to ignite the gas mixture.

Wilkins and Carros [3] further reported that the order of gas introduction into the gas gun chamber is critical. They found that smooth combustion of the gas mixture resulted either from the introduction of hydrogen, followed by helium, and finally by oxygen, or from the addition of a premixed helium and hydrogen to the oxygen, i.e., the introduction of oxygen, followed by a premixture of helium and hydrogen. We now know that Lord in his earlier experiments [2] also experienced smooth combustion because he had added a premixture of helium and hydrogen to the oxygen.

Wilkins and Carros [3] found that the order oxygen, followed by helium, followed by hydrogen gave poor results that sometimes resulted in detonation. In our first gas gun tests, because we thought it would be safer to begin with the filling of oxygen, we used this "poor" order of gas introduction. Later, we altered the order of gas introduction using commercial prepressurized, premixed gas mixtures of helium and hydrogen (see Section 8).

2.10 Statement of Work

The present report presents the status of the Contract DAJA 45-84-C-0013 and describes the benchmark validation experiments performed with the gas gun. This gas gun simulator had to be constructed and built before the experiments could be performed. The design and the selection of the gas propellant make use of the work of Lord [2] and Wilkins and Carros [3].

Part of the data reported under this Contract have been published in EMI-AFB reports [10,11,12,27]. These reports were written to summarize the work done in 1986 as required by the policy of the Fraunhofer Society and the Ministry of Defence of the Federal Republic of Germany.

An unpredictable, rather long period of time was required to build and test the ballistic simulator, because we encountered damage in the high pressure compressor, and its repair by the supplier took six months.

As stated above, the work done during the reporting period of three years completed only part of the primary envisaged tasks, since the bulk of the data were taken in the reacting muzzle flow in accordance with the Contract Monitor and the Contracting Officer. However, the foundation was laid to proceed with the simulation experiments under a new contract. This simulation is important for ballistic flow processes, for which the fundamental physics and chemistry are not understood, including:

- heat transfer to gun tube walls,
- the role of turbulence in this heat transfer,
- the process by which additive particles are deposited on gun tube walls, and
- the role of particles in reacting muzzle flows.

Therefore, we propose to continue this research with the gas gun to study interior and transitional ballistic flows in which chemical reactions are taking place. The results of the present and future experiments provide valuable clues into the details of the formation and thus the suppression of secondary gun muzzle flash and into the interior ballistic flow. Important parameters are measured which are included in interior and transitional ballistic codes, but for which there are little data.

3. DESCRIPTION OF THE EMI-AFB GAS GUN SIMULATOR

The EMI-AFB gas gun simulator, used in these experiments, had been constructed in two stages. In the first stage of construction, the gas gun chamber was employed in a closed bomb mode. The second stage in the construction included a gun tube and a projectile.

3.1 First Stage of Gas Gun (Closed Bomb Mode)

The first stage in the construction included the combustion chamber, equipped with a solid retainer and the exploding wires as an ignition source, see Figure 2.

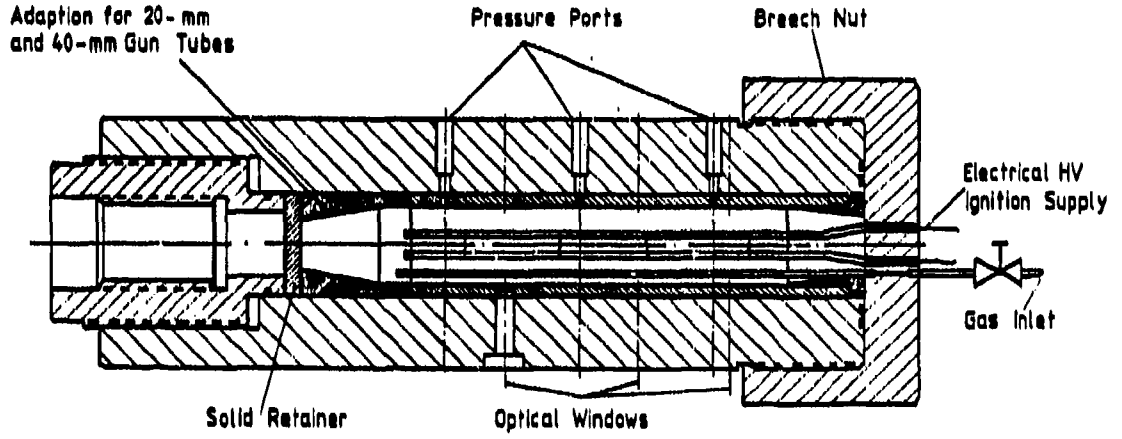

Gas Gun Chamber with Solid Retainer for Closed Chamber Combustion Studies

Fig. 2. First stage of EMI-AFB gas gun simulator

The solid retainer confines the gas mixture $3H_2 + O_2 + 8He$ so that the gun chamber can be used in a closed bomb mode.

Figure 3 shows a photograph of the gas gun chamber with the breech block containing in its center the exploding wire and the power cable. To ignite the gases, the capacitor bank is discharged into the exploding wires. The chamber is mounted to a support which holds the gas gun. The recoil of the chamber (and gun tube) is taken up by a hydrostatic device mounted at the support.

Figure 4 shows the cables connected to the two Kistler pressure gauges and the temperature gauge (emission gauge) which are mounted atop the gas gun chamber. They are used to measure the pressure and temperature histories of the gases inside the chamber during combustion.

The first stage of the EMI-AFB gas gun simulator, shown in Figures 2, 3, and 4, was used to investigate the combustion behaviour of the gas mixture $3H_2 + O_2 + 8He$ in the closed bomb mode configuration. These experimental data have been compared to thermodynamic (BLAKE) code calculations.

Fig. 3. Photograph (rear view) of gas gun chamber with the gas inlet (top) and with the power cable for the exploding wire igniter (bottom)

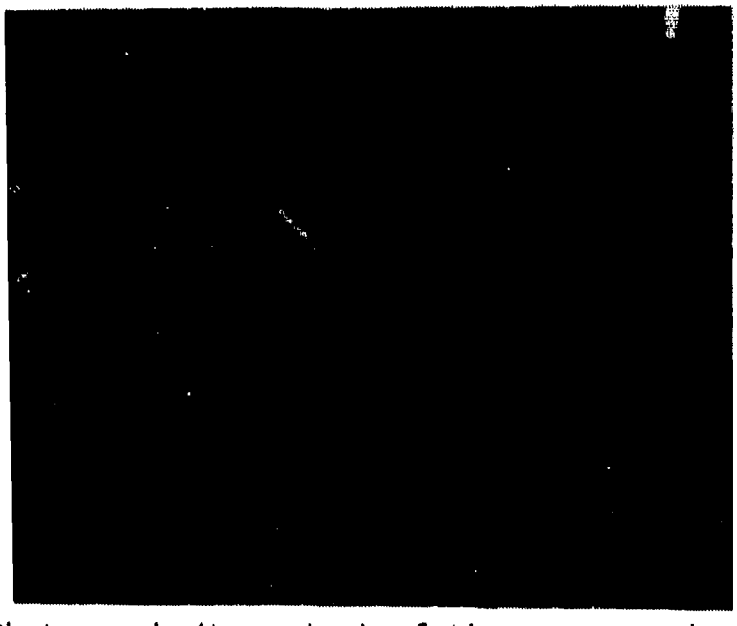

Fig. 4. Photograph (top view) of the gas gun chamber with cables to the two pressure gauges and to the temperature gauge

The gas gun chamber geometry is large when compared to conventional solid propellant 20-mm guns. The chamber has a length of 550 mm and an inside diameter of 70 mm so that its volume is approximately two liters.

For the closed chamber tests, four equally spaced exploding wires, placed axially in the chamber, were used to ignite the gas mixture. The wires were activated by releasing about 110 J of electrical energy from a 3000 Volt capacitor bank through the wires.

3.2 Second Stage of Gas Gun

The second stage in the construction of the EMI-AFB gas gun simulator included a 20-mm gun tube and the projectile, see Figure 5.

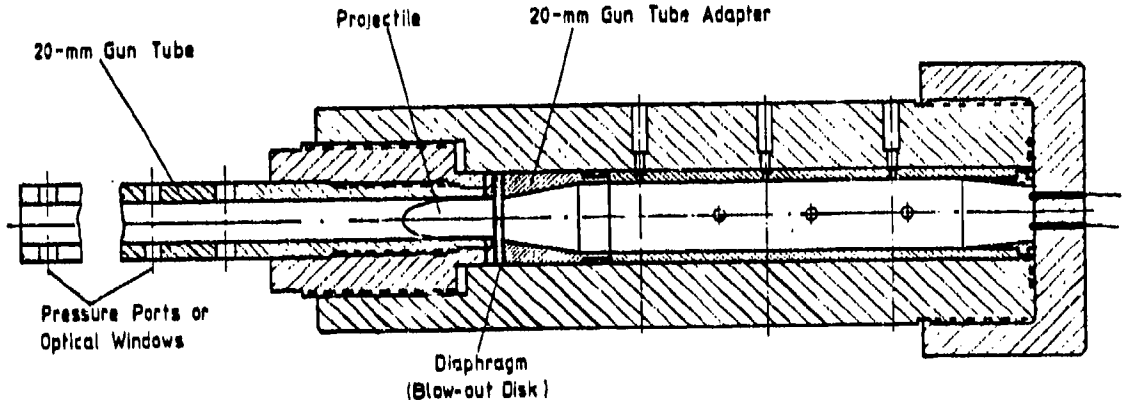

Fig. 5. Second stage of the EMI-AFB gas gun simulator

The solid retainer of the first stage of the gas gun is replaced by a blow-out disk, scored to rupture at a predetermined pressure, in order to simulate the projectile's extraction force which, for conventional 20-mm cased ammunition, is of the order of 90 MPa. If necessary, engraving forces could also be taken into account. A conventional 20-mm projectile and a 1.8 m long, 20-mm, smooth-bore gun tube were used in these experiments. To place the projectile into the tube in front of the blow-out disk, the diameter of its rotating band had to be reduced to about 20 mm. Nevertheless, this diameter still exceeded the in-bore diameter by 0.1 mm, so that the blow-by of the propellant gases was reduced.

The gas gun chamber as well as the gun tube were fitted with appropriate pressure or temperature ports and with optical windows; see Section 5. The EMI-AFB gas gun simulator therefore

can be used to simulate and study both the interior and transitional (intermediate) ballistic flows, i.e., gun tube flows and muzzle blast and flash phenomena.

Figure 6 presents a photograph of the gas gun simulator with support and 20-mm gun tube. However, in this picture, the gun tube has not yet been equipped with the measurement ports and optical windows.

In the second stage of the gas gun configuration experiments, both the ignition method and the gas introduction procedure were altered; see Section 5.

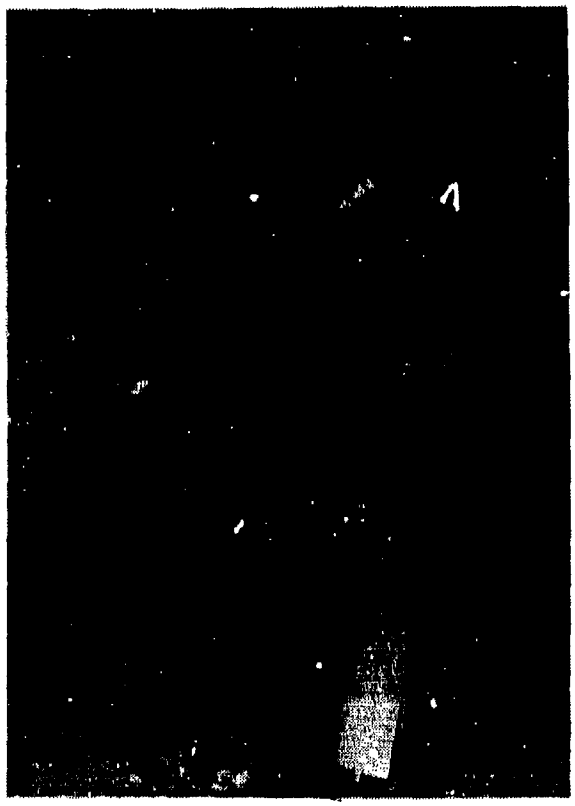

Fig. 6. Photograph of the second stage of the EMI-AFB gas gun simulator

3.3 Assembly Used for Introducing the Gases into the Gas Gun Chamber

The assembly used for introducing the gases into the gas gun chamber is shown schematically in Figure 7.

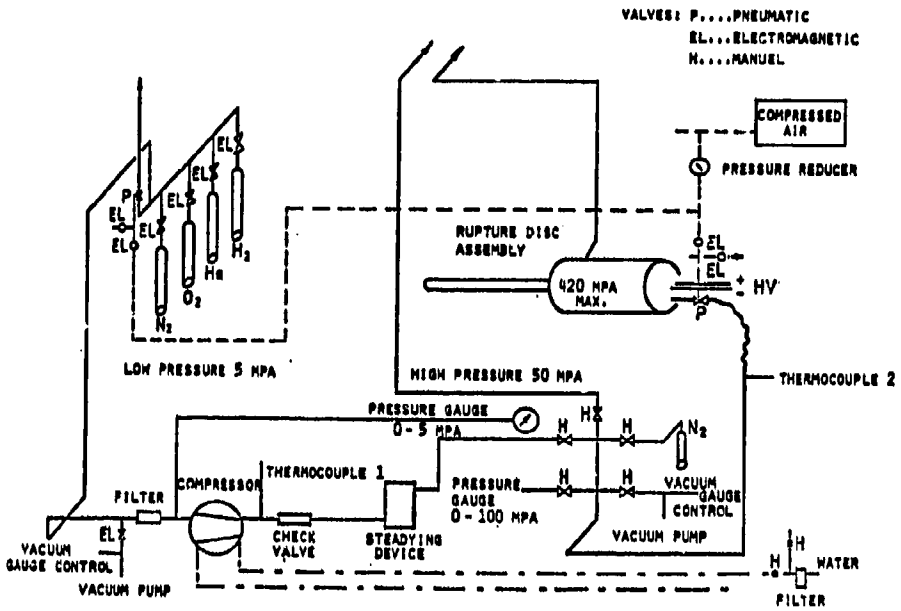

Fig. 7. Assembly used for introducing the gases into the gas gun chamber

A specially designed gas compressor is needed to prepressurize the gases. The prepressurization determines the final chamber pressure, p_F; see Figure 1 in Section 2.8. The vacuum pump evacuates the feed lines before and after a particular gas has been introduced into the gas gun chamber. Also, dry nitrogen gas is pumped through the feed lines to purge them. During the introduction of a particular gas, the gas temperature is kept constant in order to provide the correct mole fraction. The gas temperature in the feed lines is monitored by the thermocouples 1 and 2; see Figure 7. The pressure of the gases is monitored by pressure gauges. Figure 8 shows a photograph of the gas compressor, vacuum pump, and feed lines.

For safety reasons, the possible leakage of hydrogen into the test room also is monitored by an explosion warning device. This indicator is activated when the gas leakage into the test room amounts to a hydrogen concentration which corresponds approximately to 50 % of the lower gas explosion limit (4 % of hydrogen in the surrounding air). Then, this device automatically stops the filling procedure, nitrogen is pumped into the feed lines, and a room fan is turned on to remove the gases from the room.

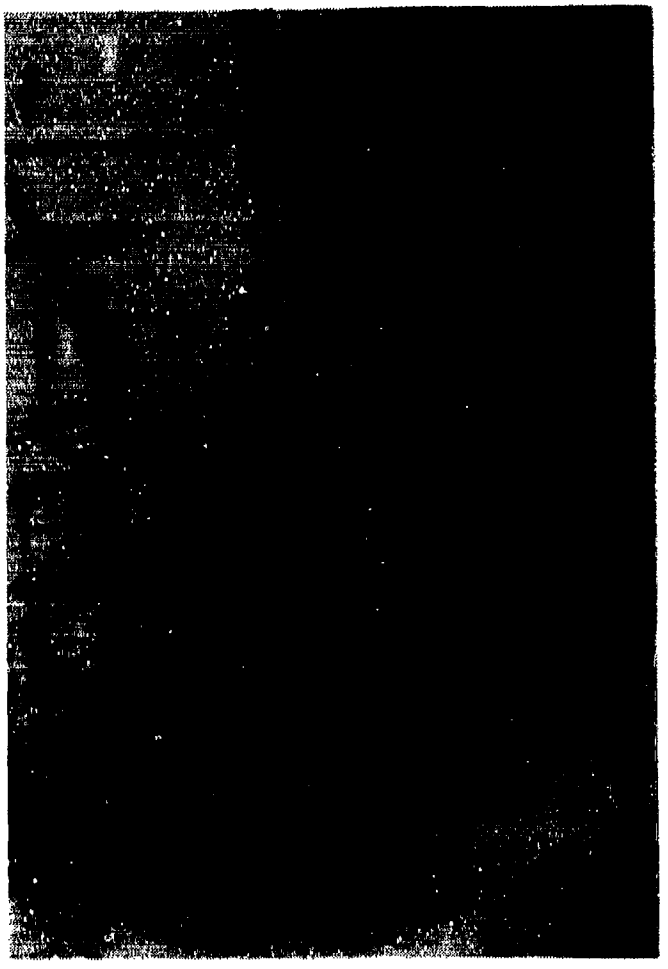

Fig. 8. Gas compressor (background), vacuum pump (foreground), and feed lines

4. THERMODYNAMIC BLAKE CODE COMPUTATIONS

4.1 Overview

As has been pointed out in Section 2, earlier studies by Lord [2] and Wilkins and Carros [3] have been conducted with hydrogen/oxygen gas mixtures diluted with helium. The primary goal of Lord's experiments was to achieve high launch velocities of the projectiles used. The EMI-AFB gas gun simulator based on Lord's apparatus was primarily designed to

- avoid the harsh environment encountered in real gun firings,

- simulate adequately interior and transitional ballistic flows which are less complex and permit optical studies,
- investigate well-controlled, better defined, single and two-phase, reacting flows with characteristics approaching those of medium caliber (20 mm to 40 mm) gun systems.

Because of the differing goals, there seemed to be no compelling reason to use only helium in the gas mixture

$$3\ H_2 + O_2 + nM \qquad (1)$$

where M denotes the diluent and n the mole proportion used. Therefore, other diluents, such as argon and nitrogen were also considered in the thermodynamic BLAKE code computations.

4.2 Considerations

There are two considerations, if one were to change the diluent for closed bomb studies:

(a) How would the substitution of diluents affect the final (combusted) chamber pressure?

(b) Could the substitution lead to a detonation?

Some concern was raised with regard to this last question because a model computation [28] predicted detonation for the mixture proportions: $2H_2 + O_2 + 7Ar$. However, the computational model itself has been called into question [28] and the matter was not resolved. From a practical point of view, it is assumed that smooth combustion is encountered, if the gas mixture proportions remain in the ratio:

$$3\ H_2 + O_2 + 8M \qquad (2)$$

where M = Ar, or M = N_2.

The first question could be answered by using thermodynamic codes for calculating the pressure time histories of various gas mixtures.

4.3 BLAKE Code Calculations

The thermodynamic BLAKE code is used at the Ballistic Research Laboratory (BRL) [29] and a version of this code was developed at the Fraunhofer-Institut für Treib- und Explosivstoffe (ICT), Prinztal-Berghausen. Most recently, a comparison of calculations done with both the BLAKE- and the ICT codes was made [30,31] to bring both programs in line with each other.

Here, we employed the ICT-code version of BLAKE. It was made operational on the VAX computer of the Fraunhofer-Institut für Naturwissenschaftlich-Technische Trendanalysen (INT), Euskirchen, which, at that time, was available for EMI-AFB use.* Under normal circumstances constant-volume (isochoric) burning calculations of the previously defined temperature T would be carried out using the ExI instruction of BLAKE. However, ERROR II (Explosion State CARD NOT ACCEPTABLE) was returned, even for the example listed on page 48 of reference 29.

A check with E. Freedman at BRL revealed that the BRL version of the code yielded the proper response. Thus, there is an error somewhere in Subroutine EXPLOS in the EMI-AFB VAX version of the BLAKE code. This difficulty was not solved directly but circumvented by using the ExP instruction, known to be operational. Since this instruction requires as input the specific volume, V_s, it was computed from the known pressure, p, and temperature, T, data using the ideal equation of state, given by

$$V_s = R T (\Sigma p_i A_i)^{-1} \tag{3}$$

where A_i denotes the atomic weight in gm/mole of the i-th species.

After some algebraic calculations, an engineering equation was developed:

$$v_s = 36,676 \ (4 \cdot 75 + A_M)^{-1} \ p^{-1} \tag{4}$$

where T has been taken as T = 298 K, R = 0.08205 liter atmospheres $(\text{molesK})^{-1}$, p as the total initial chamber pressure, and A_M the atomic weight of the diluent. The p and A_M data are summarized in Table 3.

The BLAKE code has provisions for changing the equation of state used in the computations. Here, both the ideal equation, i.e.,

$$p = R T / V_s \tag{5}$$

and the truncated virial equation of state, i.e.,

$$p = (RT/V_s) \ [1 + B/V_s + C/V_s^2] \tag{6}$$

were used.

---

* Meanwhile EMI-AFB has had a VAX computer installed at the institute.

Table 3. Computed values of the specific volume as a function of initial charge pressure for the diluents: helium, argon, and nitrogen

Charge Pressure p_I (MPa)	Specific Volume V_s (cm^3/gm) M = He	M = Ar	M = N_2
6	69.8597	13.6597	18.6648
12	34.9298	6.8298	9.3324
18	23.2865	4.5532	6.2216
24	17.4649	3.4149	4.6662
30	13.9719	2.7319	3.7329
36	11.6432	2.2766	3.1108
42	9.9799	1.9513	2.6664
48	8.7324	1.7074	2.3331
54	7.7621	1.5177	2.0738
60	6.9859	1.3659	1.8664
66	6.3508	1.2417	1.6968

4.4 Predictions

The data obtained from the BLAKE code calculations are summarized in Table 4. Also, a plot of these predictions is shown in Figure 9.

As can be seen in Figure 9, a great difference in the curves is obtained for the choice of the equation of state. The truncated virial equation of state includes the effects of finite size molecules, while the ideal equation of state does not. Therefore, the virial equation of state is judged to be a better approximation to reality. Obviously, the latter yields greater final chamber pressures than the ideal equation of state.

The reason for these deviations can be found by examining the computed final temperatures T in the gas gun chamber that

Table 4. Values of the final chamber pressure (computed using the BLAKE code) as a function of the initial chamber pressure for the diluents: helium, argon, and nitrogen and for the two equations of state

Charge Pressure p_I (MPa)	Final Chamber Pressure p_F (MPa)					
	Virial Equation of State			Ideal Equation of State		
	M = He	M = Ar	M = N_2	M = He	M = Ar	M = N_2
6	52.77	52.96	38.82	49.9	50.1	31.3
12	111.8	112.4	83.15	99.9	100.1	72.61
18	177.6	178.9	133.7	150.0	150.0	108.9
24	250.9	253.1	191.3	200.0	200.5	145.2
30	332.3	335.6	256.5	250.1	250.1	181.5
36	422.5	427.5	330.2	300.0	300.8	217.8
42	522.0	529.2	413.1	350.0	351.1	254.1
48	631.8	641.4	505.8	400.0	401.3	290.3
54	752.2	764.7	609.2	450.0	451.5	326.6
60	884.0	900.1	723.8	500.6	501.7	362.9
66	1028.0	1048.1	850.4	550.7	551.9	399.1

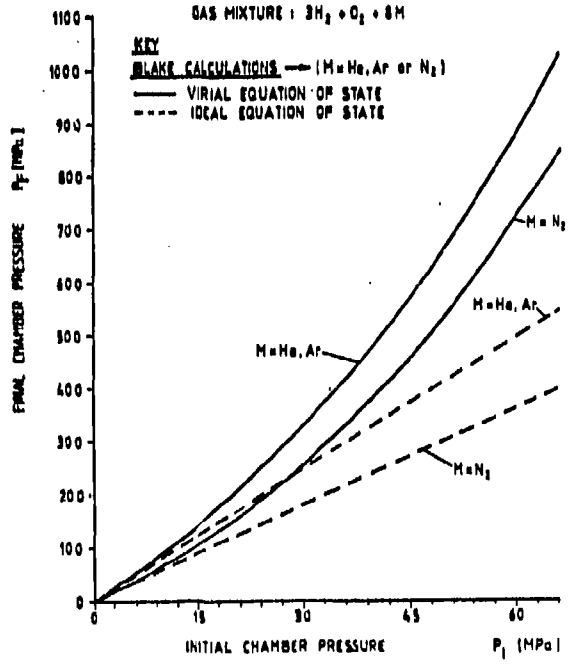

Fig. 9. Final chamber pressure, p_F, versus initial (loading) chamber pressure, p_I, as obtained from BLAKE computations

correspond to the computed final chamber pressures, p_F, listed in Table 4. These predicted temperature data are summarized in Table 5.

Table 5. Computed final chamber temperatures (K) as a function of initial chamber pressure for the diluents: helium, argon, and nitrogen and for two equations of state

Charge Pressure p_I (MPa)	Temperature T (K)					
	Virial Equation of State			Ideal Equation of State		
	M = He	M = Ar	M = N_2	M = He	M = Ar	M = N_2
6	2710	2709	1971	2705	2705	1968
12	2717	2716	1974	2709	2709	1969
18	2723	2721	1978	2711	2711	1969
24	2728	2725	1981	2712	2712	1969
30	2732	2728	1984	2713	2713	1969
36	2736	2731	1988	2713	2713	1970
42	2740	2735	1992	2714	2714	1970
48	2744	2738	1996	2714	2714	1970
54	2747	2741	2000	2714	2714	1970
60	2751	2743	2005	2714	2714	1970
66	2754	2746	2010	2715	2715	1971

For the case of the ideal equation of state and a selected diluent, we see that the computed temperature is practically constant with pressure. On the other hand, for the case of the truncated virial equation of state, the computed temperature increases slightly with increasing pressure. The temperature difference amounts to about T = 40 K over the pressure range given. This deviation is reflected in the computed final chamber pressure curves of Figure 9. It can account for the difference between the curves obtained with the two equations of state.

For a selected equation of state, we observe in Figure 9 a further deviation existing between the nitrogen (N_2) curves and the curves with the noble gases (argon and helium). The nitrogen yields lower final chamber pressures, p_F, at a given

initial loading or charge pressure, p_I, than the argon or helium diluents. Table 5 shows that, for a given pressure and equation of state, nitrogen has a lower predicted final chamber temperature than either of the noble gases argon and helium. The noble gases are monatomic molecules while nitrogen is a diatomic molecule. Thus, nitrogen has internal degrees of freedom (not available in the noble gases) that can absorb kinetic energy of the gas. Thus, its kinetic energy, i.e., the temperature, is lower than for a noble gas. This temperature reduction accounts for the lower N_2 pressure curve in Figure 9.

4.5 Comparison to Lord's Predictions

In Figure 1 of Section 2.8 we have presented Lord's predictions of the final chamber pressure, p_F, versus the initial loading pressure or charge pressure, p_I, using the gas mixture in the mole proportions:

$$3\ H_2 + O_2 + 8\ He.$$

A comparison to our corresponding predictions, i.e., for the case of helium as a diluent (M = He), reveals that there is no agreement between Lord's and our predictions, see Figures 1 and 9. Lord's data are, however, almost identical with our predictions, obtained for the case of nitrogen as a diluent ($M = N_2$). Therefore, we conclude that Lord's computations are in error.

4.6 Comparison to Experimental Data

Prior to description of the experimental results in Section 8, we present here the pressures measured by Lord [2] and under this contract for the gas mixture $3H_2 + O_2 + 8He$ in the closed bomb mode. The purpose is to compare the BLAKE code predictions with the experiment. The pressure measurements in the closed bomb mode are summarized in Table 6.

The data of Table 6 are plotted in Figure 10 together with the more realistic BLAKE code predictions, obtained by using the virial equation of state.

At the higher pressures, there is a noticeable difference in the theoretical (adiabatic) and experimental data. This difference is assumed to be due to heat losses to the chamber walls occurring during the combustion of the gas mixture, particularly at high pressures and corresponding high gas temperatures. (Lord [2] drew the conclusion that the heat loss to the chamber walls is small; however, this conclusion was based on his faulty computations.)

Table 6. Closed bomb experimental data for the mixture $3H_2 + O_2 + 8He$

Lord		Klingenberg	
Initial chamber pressure, P_I (MPa)	Final chamber pressure, P_F (MPa)	Initial chamber pressure, P_I (MPa)	Final chamber pressure, P_F (MPa)
27.2	182.8	6	60
27.2	198.1	6	64.5
40.8	246.6	12	131
40.8	261.9		
40.8	283.2	24	228
51.0	312.9	48	378
		48	406.6
57.8	356.3		

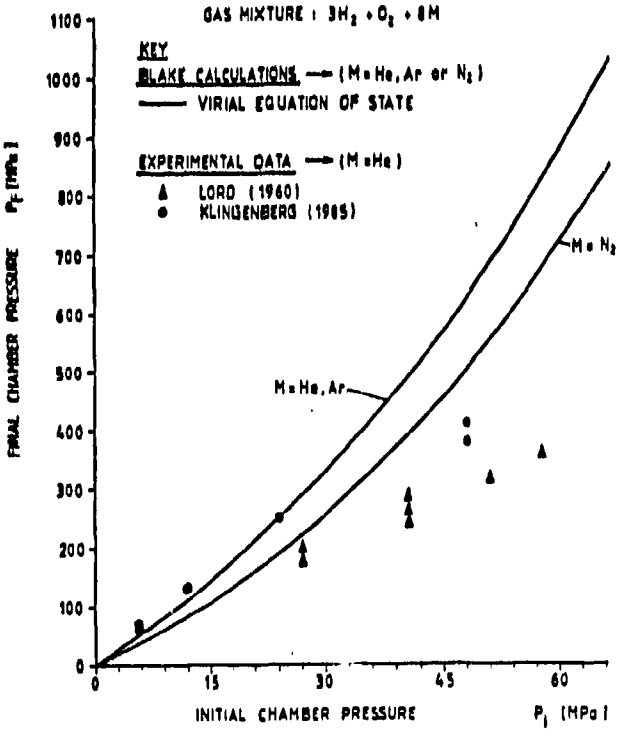

Fig. 10. Comparison of theory and experiment

4.7 Discussion

The above thermodynamic BLAKE code computations indicate that argon as well as nitrogen could be used in place of the diluent helium for the gas mixture

$$3\ H_2 + O_2 + 8\ M$$

so that we have the option to use M = helium, argon or nitrogen. However, we have presently no information whether or not a substitution in the diluent would result in a detonation. Further investigations, either experimentally or computationally, are required to answer this question. Therefore, we decided to conduct these experiments with the diluent helium (M = He) using the gas mixture investigated in references 2 and 3, i.e.,

$$3\ H_2 + O_2 + 8\ He.$$

As mentioned previously, the order of gas introduction was altered during the course of the experiments. The best results are obtained with a premixture of helium and hydrogen, added to the oxygen in the gas gun chamber. This is in accordance with the procedure used by Lord [2] and the detailed investigations of Wilkins and Carros [3].

5. EXPERIMENTAL

5.1 Test Setup

The gas gun, used in these simulator experiments, is shown schematically in Figure 11.

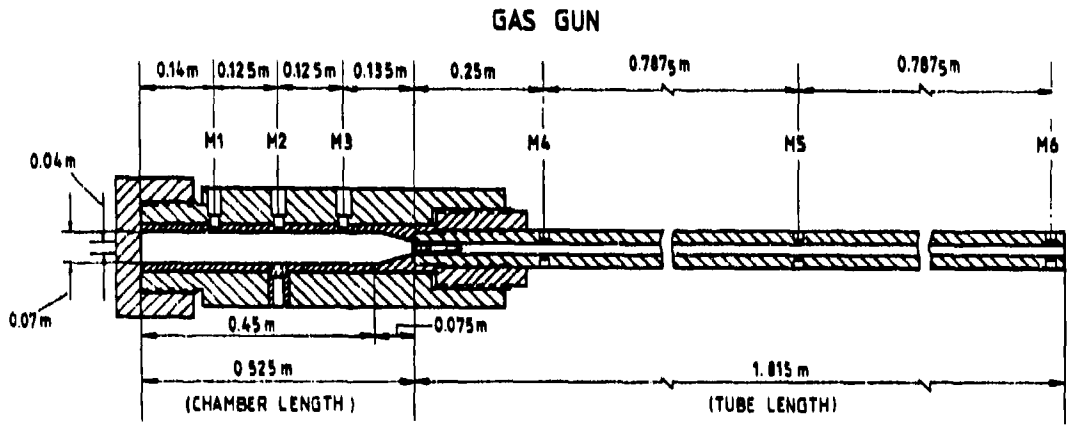

Fig. 11. Schematic of EMI-AFB gas gun simulator

Figure 11 also gives the geometry of the EMI-AFB gas gun simulator, i.e., length and diameters of both the chamber and gun tubes. Also, it shows the location of the pressure ports M 1 to M 6. Opposite to these ports are the optical windows (sapphire). The pressure port M 2 was sometimes used for temperature measurements, i.e., a temperature gauge designed by Klingenberg at EMI-AFB [12,32-36] was screwed into the measurement port at location M 2.

Since both the interior and the gun muzzle flows are investigated, Figure 12 also shows the test setup in the vicinity of the muzzle of the gas gun to study gun muzzle flash. In addition, a time-integrated open shutter photography or still picture of the muzzle flash, generated during the gas gun firing, is superimposed on the schematic drawing of Figure 12, in order to give an example of the extension of this flash. (The box seen at the far right of the picture is filled with sand to catch the projectile.)

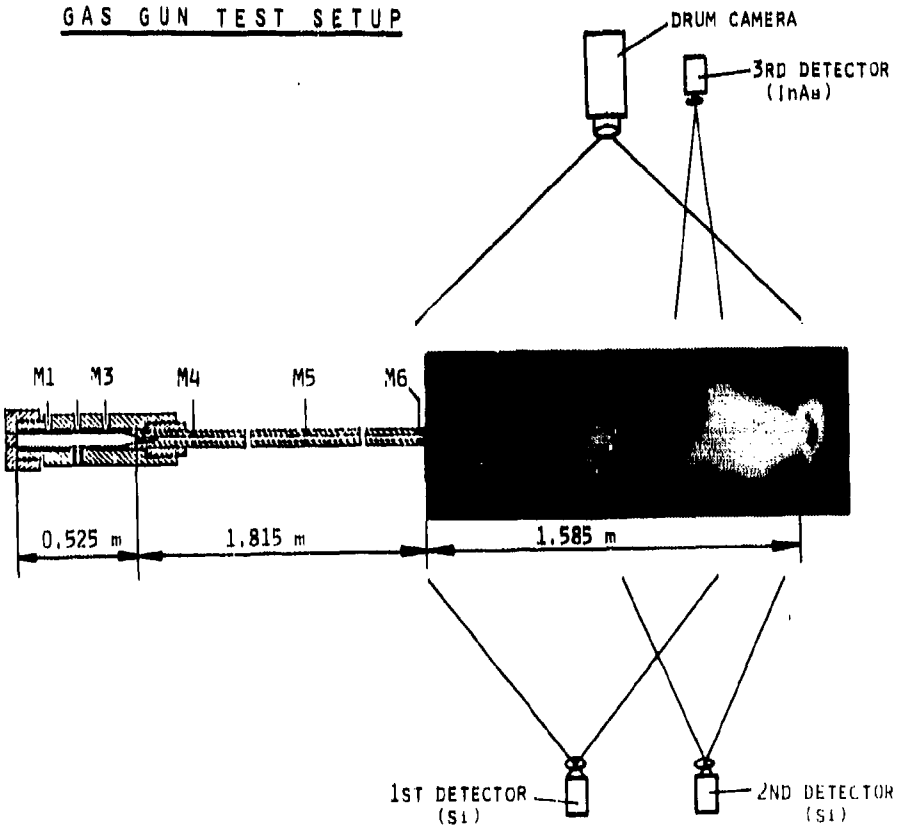

Fig. 12. Schematic of muzzle test setup with still picture of gun muzzle flash

The muzzle flash, generated by the discharge of the gas gun simulator, is investigated by using the

- open shutter camera (time-integrated photographs)
- drum camera (time-resolved photographs)
- visible light Si-detectors
- infrared InAs detector

The drum camera and the projectile catcher can also be seen in the photograph of Figure 13. This picture was selected because the gas gun muzzle flash illuminates the test room and the diagnostics.

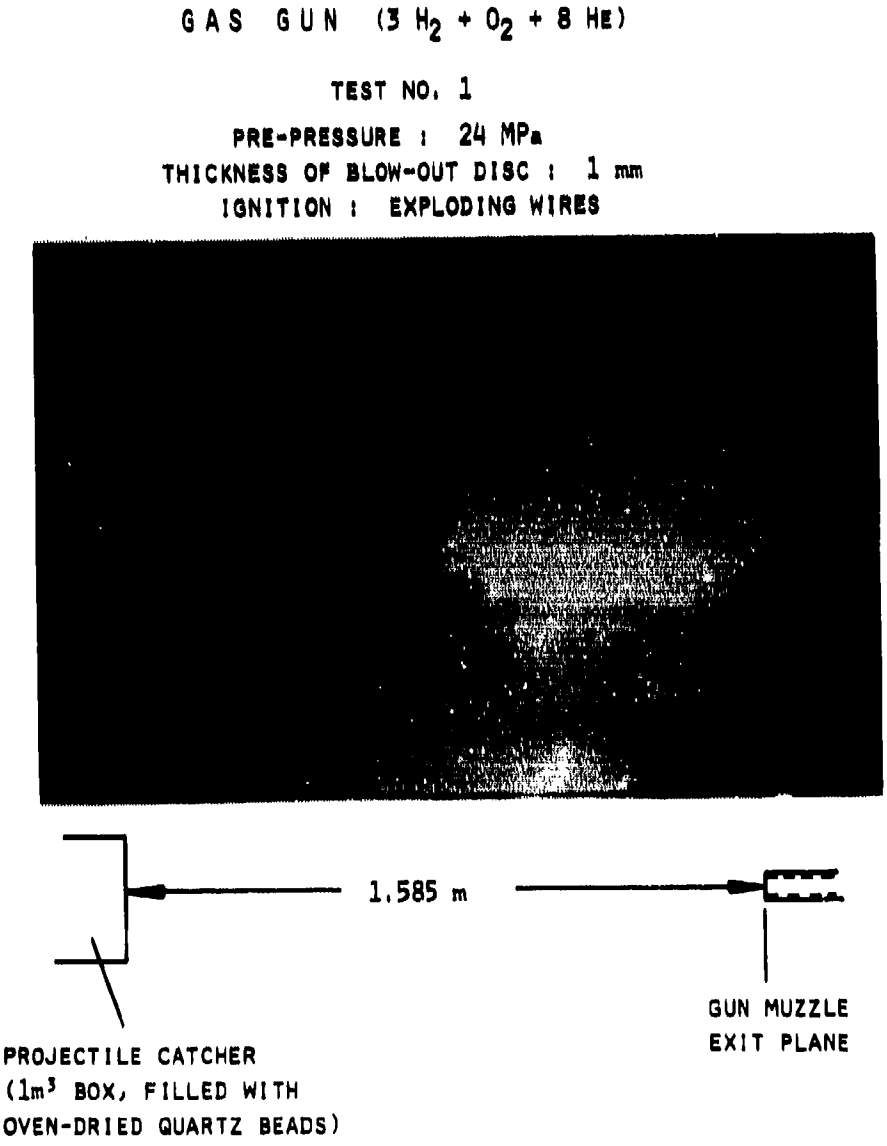

Fig. 13. Gas gun muzzle flash illuminating the test room and the diagnostics

The time-integrated, open-shutter camera photographs or still pictures of the gas gun muzzle flash were taken at pre-pressures of 12 MPa (Figure 12) and 24 MPa (Figure 13), respectively. At these two muzzle pressures, the muzzle exit conditions, expressed in terms of the gas gun muzzle exit pressure, p_e, are about two times as high for the case of p_I = 24 MPa than for p_I = 12 MPa and the intensity in the blast and flash phenomena increase accordingly. The above flash photographs confirm that gun muzzle flash is indeed generated by the combustion of hydrogen with oxygen in the gas gun chamber. Thus, it is shown for the first time that hydrogen/oxygen reactions alone can lead to muzzle flash.

The muzzle flash of Figure 13 illuminates not only the drum camera in the upper right part of the picture, but also the projectile catcher box. Here, this catcher box is located at an axial distance from the muzzle of x = 1.585 m limiting a possible further extension of the flash. The box has a volume of about 1 m^3 and contains oven-dried quartz beads. The quartz sand decelerates and stops approximately 200 projectiles of caliber 20 mm until it is used up and the box needs a refill.

5.2 Ignition Techniques

In Section 3.1, we have described the exploding wire technique and shown that four equally spaced electrodes are used for ignition, see Figure 2. The exploding wire technique resulted in reliable ignition of the gas mixture $3H_2 + O_2 + 8He$. However, it produces a rather undefined mixture of particles of various sizes into the flow. This makes it difficult to conduct well-controlled two-phase (gas/solid) flow experiments, wherein particles have to be seeded into the flow. Also, with the exploding wire technique, the reactions in the gas gun tend to go over to detonation, if the spatial energy release of the exploding wire occurs in an unexpected fashion, as, for example, at one end of the electrical wires. This may happen when a malfunction occurs in the ignition device.

To achieve "soft" ignition of the $3H_2 + O_2 + 8He$ gas mixture, the electrical heating of a tungsten wire of 0.35 mm diameter (hot wire technique) also was tested. In this technique, the single tungsten wire was placed axially into the gas gun chamber, see Figure 14.

The tungsten wire was activated by discharging a capacitor bank across the wire. The corresponding voltage pulses and current pulses were measured, and are shown in Figure 15 and 16, respectively. The maximum voltage measured for the electrical discharge is about U = 2200 Volts. The maximum current is approximately 3900 Ampères. With this pulse we obtained satis-

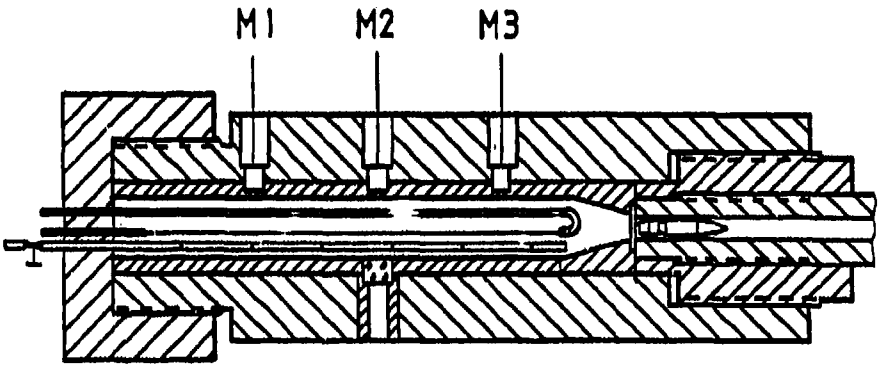

Fig. 14. Schematic of gas gun chamber with tungsten wire igniter

factory ignition. The U vs. t and I vs. t curves permit the evaluation of the power, P, and the electrical energy, E, applied across the tungsten wire. The data are given in Figures 17 and 18.

The maximum electrical energy measured amounts to about 70 Joules, see Figure 18. This is approximately the same level of energy, determined at the igniter exit of a pyrotechnic device when igniting a charge of solid gun propellants in a conventional 20-mm gun chamber [33,34].

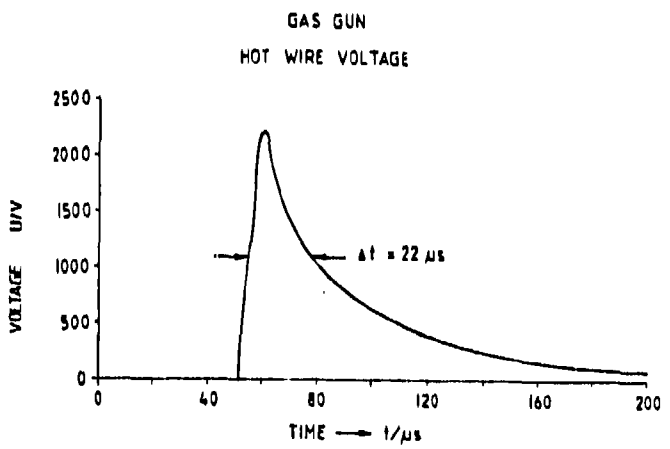

Fig. 15. Voltage versus time across the tungsten wire

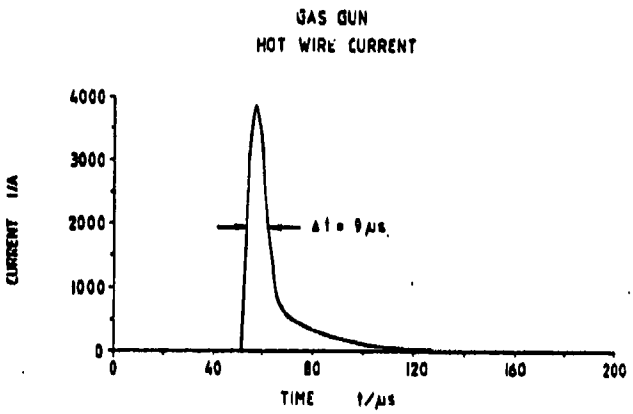

Fig. 16. Current versus time across the tungsten wire

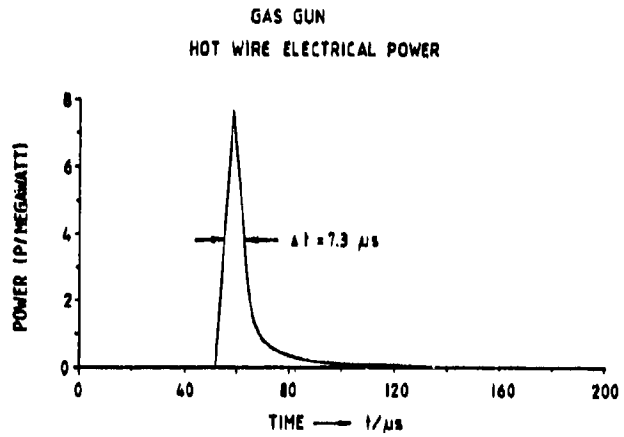

Fig. 17. Power versus time across the tungsten wire

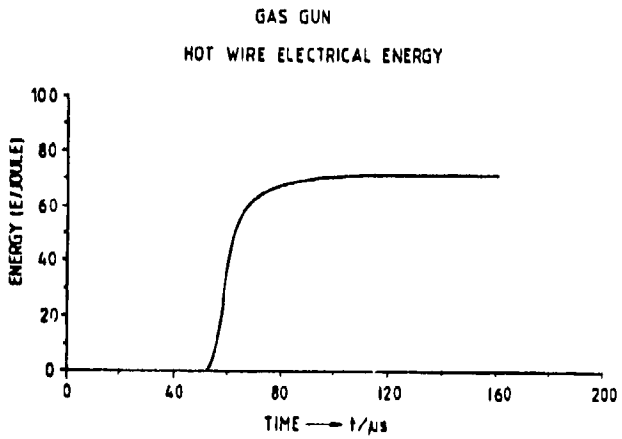

Fig. 18. Electrical energy versus time across the tungsten wire

As mentioned above, the ignition pulse applied across the tungsten wire, i.e., the hot wire igniter, yielded reliable ignition of the $3H_2 + O_2 + 8He$ gas mixture in the gun chamber. The wire was re-usable for several firings and showed no significant damage.

5.3 Test Conditions

It has been pointed out in Section 2 that we used the $3H_2 + O_2 + 8He$ gas mixture at various charge pressures, p_I. Also, it was mentioned that both the exploding wire and the hot wire technique were used to initiate the gas mixture in the gun chamber. That the order of gas introduction was changed in the course of these experiments has been also reported.

The order of gas introduction which started with the pre-pressurized oxygen, followed by helium and then by hydrogen resulted in severe pressure oscillations and - in two cases - even in detonation, in accordance with the findings of Wilkins and Carros [3]. Therefore, we altered the order of gas introduction by using commercial premixed helium/hydrogen gases. The subsequent Table 7 summarizes the test conditions used in these experiments. The results will be presented in Section 8.

Table 7: Experimental conditions
(Gas propellant mixture: $3H_2 + O_2 + 8He$)

Data in Section	Stage of Gas Gun Used	Ignition by	Order of Gas Combustion	Remarks
8.1	First Stage (Closed Bomb Mode)	Exploding Wires	Oxygen, Helium, Hydrogen	Complete combustion (Possibility of detonation)
8.2	Second Stage (Gun Configuration with 20-mm gun tube and projectile)	Exploding Wires	Oxygen, Helium, Hydrogen	Possibility of detonation, otherwise oscillations (combustion instabilities)
8.3 8.4		Exploding Wires	Oxygen, Premixture of Helium/ Hydrogen	Smooth combustion (Possibility of ignition delay)
8.5		Hot Tungsten Wire	Oxygen, Premixture of Helium/ Hydrogen	Smooth ignition and combustion

However, prior to description of the gas gun results, the new spectroscopic methods applied first in actual gun firings are described in some detail and sample results of these testings are presented in the subsequent Sections 6 and 7.

6. LASER-DOPPLER VELOCIMETRY

With the advent of modern laser based velocimeters, the velocity probing of gun muzzle flows improved significantly [37]. Compared to other laser-Doppler techniques, the Michelson laser-Doppler spectrometer, devised by Smeets and George [38, 39], gave the best results. In this technique, a phase-stabilized Michelson interferometer is used as a sensitive spectrometer. When light is scattered and Doppler-shifted by a cloud of flow-borne particles that pass through the test volume, a continuous signal, proportional to the wavelength changes of the light, is generated. The response is measured in microseconds. Thus, a near real-time velocity signal of the motion of particles is obtained. Due to the relatively high signal generation efficiency, this method is well-suited for velocity measurements in particle-laden flows of high opacity. A more detailed description and the presentation of sample results follows.

6.1 Apparatus

A schematic diagram of the experimental system is shown in Figure 19. The laser is focused into the flow and illuminates the test volume. The scattered and Doppler-shifted monochromatic radiation is then refocused and introduced into a fiber optic cable that delivers the signal to the Michelson spectrometer. It is linearly polarized, and traverses through the Pockels cell and the beam splitter tube. The beam splitter divides the signal into two beams of equal intensity that are polarized linearly parallel and vertical to the plane of the Michelson interferometer. These two beams pass through the two legs of the interferometer. The glass block in one of the legs produces an optical path difference which accounts for the wavelength sensitivity. Then the two beams are recombined and pass through a second beam-splitter cube, turned 45° with respect to the first beam-splitter cube. Thus, both the beams that arrive at the photomultiplier (PM) have complementary interferences. The interferometer is adjusted to infinite fringe spacing so that the photocathodes of the photomultipliers are uniformly irradiated. The radiant fluxes of the two exiting beams, Π_1 and Π_2, are given by [37,38]:

$$\Pi_1 = \Pi_0 \cos^2 [\pi \Delta \ell / \lambda]$$
$$\Pi_2 = \Pi_0 \sin^2 [\pi \Delta \ell / \lambda] \qquad (7)$$

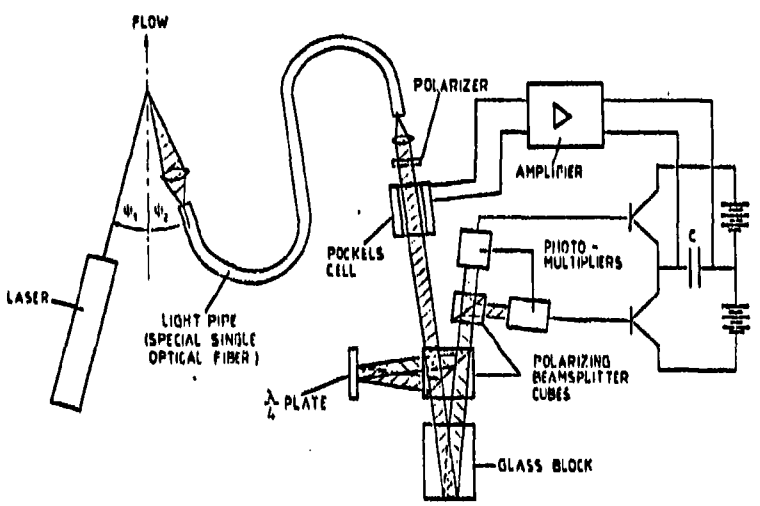

Fig. 19. Schematic of the Diehl laser-Doppler velocimeter (type ISL)

where $\Delta\ell$ denotes the optical path difference between the two beams and Π_0 the incident radiant flux. For $\Delta\ell \gg \lambda$ the interference becomes sensitive to small wavelength changes so that shifts of $\Delta\lambda/\lambda = 10^{-7}$ can be resolved [38].

The two perpendicularly polarized beams which receive a large $\Delta\ell$ within the Michelson interferometer can be additionally phase-shifted in the Pockels cell. This results in a small contribution, $d\Delta\ell$, which is proportional to the applied voltage. A fast acting phase stabilization can be realized so that the ratio $\Delta\ell/\lambda$ is kept strictly constant. A wavelength change, $d\lambda$, occurring during the scattering at the moving particles is then automatically compensated by a $d\Delta\ell$ within the Pockels cell so that

$$\frac{\Delta\ell}{\lambda} = \frac{\Delta\ell_o + d\Delta\ell}{\lambda_o + d\lambda} = \text{const.} \qquad (8)$$

The Doppler shift of the scattered radiation produces rather small relative wavelength changes, i.e., $d\lambda/\lambda \ll 1$. Then equation (8) gives

$$d\Delta\ell = \frac{\Delta\ell_o}{\lambda_o}\, d\lambda \qquad (9)$$

The phase stabilization is achieved with the simple electrical circuit shown in Figure 19. The electro-optical system maintains a phase at which there are equal radiant fluxes to both of the photocathodes. Concurrently, the photo-currents are equal and both transistors pass the same current. A sudden change in the wavelength alters the phase for an instant which, according to equation (7), leads to a difference in the two radiant fluxes.

The resulting difference current in the transistor circuit causes a variation in the charge and voltage of the capacitor. The capacitor is connected with the Pockels cell through a DC amplifier. Thus the voltage, U, and the correlated optical path difference, $d\Delta\ell$, of the Pockels cell are instantly shifted until the phase is restored.

Since the Pockels cell effect is linear, the variation of the Pockels cell voltage with time, dU(t), follows proportionally the change in the optical path difference, $d\Delta\ell$, and - according to equation (9) - proportionally $d\lambda$. The recording of dU(t) yields therefore the velocity history of the particles which pass the test volume and scatter the incident monochromatic laser light, i.e.,

$$dU(t) \sim u_p(t) \tag{10}$$

where u_p denotes the particle velocity.

6.2 Limitations

In transient flow studies, high time resolution and a wide velocity range are required. Besides the time constant given by the electrical circuit, the time resolution is dependent upon the intensity of the radiant flux, Π_0, and on the size of the test volume given by the focus of the imaged laser beam. In ballistic muzzle flow studies, an overall time constant of 10 µs was realized [37]. The velocity range of the system is rather wide. Velocities of 0.1 ms^{-1} to several 1000 ms^{-1} can be measured if the apparatus is adjusted to the flow conditions [38,39].

Severe limitations are, however, encountered for highly pressurized, opaque flows with high particle concentrations due to the signal generation efficiency. If the flow volume under study emits spectral radiation of high intensity at the selected spectral wavelength of the incident test laser beam, the measurement is impeded as well, since a reasonable high intensity ratio of the scattered radiation to the emitted spectral radiation of the flow is required in order to obtain reliable velocity signals. Therefore, only limited data can be measured, for example, in the hostile environment existing inside the actual gun tube flow even if particle-poor propellants and reduced charge weights are used.

The main advantage of Smeets' system is, however, that it is capable of continuously recording particle velocities in highly transient flows that contain a large number of residual particulates of various sizes. In muzzle flows of medium

caliber gun firings, the average size distribution of flow-borne particles is of the order of $\bar{D}_m \leq 1$ µm. Measurement of the particle velocity, u_p, provides therefore a good estimate on the gas velocity, u_{GAS} [7,37].

However, due to their inertia, these particles do not follow the gas motion across steep fronts, such as the inner shock disk of gun muzzle flow fields, but experience a slower descent [37]. The resulting particle relaxation length and time was, for example, deduced from laser-Doppler velocity measurements. For example, for particles of less than 1 µm diameter, the measured relaxation time, t_R, was in the range of $0.5 < t_R < 4$ µs [7].

Since the LDA-method is a single-point non-intrusive technique, one has to combine measurements made in a number of gun firings for analysis in order to obtain information on the whole flow field. Then it is assumed that the details of the muzzle flow field are fairly reproducible. This assumption does not appear unreasonable, if conventional cased ammunition is fired. However, in reality there will be variations between each firing so that this assumption can be only a rough approximation.

6.3 Sample Results

The laser-Doppler velocimeter was first applied in the reacting muzzle flow of an actual gun, in order to

- test the newly acquired laser-Doppler velocimeter,
- control its accuracy and reproducibility in muzzle flows, for which the flow expansion had been investigated [7] so that data were available,
- validate a hypothesis on the formation and suppression of gun muzzle flash developed for actual gun firings.

The hypothesis stated that [6,7]

- shear forces at the boundary of the supersonic jet flow induce turbulence,
- the restraints due to the blast wave results in a propellant flow which promotes turbulence throughout the entire gas plume volume,
- the turbulence is such that the formation of slip surfaces just downstream from the Mach disk is hindered or that these slip surfaces are rapidly destroyed,
- in the absence of slip surfaces, oxygen from the surrounding atmosphere can be turbulently transported toward the core of the flow,

- the transport of oxygen then permits combustion processes to take place in the intermediate flash region,
- as a consequence, the heat released by these combustion reactions adds to the shock heating to raise the temperature in the intermediate flash region so that the ignition temperature for initiating the secondary flash is attained,
- alkali salts as flash suppressants affect these "intermediate" combustion reactions,
- then the secondary flash is partially or completely suppressed.

Crucial to the hypothesis is the entrainment of oxygen from the air towards the center of the intermediate flash region. This requires the absence of slip surfaces.

In order to examine the presence or absence of slip surfaces, the laser-Doppler velocimetry method is used to measure gas velocity just downstream from the inner shock disk (Mach disk) and lateral to the main flow direction. These measurements provide the basic velocity data which can show whether or not slip surfaces are formed. An argon-ion laser radiating 1 W of power at 514.5 nm was used in the laser-Doppler velocimeter setup. The standard DM 41 ammunition was fired with a 7.62-mm gun in the velocity measurements. The ammunition DM 41 consists of a 9.45 g projectile and 2.96 g K 503 propellant with 0.8 % KNO_3 and 0.2 % Na_2SO_4 as chemical flash suppressants. The addition of these salts results in a partial suppression of the secondary flash [7].

As a sample result of these measurements [10,11], Figure 20 shows the data taken downstream from the highly underexpanded jet flow region versus the lateral distance from the flow axis, y(mm). The lateral distance is measured from the gun axis. The average of at least three measurements is shown. The "error" bars portray the maximum and minimum velocity values observed; i.e., they are not true error bars but rather a measure of the reproducibility of the data obtained from several firings. The dashed lines connecting the average velocity values are solely to aid the eye.

Figure 20 shows the lateral velocity profiles obtained downstream from the inner shock disk in the main propellant gas flow of the 7.62-mm rifle, i.e., at an axial distance from the muzzle of x = 110 mm. The distances from the inner shock disk (Mach disk) were determined from the distance of the laser focus volume measured from the muzzle of the rifle, and the inner shock disk location obtained from shadowgraphs. For distances

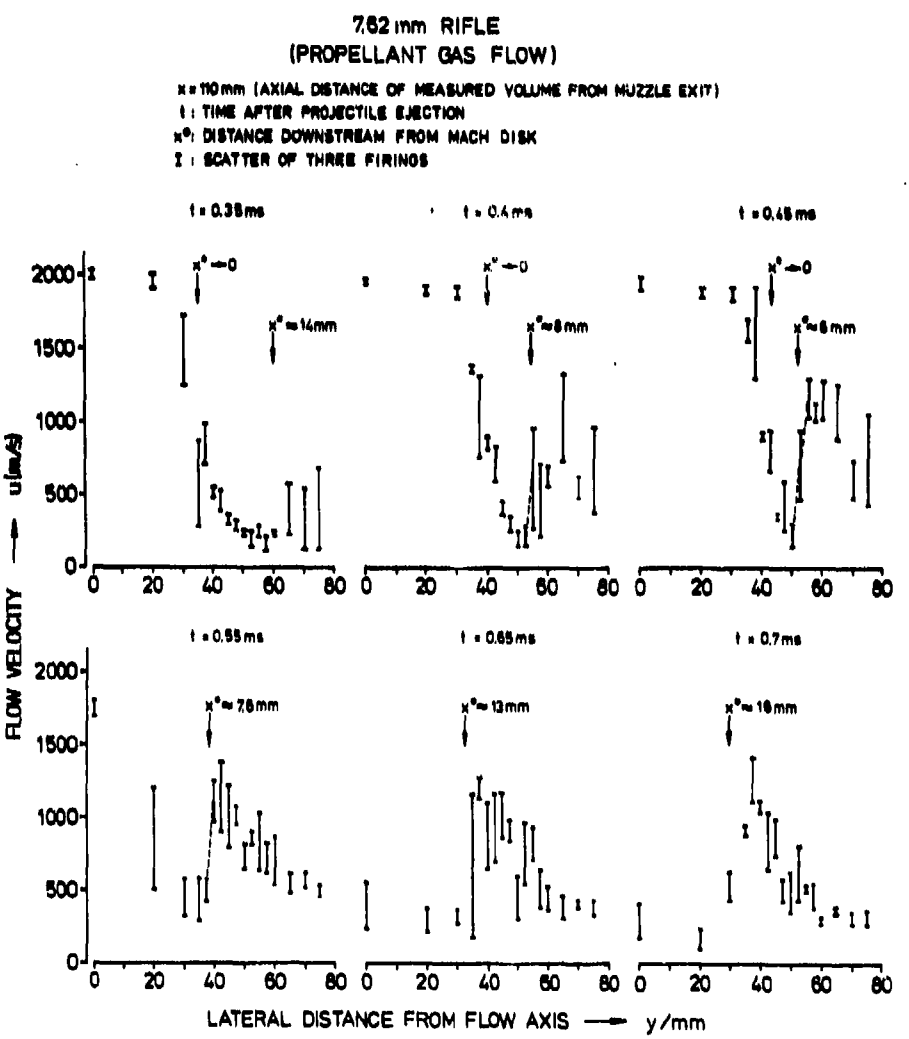

Fig. 20. Lateral velocity profiles obtained in the main propellant gas flow of the 7.62-mm rifle at an axial distance from the muzzle of x = 110 mm and times t = 0.35 to t = 0.7 ms after projectile emergence. (Selected distances x* downstream from the inner shock disk range from x* = 6 mm to x* = 16 mm.)

downstream from the inner shock disk (Mach disk) of the main propellant gas flow, i.e., for $x^* \leq 8$ mm, we observe that a steep gradient occurs between lateral distances of $30\ \text{mm} \leq y < 40$ mm. This behaviour is attributed to the formation of slip surfaces [40]. However, for $x^* > 8$ mm, no steep gradient is observed. Instead we find a smooth transition in velocity from the centerline outward. We conclude that at least for $x^* > 8$ mm slip surfaces are no longer present. This is confirmed in further results of velocity measurements, published in Refs. [10], [11], and [40]. Thus, slip surfaces in the reacting main propellant

gas flow are indeed hindered by, or rapidly destroyed by, the turbulent flow; i.e., they are absent at some relatively small distance downstream from the inner shock disk. These results were anticipated, since similar experiments in the precursor flow of the 7.62-mm rifle produced such results [40].

Photographs of the effluent as well as pressure, temperature, and flow velocity measurements in a 7.62-mm rifle [7] and in a 20-mm cannon [37] have shown remarkable similarities and strongly suggest that the development of the basic flow field of these systems would also describe the behavior of larger caliber guns [6]. Thus, we expect that the above findings can be applied to larger caliber gun systems; i.e., for all conventional guns, oxygen is transported toward the core of the flow just downstream from the Mach disk, if the gun is discharged into ambient air. Note, however, that the extension of the flow field depends upon the muzzle exit gas properties [7].

7. OPTICAL SPECTROSCOPY

Non-intrusive spectroscopic techniques have been used to measure local temperature histories in radiating muzzle flows. Methods based on the measurement of the emission and absorption along given optical paths through the flow were preferred to other popular spectroscopic techniques, such as CARS, Raman and laser-induced fluorescence, since emission-absorption methods are particularly well-suited for probing particle-laden opaque muzzle flows. The main advantage of the emission-absorption spectroscopy over other diagnostics is that it provides much higher signal levels. Reversal methods have been used to measure local temperature histories in both the intermediate and secondary flashes. The main difficulty with this technique is its inability to provide spatially resolved measurements. Abel inversion of measurements along parallel lines-of-sight at different lateral distances from the center of the field are necessary to provide information at any point in a flow field. However, this technique is limited to flow fields with suitable axisymmetric properties. The Abel inversion was therefore used to measure cross-sectional temperature data in both the primary and intermediate flashes. However, the assumption of axisymmetry is only a rough approximation particularly for the intermediate flash region [7]. The background and basis of optical spectroscopy for measuring gas temperature in radiating flows is given in Appendix I. Also, there the spectroscopic measurement methods are described in detail. Here we present briefly the essential methods and some sample results.

7.1 Modified Reversal Method

In the reversal method one assumes that temperature variations that occur during the time interval, Δt, determined by the chopper frequency are small enough to be negligible.

For example, Figure 21 shows a setup used for the measurement of temperatures by reversal in the primary flashes of simulator and - for comparison - of the 7.62-mm and 20-mm guns. In this technique, the radiation flux of a laser source (background source) is chopped by means of an acoustic-optic coupler and then passes the event. Two different laser sources, i.e., an argon laser emitting at $\lambda = 514.5$ nm and the near infrared radiation at $\lambda = 1.06$ µm of a Nd:YAG laser, were employed as background sources. The laser beam was scattered at a diffuser forming a point-line background source. To reduce errors, the

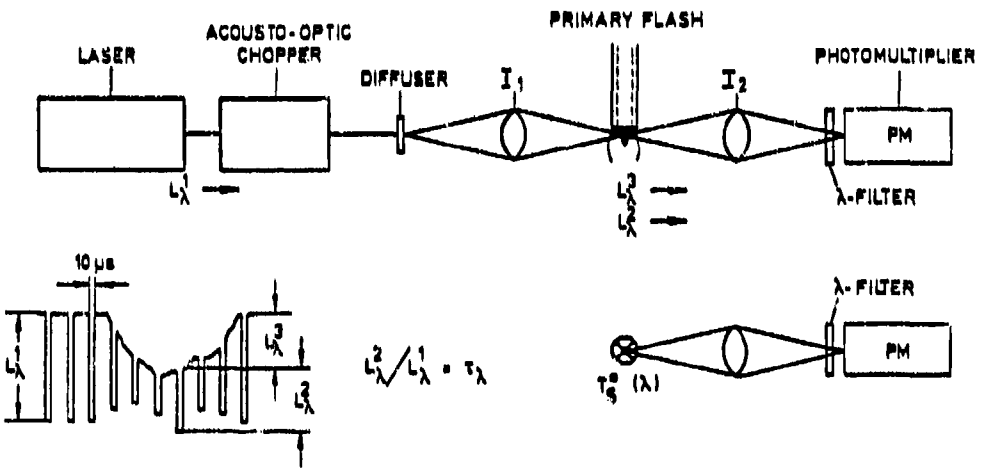

Fig. 21. Setup for reversal measurements (with the chopped radiation flux of the background source)

measurements of the spectral radiances, L_λ^1, L_λ^2, and L_λ^3, are made along identical paths. Therefore, the point source was focused into the event and then onto the photomultiplier by two lens systems, I_1 and I_2, which have the same focal length and aperture. The signal wave train is also shown in Figure 21. The spectral radiance of the laser source, L_λ^1, is measured before the flow commences and gives, together with the traversed portion L_λ^2, the transmittance, τ_λ, along the given optical path:

$$L_\lambda^2 / L_\lambda^1 = \tau_\lambda \qquad (11)$$

We obtain the reversal temperature, T, from (see Appendix I)

$$\frac{1}{T} = \frac{1}{T_S(\lambda)} - \frac{\lambda}{c_2} \ln \tau_\lambda \qquad (12)$$

However, in this technique, an appropriate calibration is required. Therefore, a calibration source is put at the location of the event. Then, the spectral radiance of the calibration source, L^*_λ, at a given brightness temperature, $T^*_S(\lambda)$, is related to the measured intensities of the photomultiplier signals, Figure 21. Thus, a relationship between L^1_λ, L^2_λ, and L^3_λ versus L^*_λ and T^*_S is obtained.

As a sample result of such measurements, Figure 22 presents the temperature measured in the primary flashes.

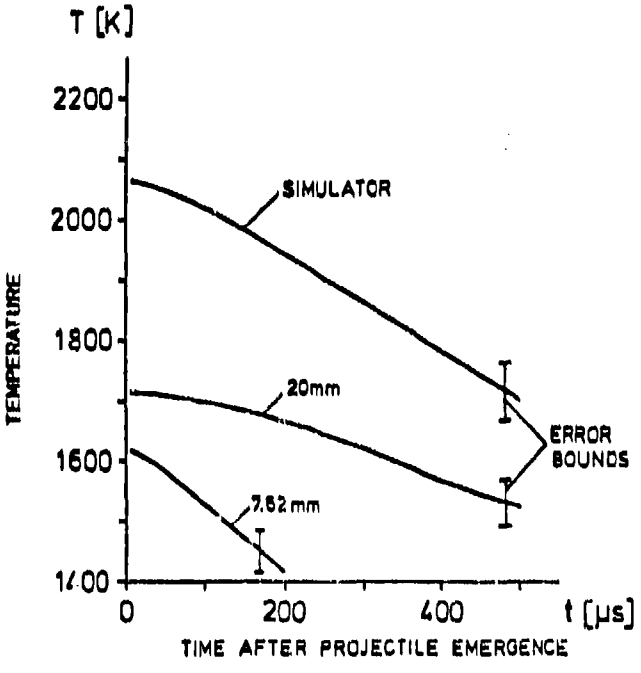

Fig. 22. Temperature versus time t measured in the primary flashes by reversal methods

The error bounds are also indicated in Figure 22. The evaluated temperatures in these experiments are considered to have an overall accuracy of about ± 50 K. It is pointed out that in the primary flash no measurable variations in the reversal temperatures at different wavelengths were obtained. Obviously, local thermal equilibrium prevails in the high-pressure area of these primary flashes.

In the intermediate flash region, however, the flow conditions are more complex. In the potassium line reversal we

measure higher temperatures than in the measurements performed at other wavelengths, if the alkali salt participates in the chemical flash suppression reaction. This behavior was anticipated, since similar experiments in the intermediate flash of the 7.62-mm rifle produced such results [7,41]. The maximum gas temperature measured in the intermediate flash of the gas gun simulator was of the order of 2100 K. Comparatively, the 20-mm gun intermediate flash has a maximum gas temperature of about 1700 K [37].

7.2 Abel Inversion Techniques

Also, experiments in the intermediate flash have been conducted using Abel inversion techniques. While in earlier investigations these measurements were made in a number of test firings combining the various measured side-on distributions of $L_\lambda(y)$ and $D_\lambda(y)$, this investigation used a method which permitted the acquisition of data in a single test firing. A schematic of the test setup used is shown in Figure 23.

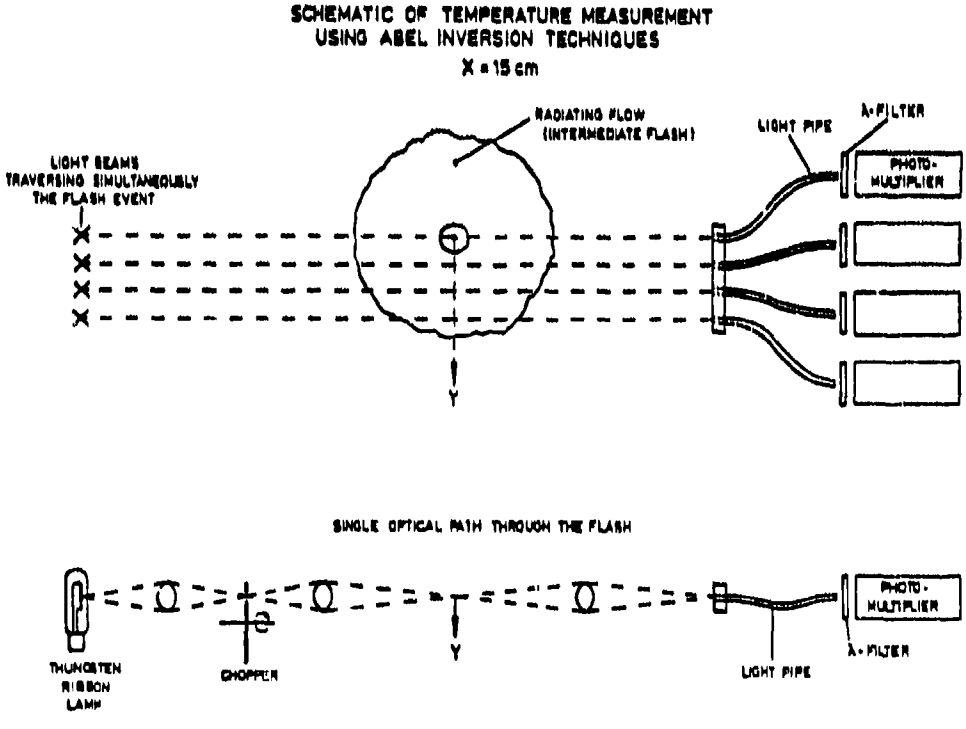

Fig. 23. Schematic of experimental setup used in the probing of the intermediate flash region

In this technique, several light beams pass simultaneously along various optical paths through a cross-section of the intermediate flash which is selected at a certain axial distance from the muzzle. A calibrated tungsten ribbon lamp is used as a background source. The light beam exiting from this lamp is chopped mechanically at 50 kHz and then divided into multiple beams by beam splitters. These multiple beams are imaged into the radiating flow and pass the cross-section under study along various optical paths with equal lateral distances y from the flow axis to the outer edge of the flow region. Then, these beams are imaged onto light pipes which transmit the signals to photomultipliers. The interference or λ-filters at the entrance sides of the photomultipliers select the desired spectral wavelength region. The photomultiplier records alternately the spectral emission and the fraction of light traversed along a given optical path, i.e., the spectral absorptance. The time interval between the emission and absorption measurements is given by the chopper frequency. Thus, the side-on distribution of both the spectral radiance, $L_\lambda(y)$, and the optical thickness, $D_\lambda(y)$, can be evaluated from the photomultiplier signals, if the same calibration procedure is applied as in the reversal method (see Appendix I). The radial distribution of temperature at the selected distance from the muzzle then is evaluated from the $L_\lambda(y)$ and $D_\lambda(y)$ using Abel inversion methods; see Appendix I.

Again, at first, we have tested this rather difficult measurement method in the intermediate flash of the 7.62-mm rifle. In these Abel inversion measurements, data in the intermediate flash of the 7.62 mm rifle were taken at an axial distance from the muzzle of x = 15 cm. The propellant used was A/S 0300. A series of tests was made, i.e.,

(a) without adding alkali salts to the propellant charge, and

(b) by adding the alkali salt $NaHCO_3$ in steps of 0.5 wt.% from 0.5 wt.% to 5 wt.% to the propellant charge.

In order to compare the results with the data obtained from the reversal measurement, the spectral data were measured at λ = 514.5 nm (continuum). The evaluated temperatures, T, were normalized to the measured gun muzzle exit temperature, T_m.

For example, Figure 24 presents the results of the Abel inversion measurements at λ = 514,5 nm and x = 15 cm in the intermediate flash of the 7.62-mm rifle when firing the propellant A/S 0300

(a) without adding alkali salts (0 %), and

(b) with 5 wt.% of $NaHCO_3$ added to the propellant charge (5 %).

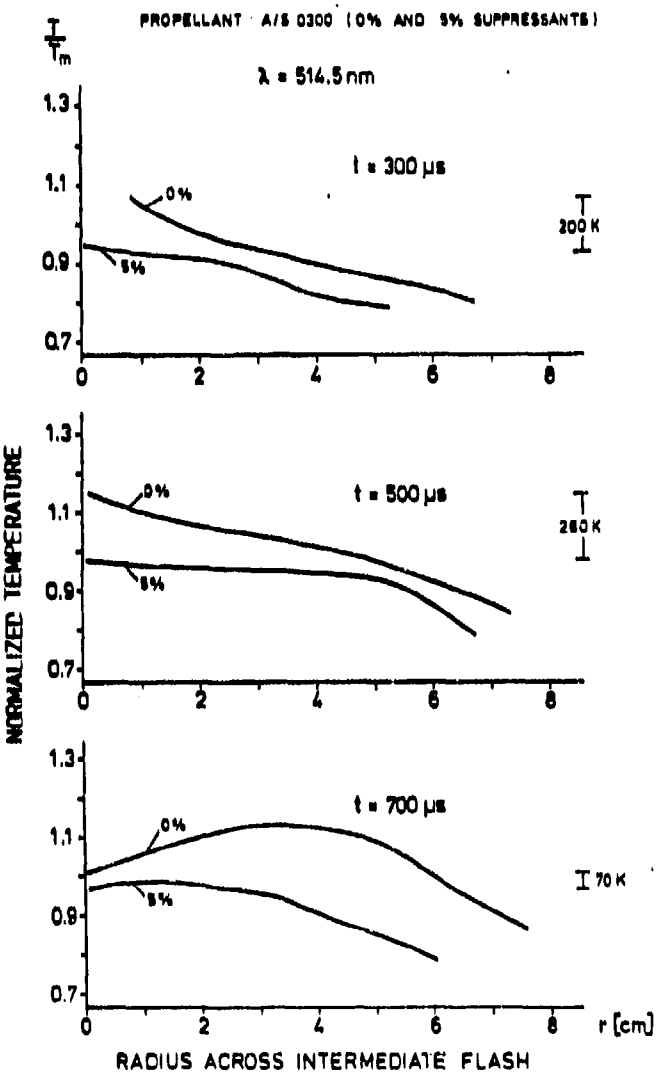

Fig. 24. Cross-sectional temperature profiles T/T_m vs. R at x = 15 cm obtained by Abel inversion measurements at λ = 514.5 nm in the intermediate flash of the 7.62-mm rifle when firing the propellant A/S 0300 (T_m = muzzle exit gas temperature; R: radial coordinate)

(a) without adding alkali salts (0 %),
(b) with 5 wt.% of $NaHCO_3$ (5 %) added to the propellant

The T/T_m versus R profile at times t = 300 μs, 500 μs, and 700 μs after projectile emergence show that the addition of 5 wt.% of $NaHCO_3$ to the propellant charge reduces significantly

the temperature in the intermediate flash region. At t = 300 μs and for a radial distance from the main flow axis of R = 1 cm, this temperature decrease is of the order of ΔT = 200 K. At t = 500 μs and for R = 0 (flow axis), the temperature decrease is ΔT = 260 K while for t = 700 μs it is only ΔT = 70 K. However, at t = 700 μs, the temperature decrease at some distance from the main flow axis is much greater than 70 K reaching its maximum at about R = 5 cm with ΔT = 280 K. At this time, the onset of the unsuppressed secondary flash raises the temperature in the 0 %-T/T_m vs. R curve so that T/T_m vs. R increases with R up to about R = 4 cm; see Figure 24.

7.3 Effect of Alkali Salts as Flash Suppressants

The tests in the 7.62-mm gun are compared to each other to control whether or not the spectroscopic techniques for measuring temperature, i.e., the reversal method and the Abel inversion, yield comparable temperature results, when alkali salts are added to the propellant charge for suppressing secondary muzzle flash. Figure 25 shows the results obtained in the intermediate flash of the 7.62-mm rifle by using the reversal method and the Abel inversion technique. The effect of alkali salts as flash suppressant is evident. Here, the percentage of KNO_3 as flash suppressant was increased in steps of 0.5 wt.% from 0 % to 5 wt.%. The data clearly show that the temperatures in the intermediate flash decrease as the percentage of alkali salts increases. The continuous reversal data represent a mean of maximum temperatures measured at various wavelengths. The Abel inversion data were taken in the flow axis (R = 0) at λ = 514.5 nm.

Figure 25 shows that the temperature decrease is about ΔT = 180 K, if 2 wt.% of KNO_3 are added to the propellant charge. The addition of 5 wt.% of $NaHCO_3$ results in a temperature decrease at the main flow axis of ΔT = 200 K for t = 300 μs, and of ΔT = 260 K for t = 500 μs after projectile emergence, respectively.

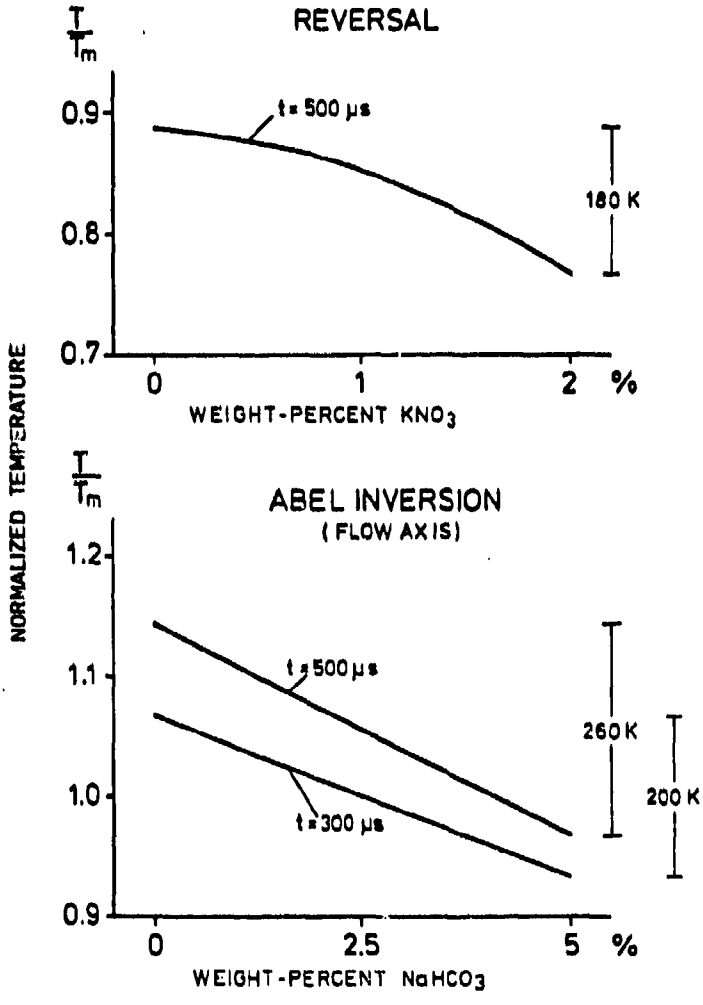

Fig. 25. T/T_m vs. wt% of added alkali salts at x = 15 cm obtained by reversal and Abel inversion measurements in the continuous radiation of the intermediate flash of the 7.62-mm rifle

7.4 Difficulties Encountered

As mentioned previously, the tests in the 7.62-mm gun and also in the gas gun simulator have shown that measurements in the spectral region of the alkali atom, involved in suppression reactions, yield much higher temperatures than measurements performed at other wavelengths.

In a series of further experiments conducted by using three different alkali salts and varying the percentage of these additives in a step-wise fashion, this behavior was

investigated. In these experiments, we increased the percentage of alkali salts in steps of 0.5 wt.% raising the percentage of

(a) KNO_3 from 0.5 wt.% to 2 wt.%

(b) K_2CO_3 from 0.5 wt.% to 5 wt.%

(c) $NaHCO_3$ from 0.5 wt.% to 10 wt.%.

Then we measured the temperature in the intermediate flash of the 7.62-mm rifle for each composition by reversal methods as well as the muzzle exit temperatures, T_m. From these investigations we found that the interacting alkali atom is indeed excited above the equilibrium temperature.

A sample result of these experiments is shown in Figure 26. It compares the data measured (a) in the Na- and K-line for the propellant K 503 which contains both the sodium and potassium salt as flash suppressant, and (b) the data measured in the continuum at wavelengths λ = 514.4 nm and 1060 nm (curves on the left). In addition, the data measured for the propellant A/S 0300 with 2 wt.% of $NaHCO_3$ as flash suppressants are shown in Figure 26. Here we compare the data obtained at the sodium

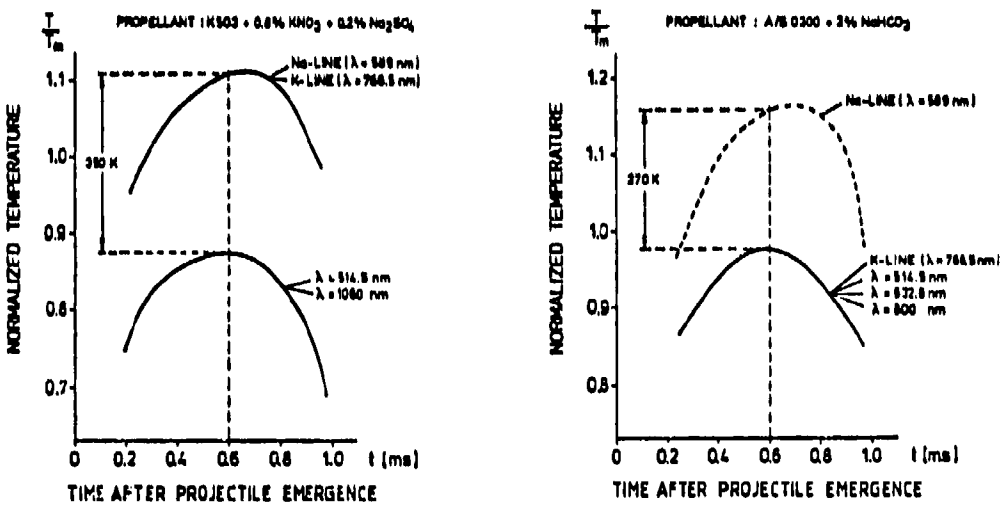

Fig. 26. T/T_m versus t at x = 15 cm obtained by reversal methods in the intermediate flash of the 7.62-mm rifle

line wavelength to the data measured at wavelengths λ = 766.5 nm (K-line), λ = 514.5 nm, 632.8 nm, and 800 nm (curves on the right). Again, the temperature is normalized by relating the data to the muzzle exit temperature, T_m. Obviously, the temperature in the intermediate flash is much higher in both the sodium and potassium line reversal measurements when these additives are present in the propellant charge than at other wave-

lengths. We conclude that temperature measurements in the resonance line wavelength of these alkali species yield at best an effective electronic excitation temperature which substantially exceeds the equilibrium gas temperature prevailing in the event. Comparatively, the temperature measured spectroscopically at other wavelengths approximates the true gas temperature that exists in the radiating gun muzzle exhaust flow.

This is confirmed by the data obtained by means of the Abel inversion technique. A sample result of these experiments is shown in Figure 27. It presents the radial or cross-sectional temperature profiles, T/T_m versus R, obtained for times t = 300 µs, 500 µs, and 700 µs, respectively, when adding 5 wt.% of $NaHCO_3$ to the propellant A/S 0300. As in the case of the

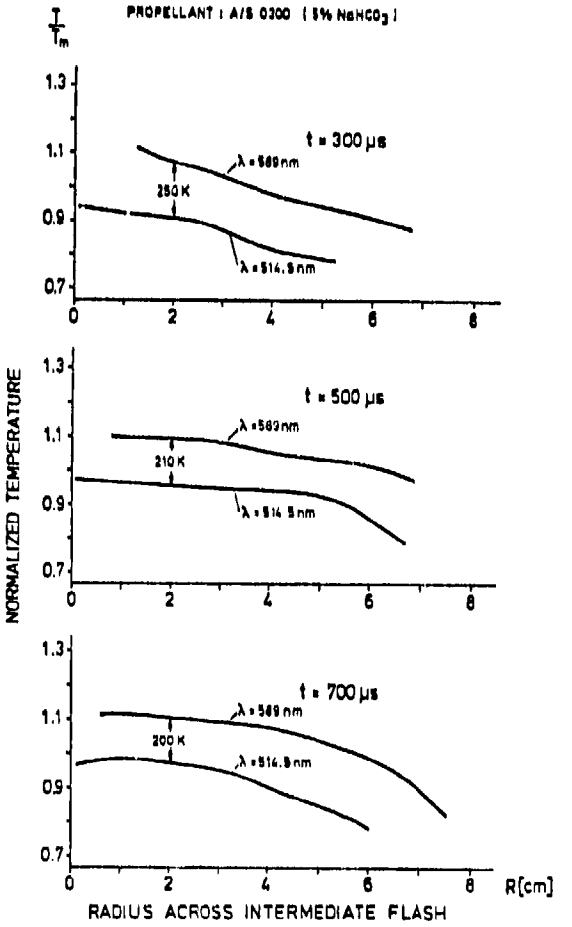

Fig. 27. Cross-sectional temperature profiles T/T_m vs. R at x = 15 cm obtained by Abel inversion measurements at λ = 589 nm and λ = 514.5 nm in the intermediate flash of the 7.62-mm rifle when firing the propellant A/S 0300 with 5 wt.% of $NaHCO_3$ added to the propellant charge

reversal measurement, a significant temperature difference was measured between the temperatures evaluated in the wavelength region of the sodium line (λ = 589 nm) and in the continuum (λ = 514.5 nm). At a radial distance from the main flow axis of R = 2 cm, this temperature difference is, for example, of the order of 250 K at t = 300 µs after projectile emergence, and it is approximately 200 K and 210 K at times t = 500 µs, and t = 700 µs, respectively.

7.5 Temperature Gauge Technique

7.5.1 Design of the Temperature Gauge

Two different types of temperature gauges have been developed and applied for intrusive temperature measurements in the combustion gases of solid and liquid gun propellants [32-36]. The first, high pressure, temperature gauge design consists of a steel tube which contains on its axis a bundle of 25 optical fibers arranged in parallel, Figure 28. The bundle of optical fibers is glued into the steel tube by epoxy. The diameter of a single fiber is 0.1 mm, and the diameter of the bundle is 0.5 mm. The surface area of the optical fiber bundle is 0.19 mm^2, and its opening angle at the end surface or flow facing side is 25°. To be able to screw the emission gauge into conventional pressure ports, both the diameter and the thread of the outer steel tube are adapted to the dimension of commercial pressure transducers, as, for example, to the dimensions of Kistler or PCB pressure gauges. The design with the bundle of 25 fibers was

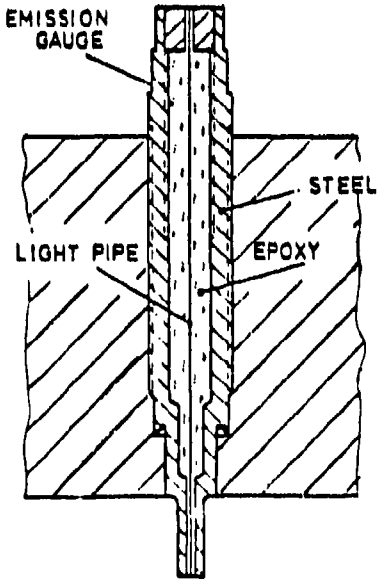

Fig. 28.
Schematic of high pressure temperature gauge (type EMI-AFB)

selected from a trial-and-error approach. The goal was to achieve an optimum transfer of radiant energy in a high pressure environment. The design shown in Figure 28 withstands a maximum gas pressure of p = 350 MPa. However, there are some limitations and constraints encountered in the application of this high pressure emission gauge. At present, the commercial optical fibers available pass only visible light and not the radiation in the near infrared portion of the spectrum. Therefore, gas temperatures evaluated from the measured spectral emission are limited to the range of T ≥ 1200 K. Also, this emission gauge does not permit a measurement of the effect of deposits at its end surface or flow facing side. Such deposits, say of soot or other condensed phase particles, can contaminate the end surface during the time of the measurement so that a change in the deduced temperature may result [32].

To overcome these difficulties, another temperature gauge has been designed. A schematic of this gauge is shown in Figure 29. In this design, a square rod with a cross-section of 6 mm^2 is glued into the steel tube by epoxy.

Fig. 29. Schematic of infrared transparent temperature gauge

The square rod of infrared (IR) transparent quartz (trade name: Infrasil) passes radiation from the visible to the IR wavelength region, i.e., to λ = 3.6 μm. Thus the measurable lower limit of the temperature is extended to about 500 K. In addition, this particular design permits a simultaneous measurement of both the emitted radiation and the effect of deposits at its end surface as a function of time. For this purpose, the upper end of the quartz rod is cut like a prism so that three surfaces are formed, the horizontal surface and two surfaces which are turned at an angle of 45° with respect to the horizontal plane, Fig. 29. Along the quartz rod, two opposite vertical surfaces are coated

with silver. The other two vertical surfaces have been roughed to improve the adhesive sealing by epoxy between the rod and the steel tube.

The effect of deposits at the end surface of the gauge then can be determined by coupling a laser beam into one of its upper end 45° surfaces. As the laser beam passes through the quartz rod, it experiences total reflection at both the coated vertical planes and at the end or flow facing surface, provided the length of the rod is adequately designed. The total reflection at the end surface is attenuated if deposits contaminate it during the measurement period. Thus, contamination at the surface of the rod can taken into account.

7.5.2 Testing

First, the setup with the infrared transparent temperature gauge is shown in Figure 30 because it has been used to control the effect of deposits while investigating the intermediate flash of an actual gun firing, i.e., the 7.62-mm rifle.

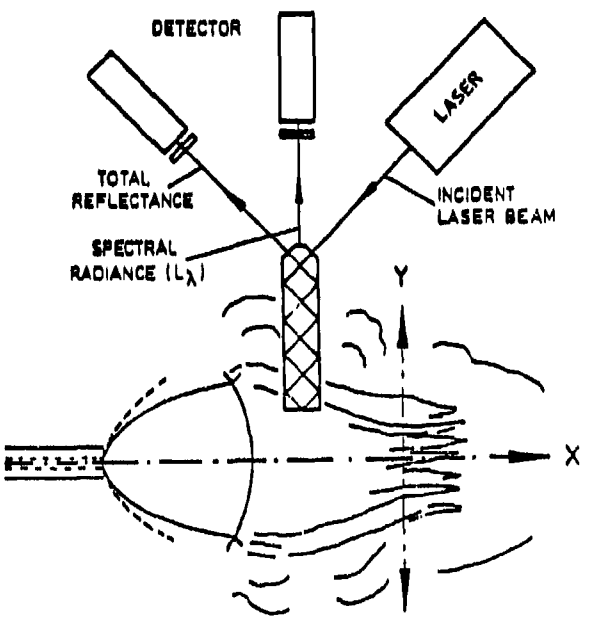

Fig. 30. Schematic of experimental setup for determining the effect of deposits in the 7.62-mm gun muzzle exhaust flow

In this technique, the monochromatic beam of a laser is sent through the 45° plane surface into the quartz rod. The laser beam passes through the quartz rod, it experiences a total reflection at both the vertical and end surfaces, and leaves the quartz rod at the second upper 45° surface, Fig. 30. Since the quartz rod functions as a light pipe, the radiance emitted by the propellant gas-particle flow is also transmitted through the gauge. Both the laser beam and the transmitted radiation then enter detectors. The detectors convert the incident radiant energy into an electrical signal. The output voltages of the detectors are proportional to the radiant energy. In order to adapt to the measurement with the previously described high pressure temperature gauge, an Argon laser beam at the spectral wavelength λ = 514.5 nm was used to determine the total reflectance.

As already mentioned, the method for measuring the time-varying effect of deposits is based on the fact that the total reflectance at the end surface of the quartz rod gauge is attenuated if the thickness of such contaminating layers increases. This is so because they reduce the transmittance, τ_λ, and the total reflectance $r_t(\lambda)$, at the end surface. In order to establish a relationship between τ_λ and $r_t(\lambda)$, a calibration procedure is required. In this calibration, the end surface of the gauge is contaminated by residual combustion products in layers of variable concentrations. Then a calibration curve τ_λ vs. $r_t(\lambda)$ is established by measuring τ_λ and $r_t(\lambda)$ as a function of the layer thickness. This calibration curve together with the measured attenuation of the laser beam allows one to quantitatively determine the effect of deposits [32].

In the probing of the 7.62-mm gun muzzle flash, however, this correction effect is very small and can be neglected. The flow expansion prevents the contamination at the end surface of the gauge due to the erasive motion of the gas flow. A significant influence of deposits was only measured at a later time after the intermediate flash has disappeared. Therefore, we believe that no corrections for deposits are required for the probing of gun muzzle exhaust flow. Thus, we can restrict our measurements to the first design of the temperature gauge; see Figure 28.

Here the measurements used two temperature gauges which were immersed in the radiating flow. With these gauges the spectral radiance at an axial distance from the muzzle of x = 15 cm and at two lateral positions y = 1 cm and y = 7 cm have been measured in the actual gun firing with the 7.62-mm rifle; see Figure 31. The light generated inside the intermediate flash is transmitted to photomultipliers. A λ-filter, i.e., an interference filter, selects the desired wavelength. Measurements were made a λ = 589 nm (Na-line) and λ = 514.5 nm in order to compare the results with data obtained by the reversal method.

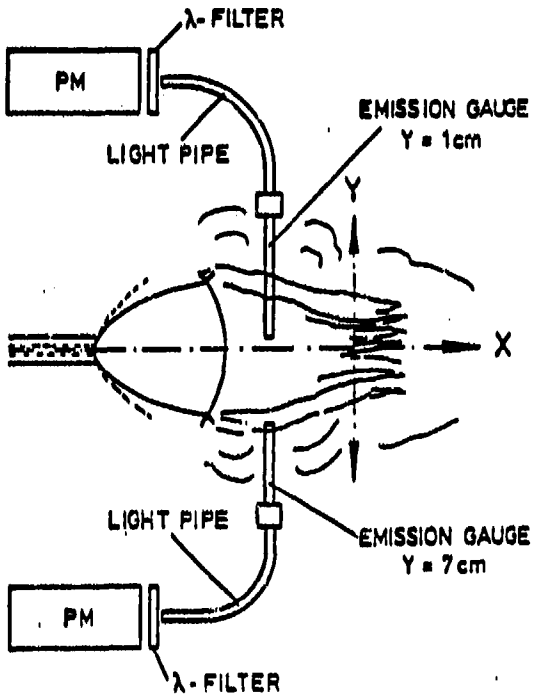

Fig. 31.
Intrusive probing of the intermediate flash of the 7.62-mm rifle by means of two high-pressure temperature gauges (design of Figure 28)

As a sample result, Figure 32 shows the temperature histories in the intermediate flash of the 7.62-mm rifle obtained with the temperature gauge technique at wavelength λ = 589 nm (sodium line) and λ = 514.5 nm (continuum) when firing the propellant A/S 0300 that contained 5 wt.% of sodium bicarbonate ($NaHCO_3$) as flash reducer. In Figure 32, the temperature gauge data are compared to the temperature histories obtained by the reversal method.

For equal wavelengths, both the temperature (emission) gauge technique and the reversal method yield approximately the same temperature history. Obviously, the brightness temperature histories $T_S(\lambda)$ vs. t, given by the temperature or emission gauge technique, approximates the temperature histories T vs. t obtained by the reversal method. Therefore, the emission gauge is applicable in the radiating gun muzzle exhaust flow. Again, there is a significant difference between the temperatures measured at the wavelength of the sodium line (λ = 589 nm) and in the continuum (λ = 514.5 nm). For λ = 589 nm, the maximum value is about 1700 K, while the continuum radiation yields approximately 1420 K, see Figure 32. Since the overall accuracy of these emission gauge measurements is estimated to be of the order of ± 5 %, the temperature difference is not due to measurement errors, but due to non-equilibrium of the alkali radiation as also measured with the other methods.

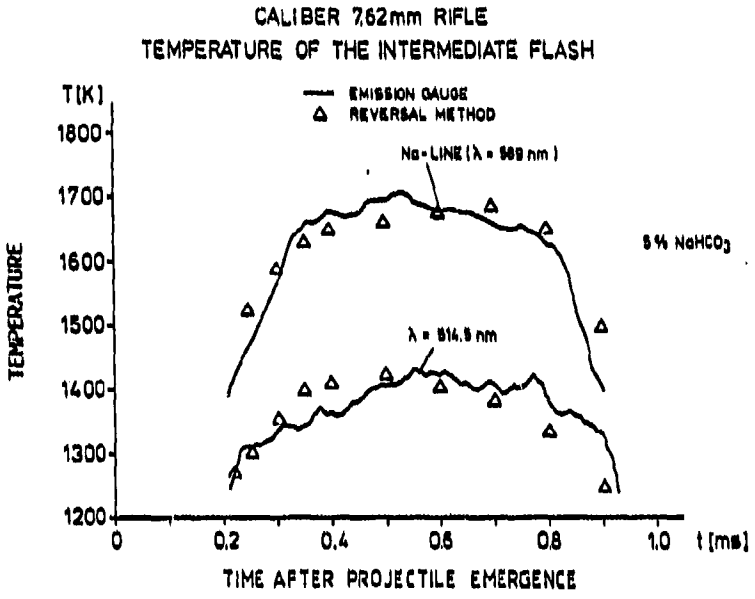

Fig. 32. Comparison of temperature histories obtained within the intermediate flash of the 7.62-mm rifle by both the temperature (emission) gauge technique and reversal method when firing the propellant A/S 0300 with 5 wt.% $NaHCO_3$ as chemical flash reducer

That reversal methods sometimes yield different temperatures in the intermediate flash of gun muzzle blast fields was already detected by Young [22] and Morton et al. [42]. They applied reversal methods in the wavelengths of the (a) sodium line (λ = 589 nm), (b) potassium line (λ = 770 nm), and (c) water band (λ = 940 nm) [42]. Different temperatures were obtained in the intermediate flashes of 0.50 caliber weapons. When the additive K_2SO_4 was added to the propellant to prevent secondary flash, the maximum temperature by potassium line reversal was 1650 K, while both the reversals at λ = 589 nm and λ = 940 nm yielded temperatures of 1510 K. According to ref.[22], the differences in temperature measurements suggest that the potassium atoms are excited above the thermal equilibrium temperature when they are involved in chemical reactions.

Recently, Mach, Werner, and Masur [43] reported on temperature measurements in the intermediate flash of the 7.62-mm rifle firing the normal DM41 round that contains the propellant K 503 with 0.8 wt.% KNO_3 and 0.2 wt.% Na_2SO_4 as chemical flash suppressant. Data were taken by reversal at λ = 589 nm (sodium line), λ = 2.7 µm (H_2O/CO_2 bands), and λ = 4.3 µm (CO_2 bands), respectively. In addition, the temperature was evaluated from the continuous

radiation of flow-borne particles by optical pyrometry. In the intermediate flash region, the reversal of the sodium line yielded much higher temperatures than the gas or particle measurements performed at the other wavelengths [43]. Thus, the excitation of alkali salts yielding temperatures which lie above the true gas temperature is confirmed by experiments.

7.5.3 Confirmation of the Hypothesis

Again, the application of the temperature gauge was tested in the actual gun firing in order to compare the results to earlier measurements. These tests included measurements performed to confirm the hypothesis on gun muzzle flash and its suppression by alkali salts [12].

To examine whether sufficient air is transported to the intermediate flash region so that the temperature is sensibly altered by combustion reactions, we changed the ambient gases from air to 100 % oxygen or to 100 % nitrogen. We then measured the temperature at two distinct locations in the intermediate flash region for these three cases. If combustion reactions significantly contribute to the temperature in the intermediate flash region, then the observed temperature will be ranked in the following order: $T(N_2) < T(air) < T(O_2)$. The specially designed intrusive temperature gauges are used to carry out these measurements.

The propellant used was A/S 0300. It is the only propellant which could be manufactured in two versions used, namely, in a charge that contained (a) no alkali salts as flash suppressant and (b) an amount of 0.5 wt.% sodium oxalate ($Na_2C_2O_4$) as chemical flash suppressant. This alkali salt has been added to the propellant during fabrication, and it suppresses completely the secondary flash. The experimental setup is shown in the schematic of Figure 33.

For surrounding atmospheres of pure nitrogen and pure oxygen, a large box was constructed. It is 1 m along the gun tube axis, 0.8 m wide, and has a volume of about 500 l. The entire box and gun tube were evacuated before filling with oxygen and nitrogen. It was found from pressure determinations that there was less than 1.3 % O_3 in the "pure" nitrogen atmospheres and less than 6 % N_2 in the "pure" oxygen atmospheres.

The axial and radial locations of the temperature gauges were somewhat arbitrarily chosen. To determine the axial locations the following information was used as a guide. Drum camera recordings of firings of the 7.62-mm rifle show that the associated intermediate flash has a spectral extent ranging from

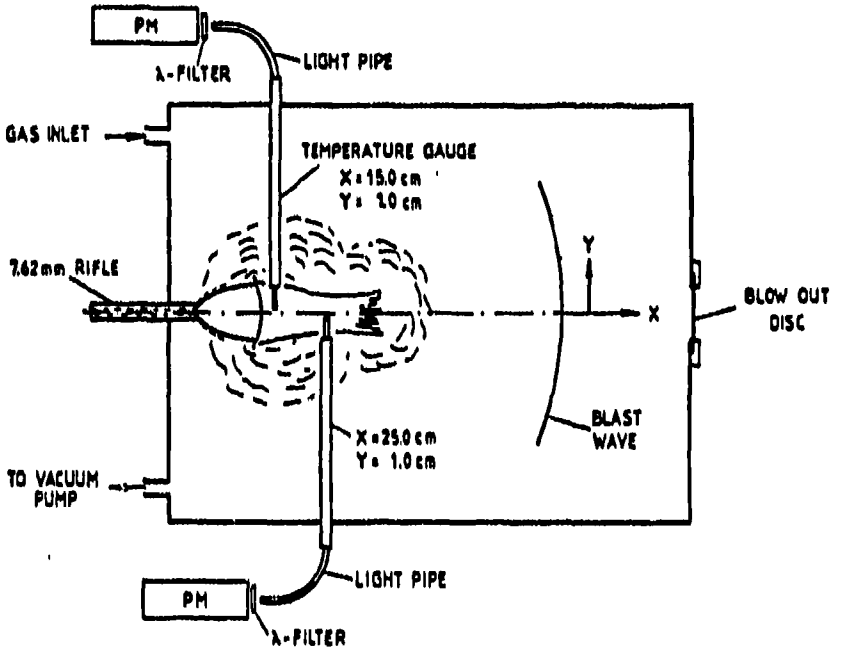

Fig. 33. Schematic of experimental setup for local temperature measurements in the propellant gas plume of the 7.62-mm rifle using two intrusive temperature gauges

about 8 cm to about 38 cm, and a temporal extent ranging from about 100 μs to about 800 μs, when the standard DM 41 ammunition is fired into air [7]. Thus, approximate "equally spaced" locations for the two gauges are at x = 15 cm and x = 25 cm.

The only constraint on the radial location is that the projectile must be allowed to pass. Here a safety factor of about y = 1 cm was used. The temperature gauge technique was employed because this technique yields more easily temperature data when compared to other methods such as the emission-absorption method or even the Abel-inversion technique.

Figure 34 shows temperature versus time plots obtained with the two temperature gauges at x = 15 cm and x = 25 cm in the propellant gas plume of the 7.62-mm rifle for A/S 0300 propellant without suppressant and with a surrounding atmosphere of air, nitrogen (N_2), and oxygen (O_2), respectively.

As before, the "error bars" are used to denote extrema in the data and are not measures of the actual error, which is of the order of ± 5 %. That is, each of these plots consists of five firings; thus the "error bars" represent the deviations, and they give an idea of the reproducibility of the data.

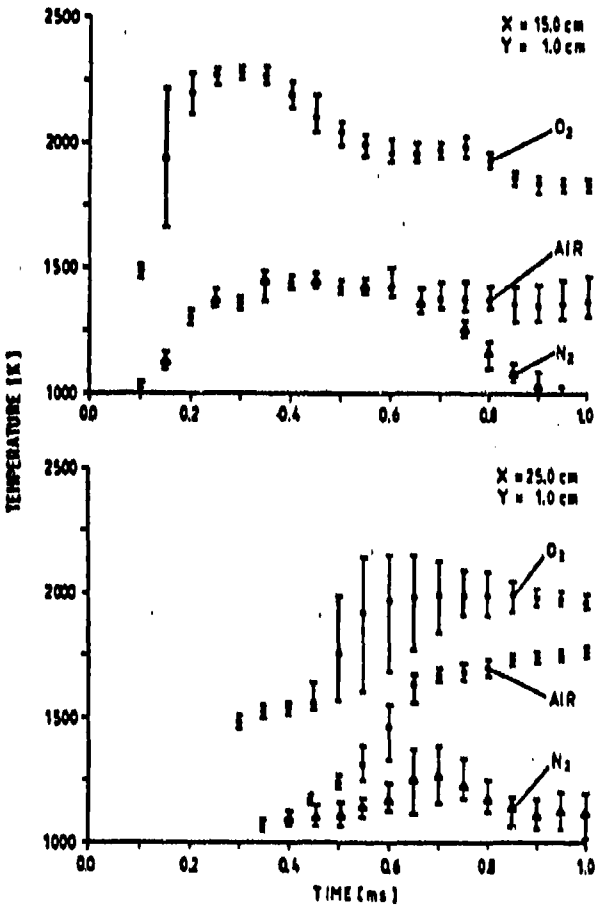

Fig. 34. Temperature versus time in the main propellant gas plume of the 7.62-mm rifle at x = 15 cm and x = 25 cm when using the propellant A/S 0300 without flash suppressants

In Figure 34, i.e., for the propellant A/S 0300 without suppressant, we see that at the earliest times the measured local temperatures in air and N_2 are the same. At times t = 0.7 ms (x = 15 cm), the temperature for discharges into air begins to depart from the temperature obtained for firings into N_2 as the surrounding gas. This is indicative that sufficient oxygen has been transported to the location denoted by (x, y) so that there is a sensible difference in these local temperatures caused by the onset of secondary combustion.

Recall that in earlier experiments with the 7.62-mm rifle it has been found that the secondary flash is observed for firings into air (and O_2), but not for firings into N_2 [7,8].

Drum camera recordings have further shown that the partially suppressed secondary flash, obtained with conventional ammunition, appears not before t = 0.8 ms [7,8].

What we are observing here is the initial process, reflected in the temperature data, leading to secondary flash. For the discharge of the rifle into ambient oxygen, so much O_2 is transported toward the inner core of the propellant gas plume downstream adjacent to the Mach disk that the temperature rise in Figure 34, i.e., for the propellant without suppressant, occurs almost immediately so that temperatures of more than 2000 K are produced locally. The same temperature rise is observed in the case of the propellant A/S 0300 with 0.5 wt.% $Na_2C_2O_4$.

Comparatively, the discharges into ambient air and nitrogen yield much lower temperatures. We could assign the temperature for firings into N_2 as due to shock heating only and the difference $T(O_2) - T(N_2)$ as due to the energy contributed by combustion reactions.

In Figure 35 the data, obtained for the propellant A/S 0300 with and without flash suppressant when firing into ambient air, are shown for comparative purposes. Those data show the effect of the flash suppressing salt. The secondary flash is completely suppressed by the addition of 0.5 wt.% $Na_2C_2O_4$ to the propellant A/S 0300, so that the local temperature decreases rapidly for times t > 0.5 ms, while high temperature develops for the propellant which contains no suppressant.

Thus, it has been confirmed by the results of these experiments that the entrainment of oxygen toward the center of the "intermediate" flow region occurs and that combustion reactions take place which affect the temperature in this flow region. Also, we have shown that the addition of 0.5 wt.% sodium oxalate as chemical flash suppressant to the propellant A/S 0300 is sufffficient nearly to suppress all the secondary flash, when the rifle is discharged into ambient air.

That the temperature of the "intermediate" flow region should control the ignition processes leading to secondary flash ought not to be so surprising, since it has already been shown that the addition of alkali salts to the propellant charge results in a decrease in temperature in the intermediate flash region. This has already led to the conclusion that the alkali salts significantly affect the chemical reactions taking place in the intermediate flash region and so prevent the ignition of the secondary flash. Thus the hypothesis has been confirmed by the results of both the velocity and temperature measurements.

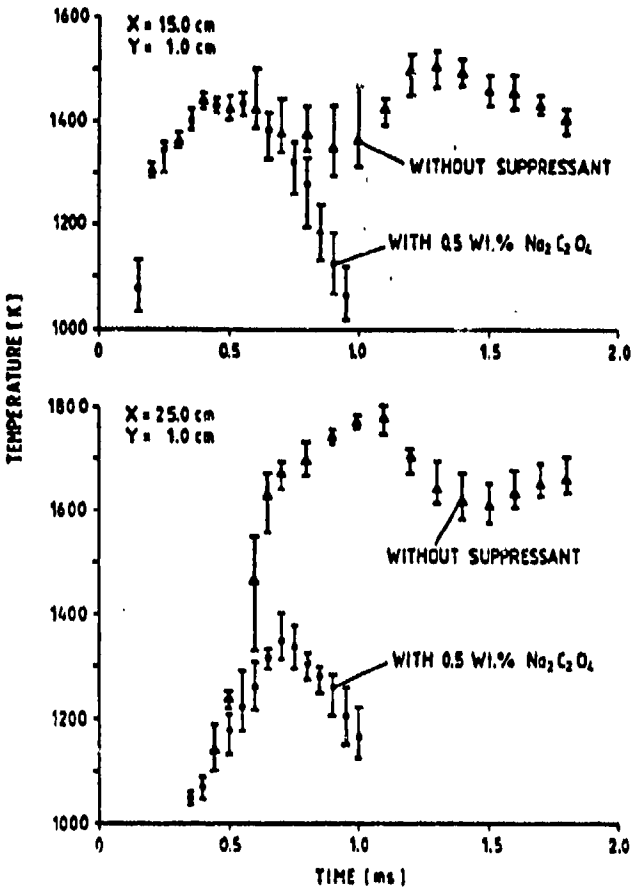

Fig. 35. Temperature versus time in the main propellant gas flow of the 7.62-mm rifle at x = 15 cm and x = 25 cm from the muzzle for the propellant A/S 0300 with and without flash suppressant, and the discharge of the rifle into air.

7.5.4 Summary of Temperature Measurements

We begin with the fact that shear forces at the boundary of the supersonic jet flow induce turbulence in the propellant gas plume developing at the muzzle of a 7.62-mm rifle and that it is promoted throughout the gas plume volume, because of the restraint by the outer blast wave. By measuring the radial velocity just downstream from the Mach disk, we have shown that the formation of slip surfaces is for the most part hindered, or rapidly destroyed by this turbulence. Once the absence of slip surfaces is established, it is possible for oxygen from the entrained air to be transported to the core of the flow in the vicinity of the Mach disk, i.e., the so-called "intermediate" flash or "intermediate" flow region. We have then employed

novel temperature (emission) gauges to measure locally the temperature downstream from the Mach disk for surrounding atmospheres of air, oxygen, and nitrogen. The comparison shows that these are sensible temperature differences with $T(O_2) > T(air) > T(N_2)$. These differences are caused by the combustion processes with the entrained oxygen.

Therefore, we conclude that the ignition sequence leading to secondary muzzle flash is governed by an ignition temperature whose value is determined by two energy sources: the well-known shock heating and the combustion reactions, discussed above.

For the conventional discharge of a gun into ambient air, these combustion reactions are affected by alkali salts so that the ignition temperature is reduced. Then the secondary flash is partially or completely suppressed.

It is pointed out that most of these data were obtained in the probing of actual gun muzzle exhaust flows. Only a few data could be measured in the flow simulated by the gas gun due to limited time. On the other hand, it was considered important to test and control the measurement techniques primarily in the actual gun firings, since in these firings we have much more data available for comparison purposes (this is also valid for the velocity measurements presented above). Nevertheless, the results obtained in the actual gun firings are very important for the fundamental understanding of the processes occurring in muzzle flashes.

8. RESULTS OF GAS GUN EXPERIMENTS

The experimental results, presented subsequently, are sample results of the simulation experiments, conducted with the FMI-AFB gas gun simulator. Here, we address primarily the simulation of gun muzzle flash. However, some data on in-bore measurements are also presented, to demonstrate that the interior as well as the transitional ballistic flows can be simulated adequately with characteristics approaching that of medium caliber gun systems. For example, a gas temperature of T = 2750 K was measured at M 2 (inside the gas gun chamber) when the final chamber pressure was 360 MPa.

8.1 Closed Bomb Data

In addition to the maximum pressure data of the closed bomb mode measurements, which have been given in Figure 10 and in Table 6 of Section 4.6, we present here two time-resolved

pressure traces taken at charge or initial loading pressures of p_I = 12 MPa and p_I = 48 MPa, see Figures 36 and 37.

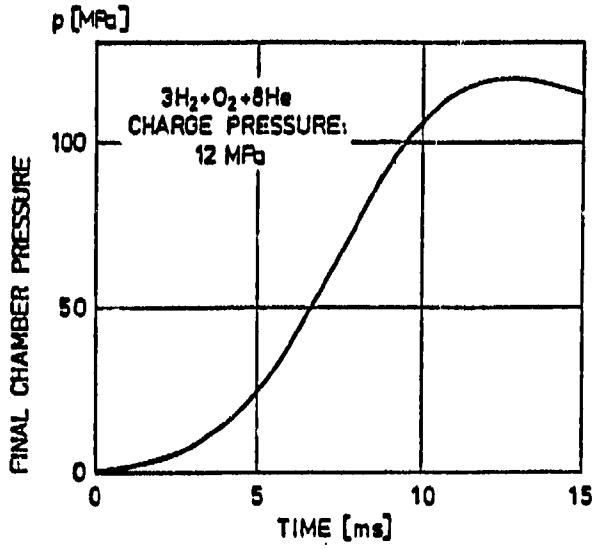

Fig. 36. Final chamber pressure versus time (Charge pressure p_I = 12 MPa; closed bomb mode)

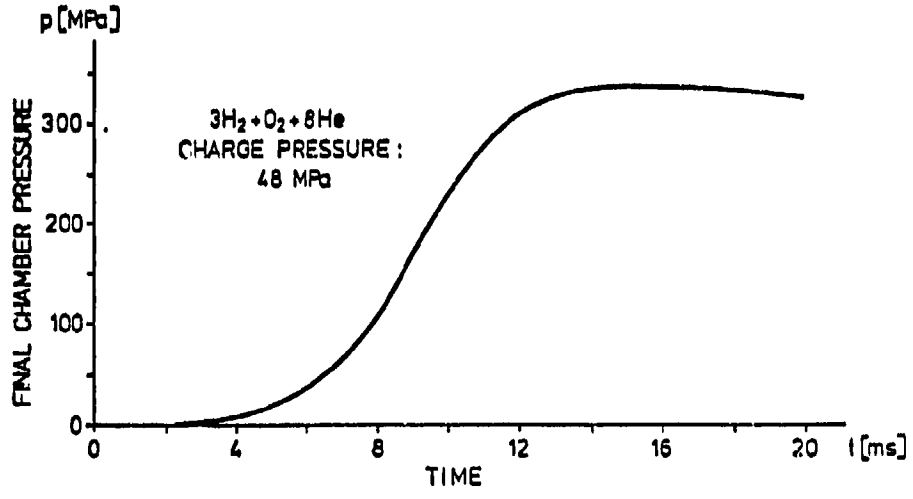

Fig. 37. Final chamber pressure versus time (Charge pressure p_I = 48 MPa; closed bomb mode)

The sample results obtained for charge pressure of 12 MPa and 48 MPa, respectively, have been selected because the bulk of the muzzle flash data were taken at charge pressures of 12 MPa, in order to reduce the gun muzzle exit pressure; see Section 8.3. The example of a charge pressure of 48 MPa is given to show that at this prepressure a rather high maximum final chamber pressure of about 360 MPa is achieved; see Fig. 37. Comparatively, for a charge pressure of p_I = 12 MPa, we measure a final chamber pressure of $p_F \approx 120$ MPa; see Figure 36. Thus, at prepressures or charge pressures of $p_I \geq 48$ MPa we generate realistic medium caliber weapon in-bore characteristics by the combustion of hydrogen with oxygen, i.e., for example, a chamber pressure of about p_F = 350 MPa at a maximum gas temperature of about T = 2700 K.

8.2 Difficulties Encountered During the Gun Firings

The second stage of gun configuration of the EMI-AFB gas gun simulator permits the study of both interior and transitional ballistics. Recall, that in the first experiments we charged the gas gun chamber with the gases in the order oxygen, followed by helium, followed by hydrogen, see Section 2.4. Following this order of gas introduction resulted, however, in difficulties regarding the combustion of the gas mixture. On two occasions, once in the closed bomb mode and once in the 20-mm gun configuration, we experienced detonation within the combustion chamber.

For cases in which there was not a detonation, we encountered severe combustion instabilities as apparent from oscillations occurring inside the gas gun chamber during the combustion of the gas mixture $3H_2 + O_2 + 8He$. For example, Figure 38 shows the pressure versus time traces of the pressure gauges at M 2 (middle of the gas gun chamber) and at M 6 (end of gun tube or muzzle exit region), taken during the gun firing. We see that severe pressure oscillations are obtained at the measuring ports M 2 and M 6. These undesirable oscillations have frequencies of 4 kHz and 40 kHz, respectively, see Figure 38.

If we place a temperature gauge instead of the Kistler gauge into the port at location M 2, we record the radiation emitted by the combustion gases. The visible light emission from the gas gun chamber, recorded by such a gauge, is shown in Figure 39. It demonstrates that the same type of oscillations is observed in the visible light emission from the chamber. This confirms that the oscillations are real and not experimental artifacts. They are apparently produced by combustion instabilities which are most likely due to incomplete mixing of the gases.

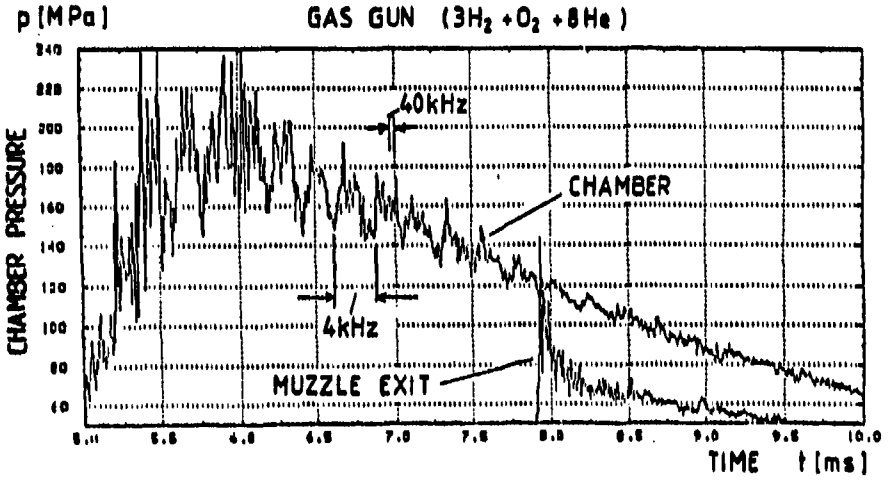

Fig. 38. In-bore pressures versus time at M 2 (chamber) and M 6 (muzzle exit); Charge pressure p_I = 24 MPa

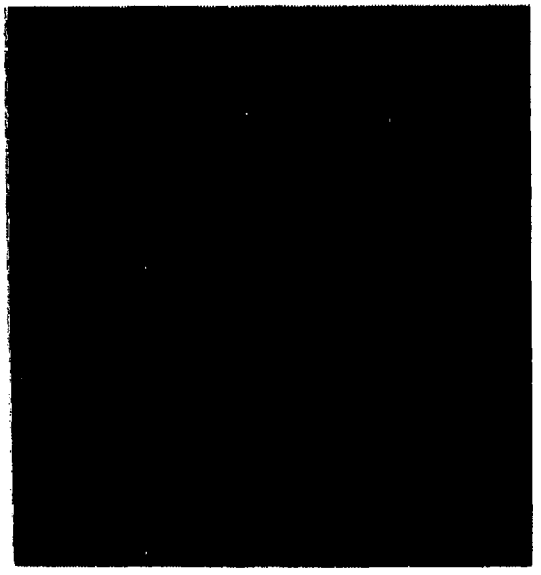

Fig. 39. Oscilloscope recording of the visible light emission from the gas gun chamber (M 2); Charge pressure p_2 = 24 MPa)

As has been pointed out in Section 2, Wilkins and Carros [3] have already reported that the order of gas introduction into the chamber is critical. They found that smooth burning of the gas mixture resulted either from the introduction of hydrogen, followed by helium and finally by oxygen, or from the addition of a premixed helium/hydrogen mixture to the oxygen. Further tests with premixed helium/hydrogen confirmed that our observed pressure oscillations were caused by the incomplete mixing of the gases, see Section 8.4.

8.3 First Gun Muzzle Flash Studies

A few gun muzzle flash studies with the EMI-AFB simulator in the gun configuration have been conducted using the critical order of gas introduction, i.e., the order: oxygen, followed by helium, followed by hydrogen. Exploding wires were used in these tests number 1 to 5 to ignite the gas mixture $3H_2 + O_2 + 8He$, and the charge pressure or initial loading pressure was p_I = 24 MPa. The thickness of the blow-out disk was 1 mm in test number 1 and 0.7 mm in the other tests.

Table 8 summarizes the maximum chamber pressures, p_F, which, in these tests, were measured at the pressure port M 1, and the maximum gun muzzle exit pressures, p_e, measured at the pressure port M 6.

Table 8. Results of gun firings (Tests No. 1 to 5)

Test No.	Thickness of Blow-out Disk (mm)	Charge Pressure p_I (MPa)	Maximum Chamber Pressure p_F (MPa)	Maximum Muzzle Exit Pressure p_e (MPa)
1	1	24	167	57
2	0.7	24	181	65
3	0.7	24	-	100
4	0.7	24	195	100

The thickness of the blow-out disk determines the pressure at which the blow-out disk ruptures, and, therefore, the percentage of combustibles released into the gun tube and finally into the surrounding air. Only in test number 1 (Table 8), the thickness of 1 mm was used. In all of the other tests, the thickness of the blow-out disk was 0.7 mm. Nevertheless, a bright flash was also recorded in test number 1, see Figure 13. The reason that the flash is relatively so intense is due to the fact that the intermediate flash is very bright.

The chamber and muzzle exit pressure data of test no. 2 are lower than the pressure data measured in tests no. 3 to 5 indicating that the combustion is incomplete. This is most likely caused by incomplete mixing of the gases.

The measured gun muzzle exit pressures in tests no. 3 and no. 4 are approximately 100 MPa. This is about twice the muzzle pressure of conventional 20-mm guns [37]. Thus, at a charge pressure of p_I = 24 MPa, we have relatively high muzzle pressures, p_e, which result in strong gun muzzle signatures, i.e., strong blast and flash phenomena. In the following experiments we have consequently reduced the charge pressure to p_I = 12 MPa, in order to lower the gun muzzle signature, and to generate a muzzle pressure which corresponds to the muzzle pressure of conventional 20-mm gun systems.

One of the goals of this investigation was the simulation of gun muzzle flash and its suppression by alkali salts.

Figure 40 shows the time-integrated photographs of the muzzle flash from the EMI-AFB 20-mm gas gun simulator precharged with 24 MPa total pressure. Here, also the critical order of gas introduction and the exploding wire technique were used. In two cases, we placed flash suppressants into the gas gun chamber, i.e., we used an amount of 1 wt.% K_2CO_3 and 2 wt.% K_2CO_3, respectively, to study the suppressant effectiveness.

A comparison of the photograph taken with no suppressant and that with 1 wt.% K_2CO_3 shows that the secondary flash (seen to the right in the uppermost photograph) is suppressed. The line of light observed on axis at distances beyond 0.8 m is due to particles, most likely particles of unreacted K_2CO_3.

A time-resolved, drum camera recording of the unsuppressed case in Figure 40 is shown in Figure 41. Though it is difficult to tell in the positive, the negative of this photograph clearly shows that the secondary flash commences at about 1.7 ms at a distance of about 0.7 m from the exit plane of the muzzle. Unfortunately, the camera angle did not permit the photographing of the entire 1.5 m distance between the muzzle and the projectile catcher box; and so - in the time-resolved photograph of Figure 41 - the initiation of the secondary flash has been masked by the intensity of the intermediate flash.

The reason that the intermediate flash is relatively so intense lies in the fact that, for the gas mixture used in the EMI-AFB simulator, only about 9 % combustibles remain after combustion in the chamber. In actual gun firings with conventional solid propellants it is known that the amount of combustibles is of the order of 50 % [6]. Nevertheless, the 9 % combustibles are sufficient to produce a secondary flash in the gas gun muzzle exhaust flow.

Thus, in these first experiments, we have determined experimentally that suitable diluted mixtures of hydrogen and oxygen are sufficient to generate secondary flash. Further it

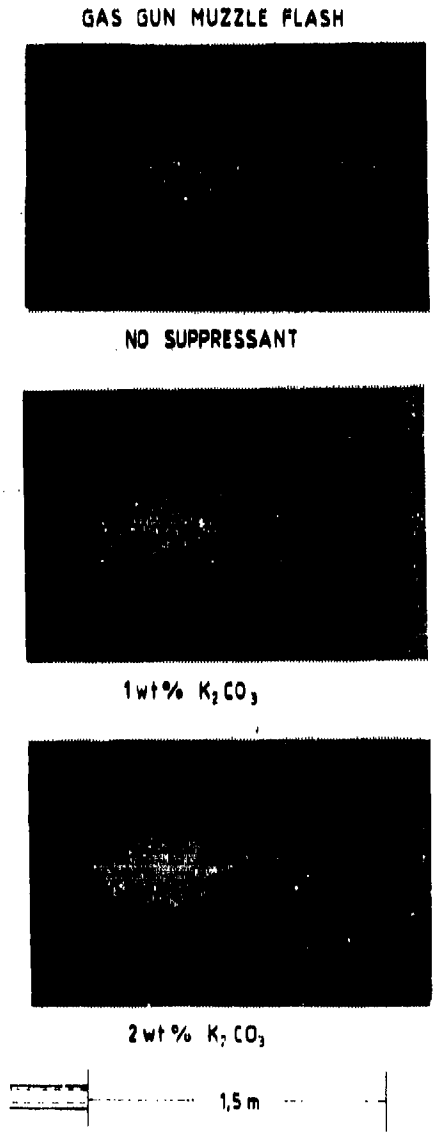

Fig. 40. Time-integrated photographs of 20-mm gas gun muzzle flashes
(Charge pressure: p_I = 24 MPa)

has been demonstrated that small amounts of alkali salts, similar to those used in actual gun systems, are sufficient to suppress the secondary flash.

The above experimental results as well as the following data support the supposition used by modellers [6] that only the hydrogen (and possibly the CO) chemistry are needed to describe the kinetics pertinent to gun muzzle flash and its chemical suppression by inhibiting alkali salts.

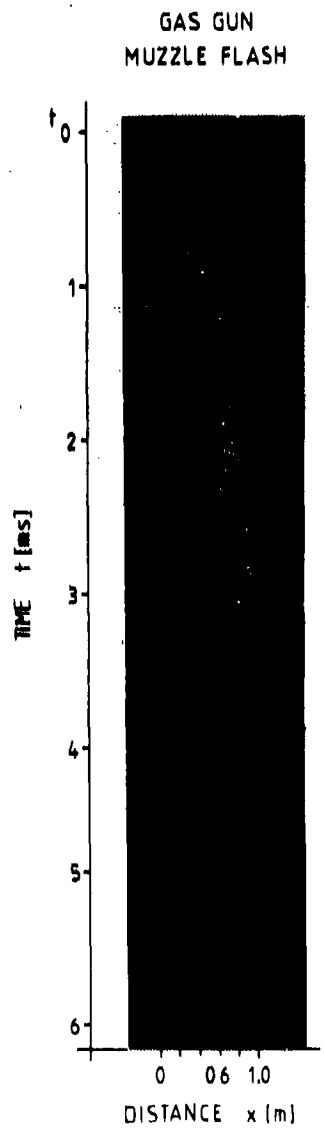

Fig. 41.

Time-resolved drum camera recording of the gas gun muzzle flash (Unsuppressed case of Figure 40; charge pressure: p_I = 24 MPa)

8.4 Studies with Premixed Helium/Hydrogen Gases and Exploding Wire Igniter

To overcome the difficulties encountered with the critical order of gas introduction, in the further studies we used commercial premixtures of helium and hydrogen. Thus, the order of gas ingroduction was changed to oxygen, followed by helium/hydrogen premixtures. The premixed helium/hydrogen gases were supplied by the Messer Griesheim Company at prepressures of 10 MPa.

8.4.1 In-Bore Pressures

The drastic change in the order of gas introduction resulted in smooth combustion, as expected from the investigations of Wilkins and Carros [3]. No further pressure oscillations were measured when using the premixture of hydrogen and helium. For example, Figure 42 shows the pressure recordings taken at the pressure ports M 1, M 3, M 4, M 5, and M 6, respectively. It is pointed out that no electrical filters were used in these pressure measurement which would cut off the noise.

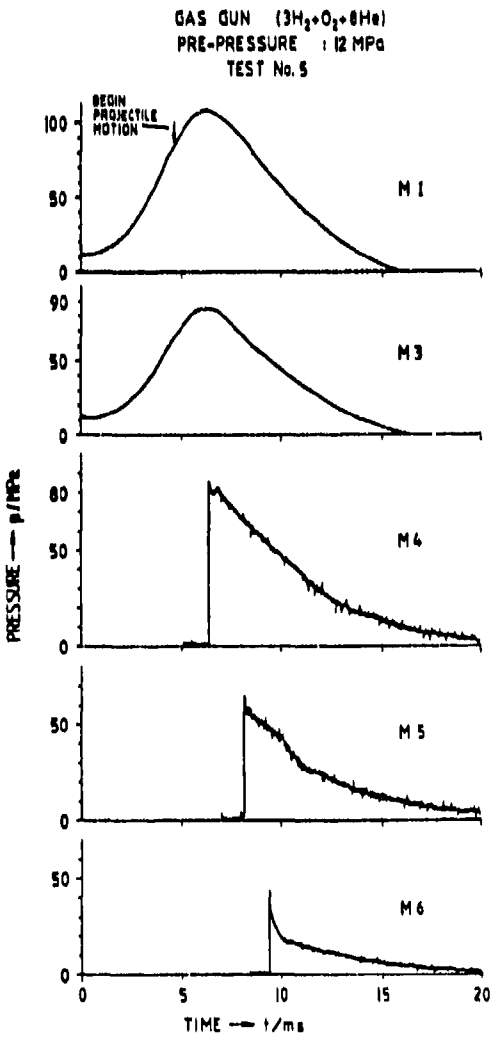

Fig. 42. Pressure versus time at M 1 to M 6 (Test No. 5; charge pressure p_I = 12 MPa)

In this test (No. 5) and the following examples (tests number 6 to 10), the $3H_2 + O_2 + 8He$ gas mixture in the gas gun chamber was prepressurized to p_I = 12 MPa (tests no. 5 to 9) and to p_I = 24 MPa (test no. 10), respectively. The thickness of the blow-out disk was always 0.7 mm. Exploding wires were used to ignite the gas mixture. Table 9 summarizes the initial data.

Table 9. Initial data of tests no. 5 to 10
(Electrical ignition through exploding wires)

Test No.	Thickness of Blow-out Disk (mm)	Charge Pressure P_I (MPa)	Amount of Alkali Additives (wt.%)	Remarks
5	0.7	12	None	Smooth in-bore combustion
6	0.7	12	None	
7	0.7	12	None	
8	0.7	12	2 %	
9	0.7	12	None	Onset of combustion delayed
10	0.7	24	None	High muzzle exit pressure

The pressure traces of Figure 42 (and of the following Figures 43 to 45) are free of oscillations. This confirms that the oscillations, encountered in the preceding experiments, are due to incomplete mixing of the gases. Thus, the altered order of gas introduction; namely, the use of premixtures of helium/hydrogen, solved the problem of combustion-related oscillations in the gas gun chamber.

Figure 42 and the following Figure 43 show that the start of the projectile motion after the burst of the blow-out disk commences at a pressure of about 90 MPa. This corresponds to the extracting force of conventional 20-mm cased ammunition [7, 37].

The above pressure-time traces show also that the in-bore pressures in the 20-mm gun tube have a rather steep increase at the pressure ports M 4 to M 6, most likely because of the

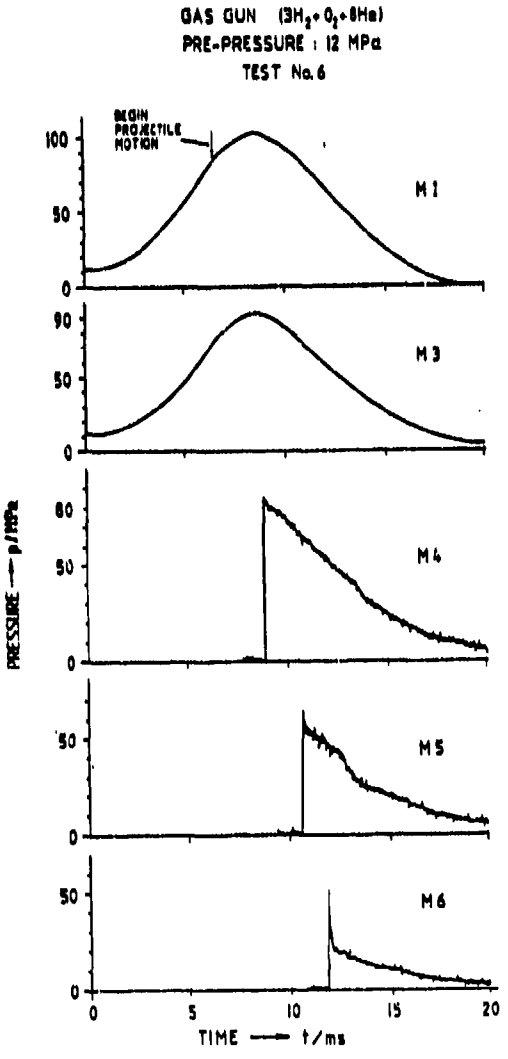

Fig. 43. Pressure versus time at M 1 to M 6 (Test No. 6; charge pressure p_I = 12 MPa)

high velocity of sound prevailing in the light gases. This is also apparent from Figure 44 which shows the pressures recorded in Test no. 7.

In these pressure traces we observe some oscillations with a small amplitude. These oscillations are thought to be due to noise inherent in the Kistler gauge technique used. The noise may also arise from vibrations induced in the small cavity that exists between both the gun tube and the gauge surfaces.

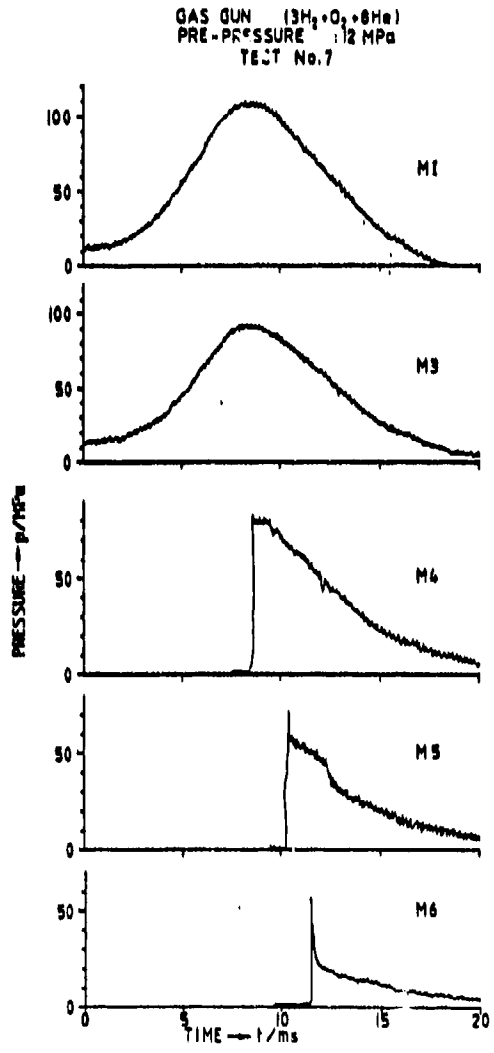

Fig. 44. Pressure versus time at M 1 to M 6 (Test No. 7; charge pressure p_I = 12 MPa)

Since the muzzle exit pressure, p_e, determines the flow expansion around the muzzle of the gas gun, Figure 45 presents the pressure recording of Figure 44 taken at the pressure port M 6 on an extended time scale. We observe that the muzzle exit pressure reaches a maximum of about 50 MPa, if the charge pressure is 12 MPa. Then, the muzzle exit pressure rapidly falls down to about 40 MPa and further down to 30 MPa.

For test number 8, 2 wt.% of the alkali additive K_2CO_3 was placed into the gas gun chamber. Figure 46 shows the pressure-time traces recorded at the pressure ports M 1 to M 6.

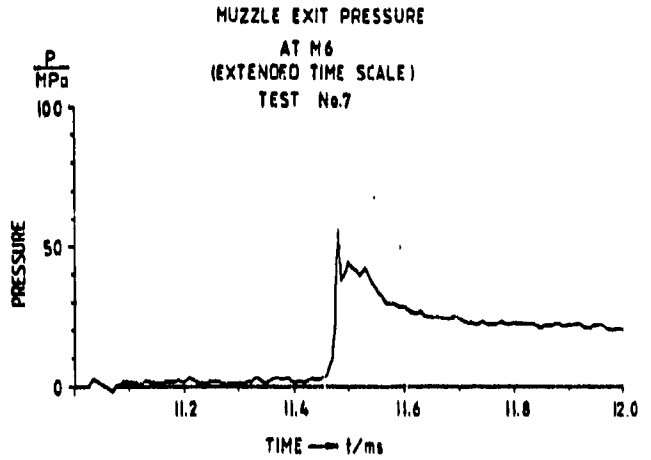

Fig. 45. Muzzle exit pressure versus time at M 6 from Figure 44 (p_I = 12 MPa)

For the above case, we observe that the pressure in the gun chamber increases faster and reaches a maximum earlier than the chamber pressures in Figures 43 and 44, where there is no suppressant. This becomes more apparent from the comparison of the two pressure-time traces taken at M 1 and shown in Figures 44 and 46. These pressure recordings are compared in the following Figure 47. Figure 47 clearly shows that the addition of 2 wt.% K_2CO_3 to the propellant gas mixture $3H_2 + O_2 + 8He$ results in a faster pressure increase, i.e., with the alkali additive the maximum pressure is reached at about t = 5 ms, while the gas propellant charge containing no suppressant salt has a pressure maximum at about t = 9 ms; see Figure 47.

Obviously, the combustion rate or "vivacity" of the gas mixture $3H_2 + O_2 + 8He$ is affected by the presence of alkali salt in the gun chamber. We conclude that the hydrogen/oxygen reaction sequence is altered by the alkali during the combustion process in the gun chamber.

The pressure versus time recordings of test no. 7 are shown in Figure 48. Here we observe a relatively large ignition delay, i.e., the maximum pressure at M 1 to M 6 is established much later than in the preceding gun firings. For example, at M 1 the maximum chamber pressure shown in Figure 48 is measured at about t = 18 ms while in Figures 43 and 44 we have the maximum chamber pressure at about t = 8 ms. The long ignition delay is most likely due to the relatively longer response time of the exploding wire igniter. This indicates that the exploding wire technique is not the most favorable ignition device for hydrogen/oxygen gas mixtures.

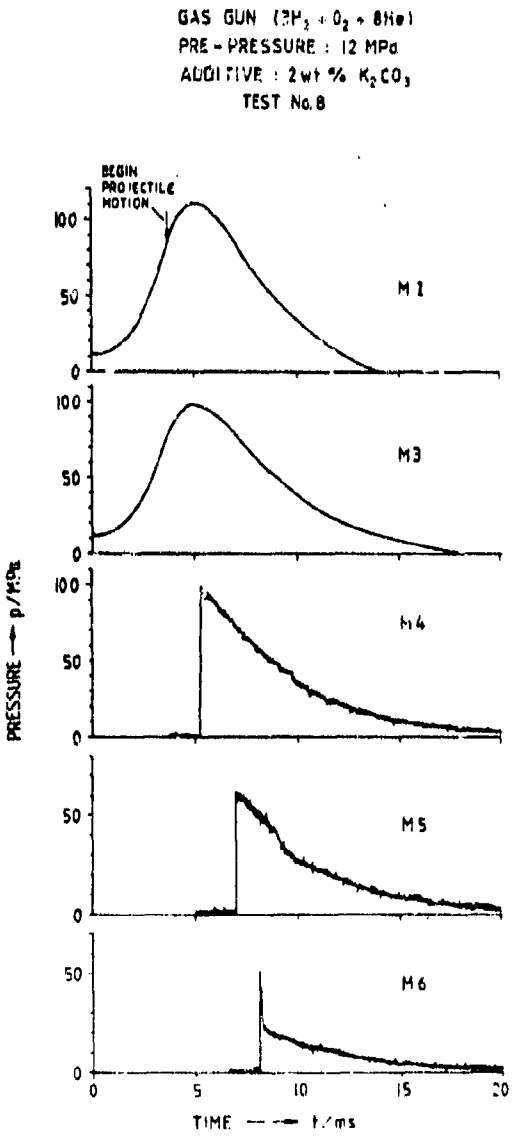

Fig. 46. Pressure versus time at M 1 to M 6 (Test No. 8; charge pressure p_I = 12 MPa; 2 wt.% of K_2CO_3)

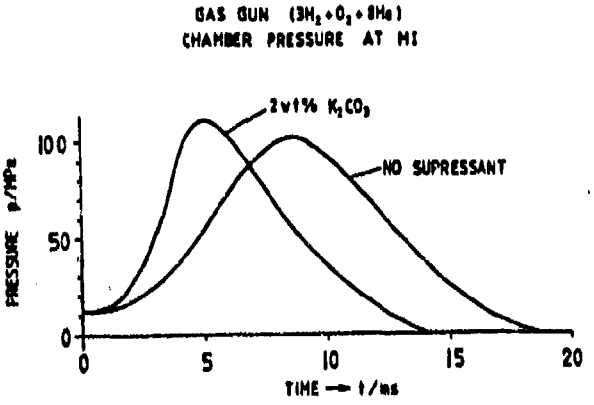

Fig. 47.

Pressure versus time at M 1 from Figures 42 and 46 (p_I = 12 MPa)

(a) with 2 wt.% K_2CO_3

(b) without suppressant alkali salt

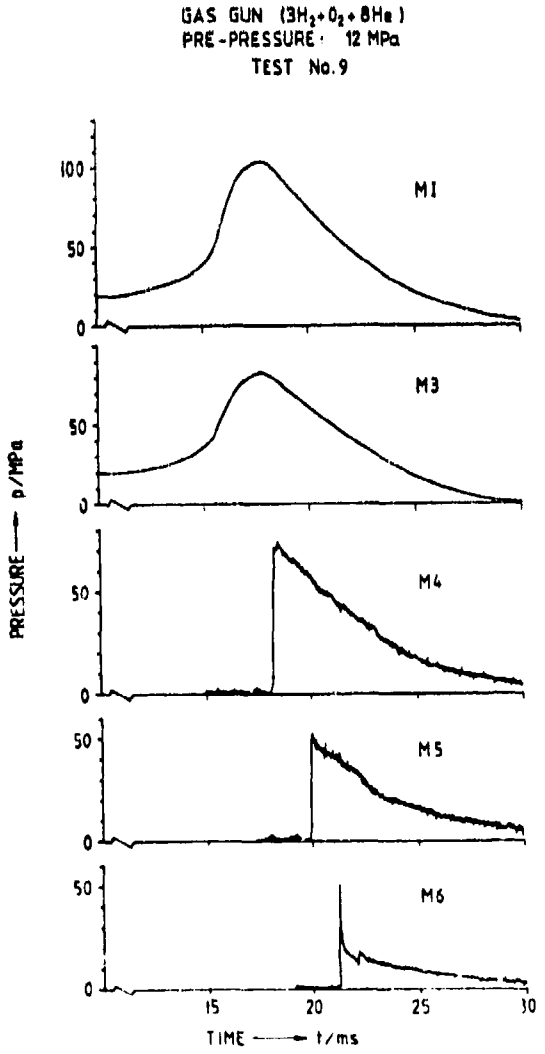

Fig. 48.

Pressure versus time at M 1 to M 6
(Test No. 9; p_I = 12 MPa)

Figure 49 shows finally the pressures recorded in test number 10. Here, the prepressure or charge pressure was p_I = 24 MPa.

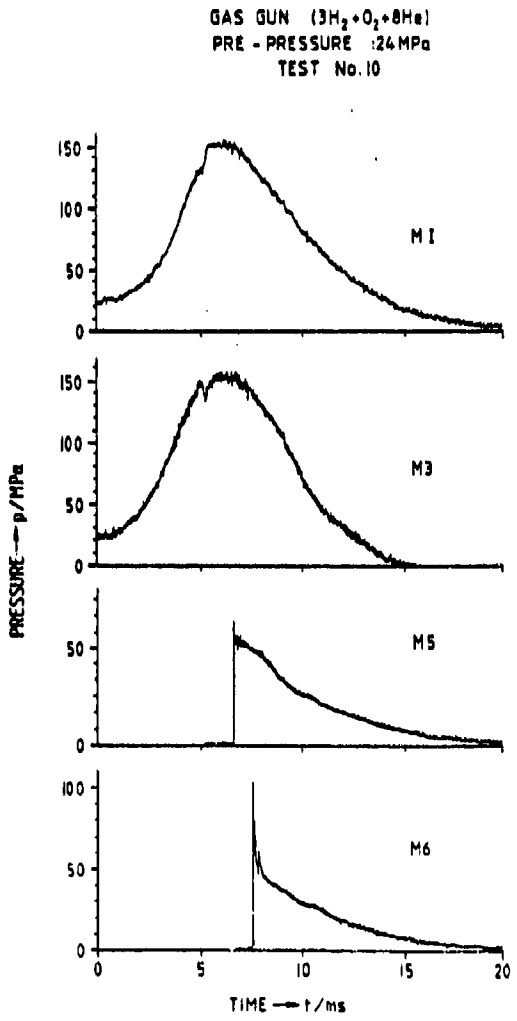

Fig. 49. Pressure versus time at M 1 to M 6 (Test No. 10; charge pressure p_I = 24 MPa)

For a higher charge pressure of p_I = 24 MPa we have higher in-bore pressures with a muzzle exit pressure of about p_e = 100 MPa. Again, the pressure recording at M 6 is shown on an extended time scale, see Figure 50, in order to resolve the initial decay of the muzzle exit pressure. A comparison to Figure 45 shows that the increase of the charge pressure from p_I = 12 MPa to p_I = 24 MPa yields about twice the muzzle exit

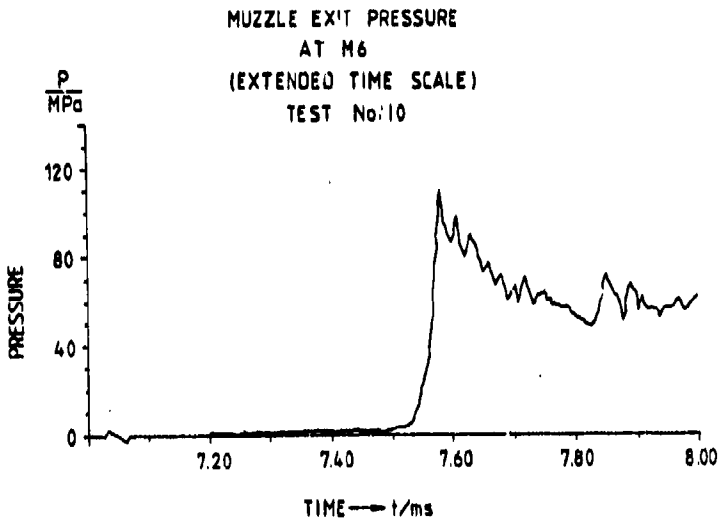

Fig. 50. Pressure versus time at M 6 from Figure 49 (charge pressure p_I = 24 MPa)

pressure at the measuring port M 6. As has been pointed out above, the muzzle exit pressure of about p_e = 100 MPa (see Figure 50) is about twice the muzzle pressure of conventional 20-mm guns. Most of the gun muzzle flash studies therefore were performed at charge pressure of p_I = 12 MPa (p_e ~ 50 MPa).

We conclude the presentation of in-bore pressure data with Table 10 which summarizes the maximum gas pressures measured at the measuring ports M 1, M 3, M 4, M 5, and M 6, respectively. Since the performance of gun systems is often measured in terms of the projectile launch velocity, v_o, attained during the gun firings, the launch velocities were also measured and are listed in Table 10. Evidently, the launch velocity of the projectile depends upon the charge pressure; i.e., the interior ballistics and gun performance is determined by the initial loading or charge pressure, p_I. For p_I = 12 MPa we measure a launch velocity of about v_o = 750 m/s, while for a charge pressure of p_I = 24 MPa we have a launch velocity of about v_o = 950 m/s. The weight of the 20-mm projectile used is 120 g.

Lord [2] reported that a projectile of 40 g could be accelerated to about 4000 m/s when the final chamber pressure was increased to about 400 MPa. The high velocity is due to the fact that the molecular weight of the combustion gases is low and/or their sonic speed is high. Also, Lord [2] pointed out that the obvious limitations of a gas gun is its sonic speed. For a fixed sonic speed and projectile mass, the only way of

Table 10. Maximum gas pressures and projectile launch velocities (Tests No. 5 to 10)

Test No.	Charge Pressure p_I (MPa)	Maximum Gas Pressure at Ports					Projectile Launch Velocity v_o (m/s)
		M 1	M 3	M 4 (MPa)	M 5	M 6	
5	12	108	86	84	64	45	-
6	12	104	93	84	64	52	787
7	12	108	92	82	72	57	732
8 *	12	111	98	98	62	50	775
9	12	104	85	74	52	49	723
10	24	152	154	--	--	103	957

* with 2 wt.% K_2CO_3

achieving higher projectile velocity is by increasing the chamber pressure. For example, at a chamber pressure of about p_I = 650 MPa one could accelerate a 60 g projectile to about v_o = 4300 m/s, if complete combustion of the gases is possible [2].

The EMI-AFB gas gun simulator is designed for maximum final chamber pressures of about 450 MPa. Our gas gun therefore is capable of accelerating projectiles to velocities of about v_o = 3000 m/s. However, a drastic increase of the projectile launch velocity would be possible, if a two-stage gas gun were built which used the principle of conventional light gas guns, but employed instead of solid propellant charges only light gases as a propellant.

8.4.2 Flash Photography

The muzzle flashes generated in tests no. 5 to 10 have been photographed using time-integrated open-shutter and drum cameras. For example, Figure 51 presents the open-shutter or still pictures taken in tests no. 5 to 8.

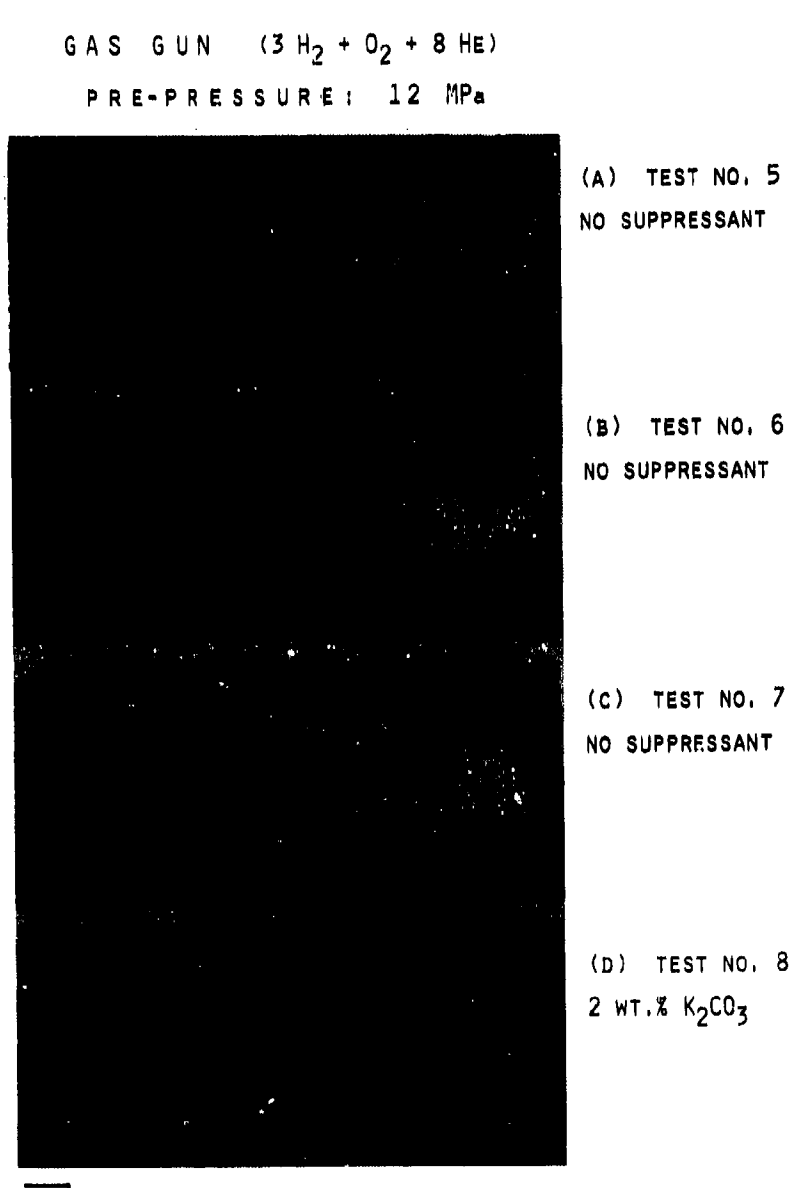

Fig. 51. Time-integrated photographs of muzzle flash (Tests No. 5, 6, 7, and 8; charge pressure p_I = 12 MPa)

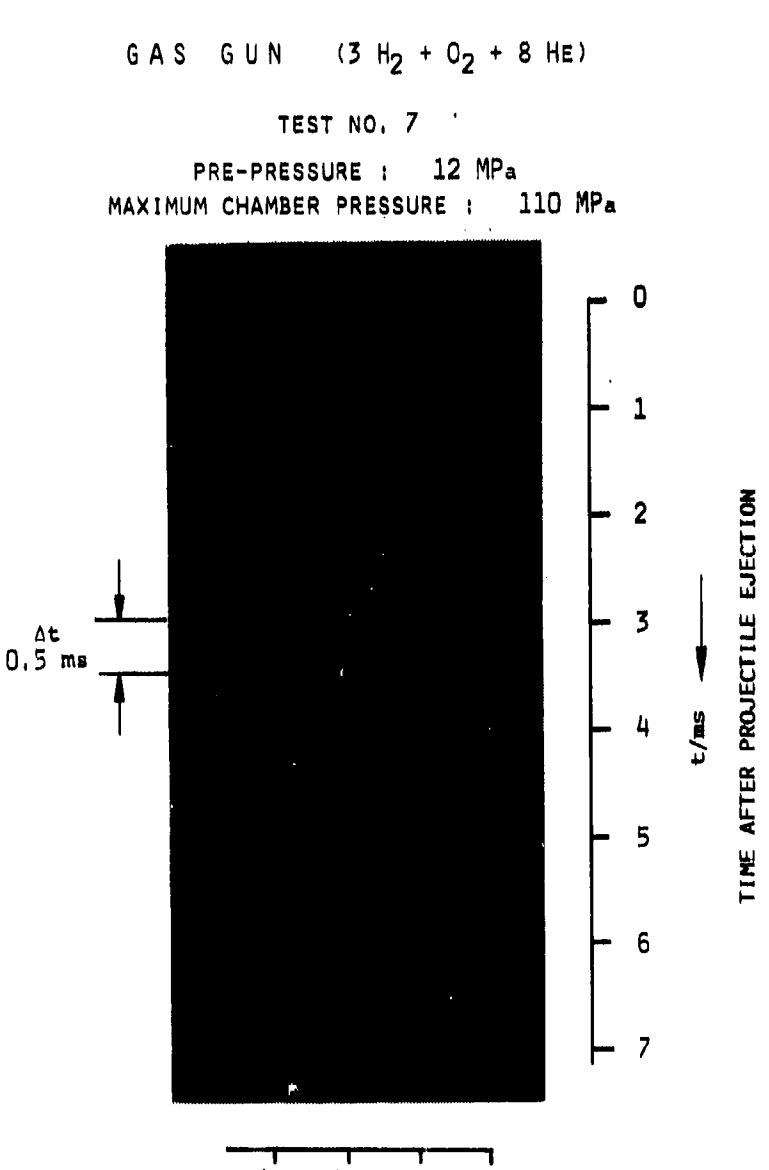

Fig. 52. Drum-camera recording of muzzle flash (Test No. 7; charge pressure p_I = 12 MPa)

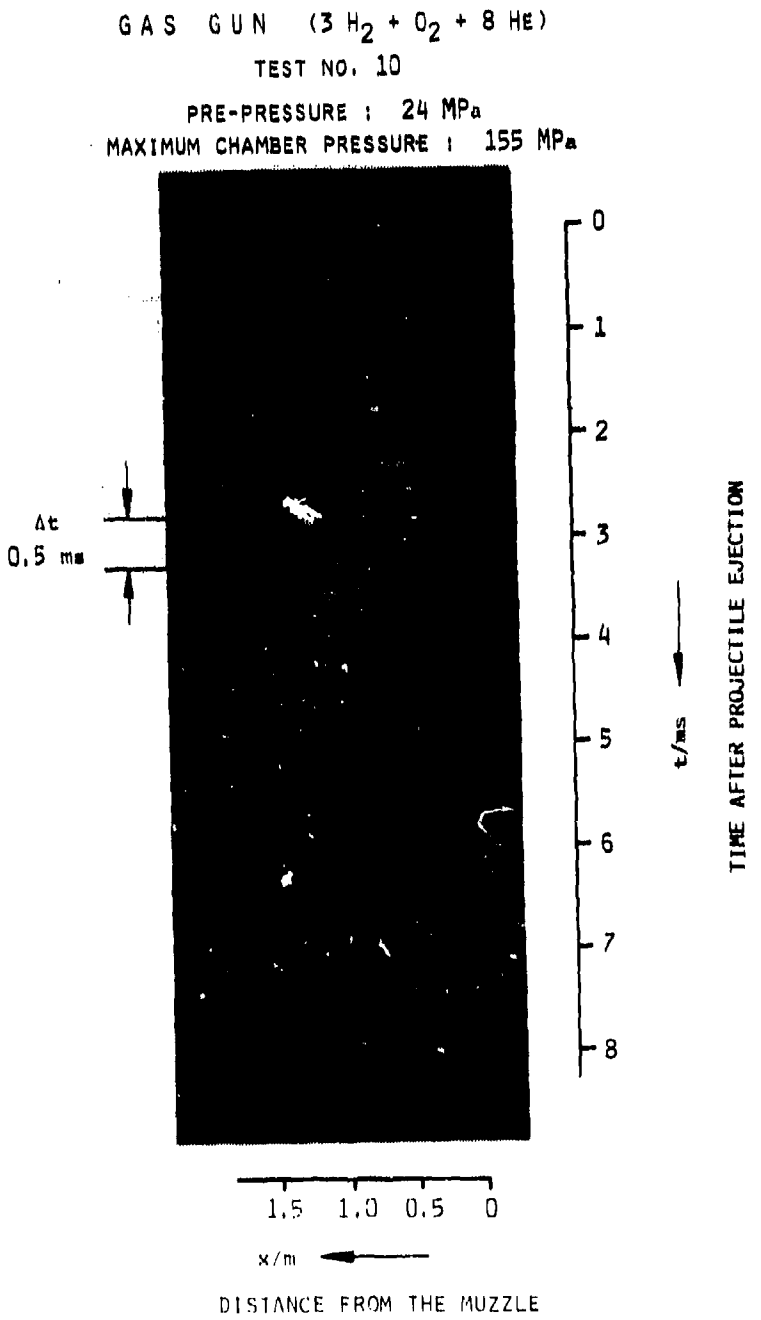

Fig. 53. Drum-camera recording of muzzle flash (Test No. 10; charge pressure p_I = 24 MPa)

As sample results, Figures 52 and 53 further show the time-resolved drum-camera recordings of tests number 7 and 10, i.e., unsuppressed muzzle flashes generated at charge pressures of p_I = 12 MPa (Figure 52) and p_I = 24 MPa (Figure 53), respectively.

In Figure 51 (A), (B), and (C) we demonstrate that the secondary flash is generated and varies from shot to shot in its intensity. In Figure 51 (D) the effect of 2 wt.% K_2CO_3 is shown. Obviously, the secondary flash is completely suppressed since the remaining luminosity in Figure 51 (D) is caused by the intermediate flash.

The time-resolved drum-camera recording of the unsuppressed flash in Figure 52 shows that at a charge pressure of p_I = 12 MPa we have a flash with a spatial extension going up to the projectile catcher box (1.5 m) and a duration of about t = 5 ms. Comparatively, the unsuppressed muzzle flash of a 20-mm cannon firing conventional solid gun propellants has a spatial extension of about x = 1.5 m and a duration of about t = 10 ms [37].

The brightness and duration of the unsuppressed gas gun muzzle flashes increase with greater charge or chamber pressures, see Figure 53. At p_I = 24 MPa the flash is much brighter than at p_I = 12 MPa, and its duration increases slightly. In particular, the brightness of the intermediate flash, existing during the time interval $0 < t < 2$ ms, is drastically increased. Also, for axial distances from the muzzle of $0 < x < 1$ m luminosity appears in the secondary flash during $2 < t < 6$ ms, see Figure 53. Comparatively, in Figure 52 (at p_I = 12 MPa), we do not see a blackening of the film in this flow area, because the radiation is much weaker or even suppressed.

Again, we have experimentally confirmed that mixtures of hydrogen and oxygen, suitably diluted with helium, are sufficient to cause muzzle flash. In addition, it has been demonstrated once more that small amounts of alkali salt, here 2 wt.% K_2CO_3, are sufficient to affect the secondary flash. Evidentially, the hydrogen/oxygen reactions alone can lead to secondary flash, and this flash can be suppressed by the addition of alkali salts.

8.4.3 Detector Recordings

Sample results of the Si- and InAs-detectors recordings of the unsuppressed gas gun muzzle flash are shown in Figure 54 and the following Figures in this Section. The location of these detectors has been shown in Figure 12. Figure 54 displays the emission recordings of the first and second Si-detectors (visible) and the emission recording of the InAs-detector (near infrared).

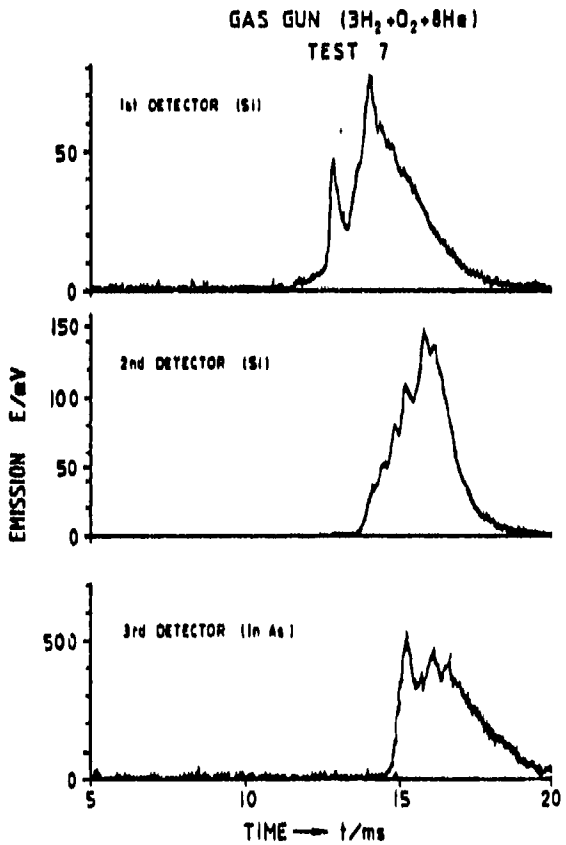

Fig. 54. Emission versus time
Si- and InAs-detectors recordings of
unsuppressed muzzle flash
(Test No. 7; p_I = 12 MPa)

Figure 55 shows similar emission recordings for the case of flash suppression (test no. 8), i.e., when 2 wt.% of K_2CO_3 is added to the propellant charge.

In the suppressed case of Figure 55, we measure much less intensity of the emitted radiation; especially for the Si-detectors, i.e., in the visible region of the spectrum. Also the duration of the detector pulses is somewhat reduced in the suppressed case of Figure 55, when compared to the unsuppressed case of Figure 54.

Figure 56 shows another sample result of these detector recordings; namely, for the case when the chamber pressure is increased to p_I = 24 MPa (test no. 10).

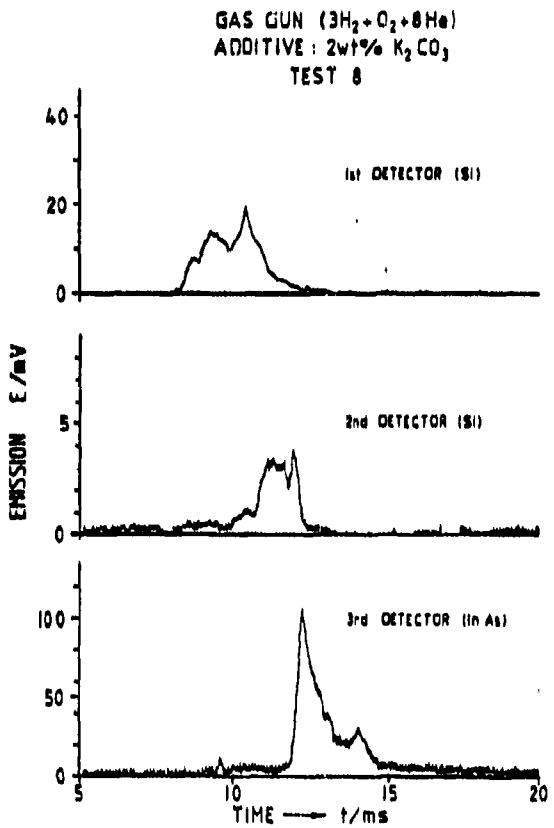

Fig. 55. Emission versus time; Si- and InAs-detectors recordings of suppressed muzzle flash (2 wt.% K_2CO_3) (Test No. 8; p_I = 12 MPa)

For the case of unsuppressed gas gun muzzle flash at a charge pressure of p_I = 24 MPa, the intensity of the measured radiation is much higher. The Si-detector recordings show that the intensity in the visible region is about ten times the intensity of the flash when a charge pressure of p_I = 12 MPa is applied. Comparatively, the intensity recorded by the InAs-detector is only increased by a factor of 2.2, see Figures 54 and 55.

Since the detectors were not calibrated, these emission recordings yield only relative data of the muzzle flash development.

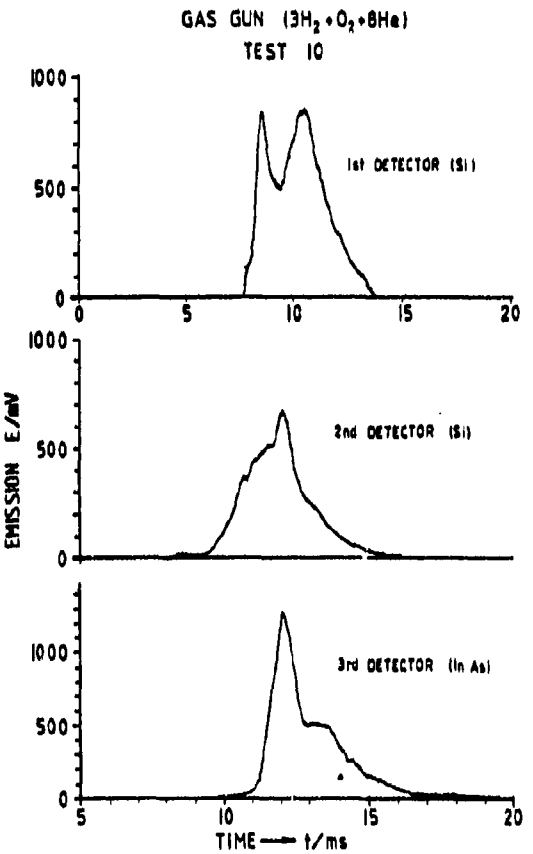

Fig. 56. Emission versus time
Si- and InAs-detectors recordings of unsuppressed muzzle flash
(Test No. 10; p_I = 24 MPa)

8.5 Studies with Premixed Helium/Hydrogen and Hot Wire Igniter

As described in Section 5.2, an electrically heated tungsten wire of 0.35 mm diameter was used as a hot wire igniter to initiate smoothly the combustion of the prepressurized gas mixture $3H_2 + O_2 + 8He$ in the gas gun chamber.

A sample result of the pressure measurements, performed at a charge pressure of p_I = 12 MPa with the premixed helium/hydrogen and the oxygen using the hot wire igniter, is shown in Figure 57. Here, only the pressure versus time traces at locations M 1 and M 6 are presented, because there was no significant difference between the pressure recordings taken with the

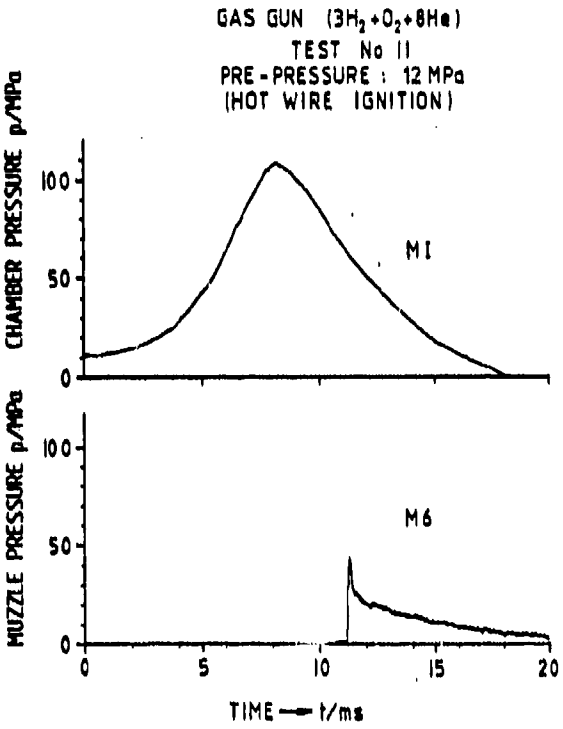

Fig. 57. Pressure versus time at M 1 and M 6 (Test No. 11; p_I = 12 MPa; hot wire igniter)

exploding wire technique and shown in Figures 43, 44, and 48 and the recordings taken with the hot wire igniter in Figure 57. With the hot wire igniter in test no. 11, we measure a maximum final chamber pressure of p_F = 110 MPa and a maximum muzzle exit pressure of about p_e = 45 MPa.

Again, we have smooth combustion of the gases, as apparent from the pressure time traces in Figure 57. The hot wire ignition is satisfactory. Apparently, the hot wire igniter should be preferred to the exploding wire technique. It advantageously avoids the production of undefined particles into the flow. In addition, with the hot wire ignition we have a better defined, smooth initiation of the gas mixture and we can easily determine the electrical energy needed for the ignition of the gas propellants.

9. PARTICLE EFFECTS

Only a few preliminary investigations could be performed on two-phase flow effects. This was due to the fact that the probing of the temperature and velocity took too much time. However, we performed some tests implementing TiO_2 into the flow. We glued the inert particles onto the surface of the hot wire igniter to obtain a good distribution in the expanding flow. First velocity data confirm that this procedure is applicable.

Also reacting particle seeding was obtained when inserting the alkali salt KNO_3 into the gas gun chamber. These particles experience condensation during the expansion especially in the muzzle flow of the gas gun. After production of the muzzle flash, these reacting particles are involved in the chemical reaction sequence, since they are vaporized and combusted after they have passed the inner shock disk (Mach disk). However, only preliminary data could be taken until this contract had expired. Thus, further investigations are delayed to a new contract proposed recently to the Ballistic Research Laboratory and to the European Research Office, London [44].

10. SUMMARY AND RECOMMENDATIONS

Gun muzzle flash studies were conducted combusting oxygen/hydrogen/helium mixtures in the EMI-AFB gas gun simulator. These experiments were supported by measurements performed in actual gun firings.

The gas gun simulator, pre-charged with suitably diluted mixtures of hydrogen and oxygen permits the generation of relatively clean, reacting gas flows with realistic ballistic gas pressures and temperatures, i.e., at pressures of 400 to 450 MPa and temperatures of 2700 to 3000 K. Thus, fundamental studies of single and two-phase interior and transitional ballistic flows can be conducted.

The gas gun is capable of simulating both the interior ballistics and muzzle flash phenomena with particularly simple chemistry. Basic studies of the ballistic flow should include the chemistry. For example, if pressure waves are generated by ignition or combustion related instabilities inside the gun, then a more accurate interior ballistic predictive code is needed which can take into account the chemical reactions. A first response to this problem was undertaken at the Ballistic Research Laboratory (BRL), Aberdeen Proving Ground, Maryland, USA. A new derivative of the NOVA code, named XNOVAK, has been

developed at the BRL (IBD) to provide the capability of addressing chemical reactions within the framework of a one-dimensional, two-phase interior ballistic model. The development of this code was driven by the fact that experience with low-vulnerability (LOVA) compositions had occasionally revealed large discrepancies between theoretical predictions and actual performance [5]. These developments need support from the experimental side, in order to verify the theoretical solutions and their underlying assumption. Therefore, the continuation of this research work is recommended.

The secondary muzzle flash produced by the combustion of the pure hydrogen-oxygen gas mixtures, is suppressed by the addition of alkali salts, here K_2CO_3, to the propellant charge. These experimental findings support the supposition of the modelling community [6]; namely, that only the hydrogen (and possibly the CO) chemistry are needed to describe properly the kinetics pertinent to gun muzzle flash and its suppression by chemical alkali salts suppressants. However, the kinetics to be developed and incorporated into a future improved flash prediction code also needs experimental support.

It is my view that the EMI-AFB gas gun simulator is a tool capable of providing the experimental support. Therefore, a further three years program is envisaged at EMI-AFB to lay the foundation for the construction of plausible chemical reaction kinetics, and to assist in the development of adequate reactive flow codes. This proposed task should include fundamental studies of

- the combustion of $H_2/O_2/He$ and CO gas mixtures
- reacting and particle-laden flows

and requires the extension of our present test facility as well as the development of adequate diagnostics.

ACKNOWLEDGEMENT

The author would like to acknowledge the support and sponsorship of the U.S. Army Research, Development and Standardization Group (UK), London. Also, he would like to thank Dr. Fritz Oertel of the U.S. Army Research, Development and Standardization Group (UK), London, as well as Dr. H. Schmidt of the Ministry of Defence of the Federal Republic of Germany (Rü VII 7) and Dr. G.A. Schröder, Chief: EMI-AFB, for their support. Special thanks are due to Dr. J.M. Heimerl of BRL who participated in these investigations as an Exchange Scientist with EMI-AFB from January 1985 to April 1986. Finally, the author would like to express his gratitude to Mr. O. Wieland for his help in the experiments, to Mrs. E. Messner for preparing the manuscript so well, and to Dr. T. Minor and Dr. G. Keller, BRL, for supporting the work and reviewing the manuscript.

11. REFERENCES

[1] Klingenberg, G., and Banks, N.E., "Review on Interior Ballistics Research: State-of-the-Art of Computational and Experimental Efforts", Proceedings of the Sixth International Symposium on Ballistics, Orlando, Florida, USA, October 1981

[2] Lord, M.E., "Performance of a 40-mm Combustion Heated Light Gas Gun Launcher", Arnold Engineering Center, Inc., Report October 1960

[3] Wilkins, M.E., and Carros, R.J., "Combustion Tests of Oxygen-Hydrogen-Helium Mixtures at Loading Pressures up to 8,000 Pounds per Square Inch", NASA Technical Note, NASA-TN-D-1892, October 1963

[4] Horst, A., Keller, G., and Minor, T., "A Plan for the Future of Interior Ballistic Model Development, Validation, and Application in the Interior Ballistic Division of the Ballistic Research Laboratory", BRL, July 1986

[5] Horst, A., Keller, G., and Gough, P., "A Two-Phase Flow Simulation of LOVA Propellant Interior Ballistic Behaviour Using the XNOVAK CODE", Proceedings of the Ninth International Symposium on Ballistics, Shrivenham, England, April/May 1986

[6] Heimerl, J.M., Keller, G.E., and Klingenberg, G., "Muzzle Flash Kinetics and Modelling", Fraunhofer-Institut für Kurzzeitdynamik, Weil am Rhein, FRG, EMI-AFB Report No. 1/85, May 1985

[7] Klingenberg, G., "Experimental Diagnostics in Reacting Muzzle Flows", Fraunhofer-Institut für Kurzzeitdynamik, Weil am Rhein, FRG, EMI-AFB Report No. E 12/84, December 1984

[8] Klingenberg, G., and Mach, H., "Investigation of Combustion Phenomena Associated with the Flow of Hot Propellant Gases - I: Spectroscopic Temperature Measurements Inside the Muzzle Flash of a Rifle", J. Combustion and Flame, Vol. 27, 1976, pp. 163-176

[9] Klingenberg, G., "Investigation of Combustion Phenomena Associated with the Flow of Hot Propellant Gases - III: Experimental Survey of the Formation and Decay of Muzzle Flow Fields and of Pressure Measurements", J. Combustion and Flame, Vol. 29, 1977, pp. 289-309

[10] Heimerl, J.M., and Klingenberg, G., "Combustion Following Turbulent Mixing in Muzzle Flows", Fraunhofer-Institut für Kurzzeitdynamik, Weil am Rhein, FRG, EMI-AFB Report No. 6/86, August 1986

[11] Klingenberg, G., Heimerl, J.M., and Wieland, O., "Laser-Doppler-Velozimeter-Messungen in der Pulvergasglocke des NATO-Gewehres G 3", Fraunhofer-Institut für Kurzzeitdynamik, Weil am Rhein, EMI-AFB Report No. 4/86, July 1986

[12] Klingenberg, G., Heimerl, J.M., and Wieland, O., "Lokale Temperaturmessungen in der Pulvergasglocke des NATO-Gewehres G 3", Fraunhofer-Institut für Kurzzeitdynamik, Weil am Rhein, FRG, EMI-AFB Report No. 5/86, August 1986

[13] Engineering Design Handbook: Spectral Characteristics of Muzzle Flash, AMCP-706-255 (June 1967)

[14] Schmidt, E.M., "Secondary Combustion in Gun Exhaust Flows", Ballistic Research Laboratory, Technical Report ARBRL-TR-02372, October 1981 (ADA 107312)

[15] Heimerl, J.M., "Secondary Combustion in Gun Exhaust Flows", Ballistic Research Laboratory, Technical Report ARBRL-TR-02479, March 1983 (ADA 126-129)

[16] Morrison, W.F., Knapton, J.D., and Klingenberg, G., "Regenerative Injection Liquid Propellant Guns", J. of Ballistics, Vol. 8, No. 3, 1985, pp. 2026-2060

[17] Wuest, H., and Kegler, W., "Untersuchungen zum Problem rückstoßfreier Waffen", Report ST 5/62, German-French Research Institute, St. Louis, France, ISL, January 1962

[18] Kesslau, H., "Das Mündungsfeuer bei Geschützen und Raketen", Institut St. Louis, France, Report No. 11/48, 1948

[19] Heimerl, J.M., "The Muzzle Flash of Guns and Rockets: A Translation", Ballistic Research Laboratory, Special Publication BRL-SP-50, December 1985

[20] Bracuti, A.J., Bottei, L.A., and Davis, R., "Evaluation of Potential Multipurposes Propellant Additives: Flash-Erosion-Suppressant", J. of Ballistics, Vol. 7, 1983, pp. 1609-1629

[21] Klingenberg, G., "Mündungsfeuer und Rauchbildung", Fraunhofer-Institut für Kurzzeitdynamik, Weil am Rhein, FRG, EMI-AFB Report No. E 16/81, December 1981

[22] Young, H.H. (Ed.), "Smoke and Flash in Small Arms Ammunition 1948-1954", Midwest Research Institute, Report Sept. 30, 1954

[23] Klingenberg, G., "Gun Muzzle Flash Research at the Fraunhofer-Institute EMI-AFB", J. of Ballistics, Vol. 9, No. 1, 1986, pp. 2129-2167

[24] Klingenberg, G., Schmolinske, E., Mach, H., and Seiler, F., "Flow Simulation Experiments in Ballistics", J. of Ballistics, Vol. 8, No. 4, 1985, pp. 2098-2117

[25] Klingenberg, G., Heimerl, J.M., and Schmolinske, E., "Simulation Experiments - Gas Gun Simulator", Proceedings of the Ninth International Symposium on Ballistics, RMCS, Shrivenham, England, April 1986

[26] Bicen, A.F., Khezzar, L., and Whitelaw, J.H., "Subsonic Single-Phase Flow in a Gun Simulator", Imperial College of Science and Technology, Department of Mechanical Engineering, London, England, Report FS/86/03, March 1986

[27] Klingenberg, G., and Heimerl, J.M., "Simulation Experiments on Reacting Muzzle Flows", Fraunhofer-Institut für Kurzzeitdynamik, Weil am Rhein, FRG, EMI-AFB Report No. 9/86, December 1986

[28] Capellos, C., and Walker, R.F., "Fast Reactions in Energetic Systems", Reidel, 1981

[29] Freedman, E., "BLAKE - A Thermodynamic Code Based on TIGER: User's Manual and Guide", Ballistic Research Laboratory, Technical Report ARBRL-TR-02441, July 1982

[30] Bathelt, H., and Volk, F., "Vergleichende thermodynamische Berechnungen mit dem BLAKE- und dem ICT-Code", Fraunhofer-Institut für Treib- und Explosivstoffe, Pfinztal-Berghausen, FRG, ICT Report No. 9/84, December 1984

[31] Heimerl, J.M., "A Comparison of Thermodynamic Calculations of the BLAKE- and the ICT Code (A Translation)", Fraunhofer-Institut für Kurzzeitdynamik, Weil am Rhein, FRG, EMI-AFB Report No. T 4/86, April 1986

[32] Klingenberg, G., "Invasive Spectroscopic Techniques for Measuring Temperature in Highly Pressurized Combustion Chambers", J. Optical Engineering, Vol. 24, No. 4, 1985, pp. 692-296

[33] Klingenberg, G., "Investigation of Two Different Propellants During the Ignition and Combustion in a 20-mm Gun Chamber", J. Propellants, Explosives, Pyrotechnics, Vol.10, 1985, pp. 31-38

[34] Klingenberg, G., "Temperature History of the Interior Ballistic Flow of a 20-mm Cannon", J. of Ballistics, Vol. 8, No. 2, 1985, pp. 1896-2008

[35] Klingenberg, G., "Measurement of Important Ballistic Flow Properties by Spectroscopic Techniques", Proceedings of the AGARD Propulsion and Energetics Panel, 66th (B) Specialists' Meeting "Interior Ballistics of Guns", Florence, Italy, September 1985 (AGARD Paper No. 392)

[36] Klingenberg, G., "Application of Novel Temperature Gauges to Study the Combustion of Liquid Gun Propellants", Proceedings of the Ninth International Symposium on Ballistics, Shrivenham, England, April 1986

[37] Klingenberg, G., Mach, H., and Smeets, G., "Flow Fields Measurements of an Unsteady Reacting Muzzle Exhaust Flow", J. of Heat Transfer, Vol. 105, 1983, pp. 884-888

[38] Smeets, G., and George, A., "Instantaneous Laser-Doppler-Velocimeter Using a Fast Wavelength Tracking Michelson", J. Review Sci. Instrum., Vol. 29, 1977, pp. 1589 ff.

[39] Smeets, G., and George, A., "Michelson Spectrometer for Instantaneous Velocity Measurements", J. Phys. E., Sci. Instrum., Vol. 14, 1981, pp. 838-845

[40] Heimerl, J.M., and Klingenberg, G., "New Evidence for the Role of Turbulence in the Ignition of Secondary Flash", Proceedings of the Ninth International Symposium on Ballistics, Shrivenham, England, April 1986

[41] Klingenberg, G., and Heimerl, J.M., "The Effect of Chemical Flash Suppressants on Intermediate Flash", Proceedings of the Eighth International Symposium on Ballistics, Orlando, Florida, October 1984

[42] Morton, A.W., Agnew, J.T., "Basic and Technical Work on Military Propellants", The Franklin Institute, Philadelphia, Pennsylvania, Final Report No. F-2092-15, December 1949

[43] Mach, H., Werner, U., and Masur, H., "Messungen an der Zweiphasenströmung im Ausströmbereich eines Gewehres vom Kaliber 7,62 mm", German-French Research Institute, St. Louis, France, ISL Report No. R 110/84, 1984

[44] Klingenberg, G., "Investigation of Highly Pressurized, Two-Phase, Reacting Flow", Proposal to BRL and the U.S. Army Research, Development and Standardization Group (UK), London, July 2, 1986

[45] Driscoll, W.G., and Vaugham, W. (Edts.) "Handbook of Optics", McGraw-Hill Book Company, New York, 1978

[46] Meiners, D., "Spektroskopische Methoden zur Messung der Temperatur in Plasmen mit Selbstabsorption", BMBW-FB Report, No. 72-22, November 1972

12. APPENDIX I

FUNDAMENTALS OF SPECTROSCOPIC TEMPERATURE MEASUREMENTS

12.1 Nomenclature

ΔA	: unit area of a radiation source
a	: absorptance
$a_\lambda(T)$	: spectral absorptance at wavelength λ and temperature T
$a^*_\lambda(T)$	: spectral absorption coefficient at wavelength λ and temperature T
c_1	: first radiation constant = 3.7415×10^{-16} watt m^2
c_2	: second radiation constant = 1.4388 cm deg K
D	: optical thickness
$D_\lambda(T)$	: optical thickness at wavelength λ and temperature T
d	: diameter (gun tube in-bore diameter = caliber)
d_m	: median particle diameter
f	: function
Δf	: distance between main flow axis and "effective film location"
I	: imaging optic (lens)
K	: degree Kelvin
$L_\lambda(T)$	: spectral radiance at wavelength λ and temperature T
$L^b_\lambda(T)$	: spectral radiance of a blackbody
L^*_λ	: spectral radiance of a calibrated source
L^1_λ	: spectral radiance of a background source
L^2_λ	: non-absorbed fraction of L^1_λ after it has passed the event
L^3_λ	: spectral radiance emitted by the event
ℓ	: optical path length
$\Delta\ell$	: optical path difference
M_e	: Mach number of flow exiting the gun muzzle
R	: radial coordinate
r	: reflectance
$r_\lambda(T)$	: spectral reflectance at wavelength λ and temperature T
$r_t(\lambda)$	: total reflectance at wavelength λ
T	: temperature
T_m	: gas temperature of flow exiting the gun muzzle

$T_S(\lambda)$	: brightness temperature at wavelength λ
$T_S^*(\lambda)$	: brightness temperature of calibrated source at wavelength λ
t	: time
α	: unit solid angle about a radiation source
β	: unit angle of radiant beam
γ	: specific heat ratio
Δ, ∂, d	: differential increments
$\varepsilon_\lambda(T)$	: spectral emissivity at wavelength λ and temperature T
$\varepsilon_\lambda^*(T)$	: spectral emission coefficient at wavelength λ and temperature T
λ	: wavelength
Π	: radiant flux
$\Pi_\lambda(T)$	: spectral radiant flux at wavelength λ and temperature T
τ	: transmittance
$\tau_\lambda(T)$	: spectral transmittance at wavelength λ and temperature T

12.2 Data Reduction Procedure

12.2.1 Radiation Laws

In differential form, the spectral radiance, $L_\lambda(T)$, is defined as the radiant flux, $\Pi_\lambda(T)$, emitted by a source per unit spectral wavelength $\Delta\lambda$, per unit area of the source ΔA, per unit solid angle α about the source, per unit angle β of the emitted beam [45]:

$$L_\lambda(T) = \frac{\partial^3 \Pi}{\partial \lambda \, \partial A \, \partial \, \alpha \cos\beta} \quad * \qquad (13)$$

When a radiant beam of spectral radiance $L_\lambda(T)$ is incident upon a medium, it can be attenuated by absorption, reflection, and scattering. If no scattering occurs, the fractions of an incident beam which are absorbed, transmitted, and reflected are defined as spectral absorptance, $a_\lambda(T)$, spectral transmittance, $\tau_\lambda(T)$, and spectral reflectance, $r_\lambda(T)$. Envoking conservation of energy yields:

$$a_\lambda + \tau_\lambda + r_\lambda = 1 \qquad (14)$$

A thermal radiator is a source in thermal equilibrium which emits radiation solely because of its temperature. The thermal radiator is called a "blackbody" if it absorbs all of the incident radiation:

$$a_\lambda(T) = 1 \; ; \qquad \tau_\lambda(T), \, r_\lambda(T) = 0 \qquad (15)$$

At any wavelength λ, the spectral radiance of a blackbody, $L^b_\lambda(T)$, is given by the radiation law of Planck or by Wien's approximation:

$$L^b_\lambda(T) = \frac{c_1}{\lambda^5 (e^{c_2/\lambda T} - 1)} \qquad \text{(Planck)} \qquad (16)$$

$$L^b_\lambda(T) = \frac{c_1}{\lambda^5 e^{c_2/\lambda T}} \qquad \text{(Wien)} \qquad (17)$$

---

* The use of the subscript λ for denoting a function of wavelength is customary in the field of optical spectroscopy [7]. The more standard notation $f(\lambda)$ instead of f_λ is only used when subscripts are needed to identify a specific case as, e.g., in the definition of the "brightness" temperature $T_S(\lambda)$. This holds for all the radiative quantities introduced in this report.

where c_1 and c_2 are the well-known radiation constants, i.e., $c_1 = 3.7415 \times 10^{-16}$ [Wm^2], $c_2 = 1.4388$ [cmK].

Wien's approximation is found to be accurate within 1 % for values of $\lambda T < 3000$ [μmK]. Therefore, this approximation is applicable in combustion and ballistics, since frequently $T < 3000$ K and $\lambda < 1$ μm.

For a non-blackbody thermal radiator, the emitted spectral radiance, $L_\lambda(T)$, is related to that of a blackbody through its spectral absorptance, $a_\lambda(T)$, i.e., Kirchhoff's law:

$$L_\lambda(T) = a_\lambda(T)\, L_\lambda^b(T) \tag{18}$$

The spectral emissivity, $\varepsilon_\lambda(T)$, of the non-blackbody thermal radiator is defined as the ratio of the emitted spectral radiance, $L_\lambda(T)$, to the spectral radiance of a blackbody, $L_\lambda^b(T)$, at the same temperature:

$$\varepsilon_\lambda(T) = \frac{L_\lambda(T)}{L_\lambda^b(T)} \tag{19}$$

Substituting equation (19) into equation (18) yields

$$\varepsilon_\lambda(T) = a_\lambda(T) \tag{20}$$

which is an alternative statement of Kirchhoff's law. A thermal radiator is called a "greybody", if the emissivity is independent of wavelength λ.

In general, radiating gases are neither blackbody nor greybody radiators. Their emissivity and absorption varies strongly with wavelength. Spectroscopic methods for temperature measurements therefore are based on measurements of the radiative quantities at one wavelength [7]. The attenuation of a monochromatic beam of radiation that passes along a certain optical path, ℓ, through the investigated gas volume, and the emitted spectral radiance along ℓ is given by the radiation transport equation [45]. Provided losses caused by reflection and scattering processes are negligible, and local thermal equilibrium (LTE) prevails in the test volume, the solution of the radiation transport equation defines the spectral emission and absorption coefficients. The ratio of these spectral coefficients are equal to the spectral radiance of a blackbody, i.e., the modified form of Kirchhoff's law [7]:

$$\frac{\varepsilon_\lambda^*(T)}{a_\lambda^*(T)} = L_\lambda^b(T) \tag{21}$$

where $\varepsilon^*_\lambda(T)$ [W/cm^{4}ster] denotes the spectral emission coefficient, and $a^*_\lambda(T)$ [m^{-1}] the spectral absorption coefficient. In this case, the relation between $a_\lambda(T)$, $\tau_\lambda(T)$, and the "optical thickness", $D_\lambda(T)$, are given by:

$$a_\lambda(T) = 1 - \tau_\lambda(T) = 1 - e^{-a^*_\lambda(T)\,\ell} \tag{22}$$

$$D_\lambda(T) = a^*_\lambda(T)\,\ell = -\ln \tau_\lambda(T) \tag{23}$$

The optical thickness, $D_\lambda(T)$, increases with the pathlength, ℓ, and the absorption coefficient, $a^*_\lambda(T)$, which, in turn, is dependent on the density of absorbing chemical species and/or particles present in the test region. For large values of $D_\lambda(T)$, the gas is said to be optically thick. For optically thick gases, almost all of the incident radiation is absorbed so that

$$a_\lambda(T) = 1 - e^{-D_\lambda(T)} \to 1 \tag{24}$$

and

$$L_\lambda(T) \to L^b_\lambda(T) \tag{25}$$

i.e., the emitted radiation approaches blackbody radiation. Measurements of the locally emitted spectral radiance, $L_\lambda(T)$, in optically thick gases therefore yield an estimate of gas temperature.

Gas temperature measurements by absorption and/or emission methods are based upon the above definitions. However, these radiative equations suppose that

(1) radiation losses due to reflection and scattering are negligible,

(2) the system is in local thermal equilibrium.

The validity of the first supposition depends upon the type, size, and concentration of particles present in the investigated gas volume. In the main muzzle flash regions of the gun muzzle blast field, most of the propellant combustion particulates exiting at the muzzle will be vaporized and/or consumed during the shock-heating and subsequently induced exothermic chemical reactions. The possible formation of soot during the chemical reactions would result in an increase of the spectral absorptance, but it would have a minor effect on the reflection and scattering. Therefore, the first supposition is considered to be a reasonable approximation of the conditions that prevail in the gun muzzle flash region.

The validity of the second supposition remains to be assessed. As a rule, local thermal equilibrium (LTE) exists if [7,45]:

- small gas test volumes are of the same temperature, T,
- radiation is a function of temperature,
- particle mean free path is short compared to the gas test volume,
- energy transfer is due mainly to collisions and not to radiation.

In transient flows, the relaxation time for LTE depends on the collision frequency and sometimes exceeds a characteristic flow time, giving a non-equilibrium condition. However, as long as the relaxation time is short in comparison with the flow residence time, the LTE assumption is good. This is commonly the case in gun propellant flows, pressurized to or above atmospheric pressure, due to the high collision frequency. On the other hand, non-equilibrium has been observed in chemically reacting gases or flames and in shock-heated gases [7]. For example, chemical processes may lead to the formation of an abnormally high population in the excited state of a molecule so that we have chemiluminescence [7]. Apart from the chemical excitation which per se excludes LTE, it is possible that in chemically reacting flows there may be departures from thermal as well as from chemical equilibrium. The meaning of temperature then becomes doubtful and we have at best an effective temperature [7].

12.2.2 Brightness Temperature

In practice, it is advantageous to characterize a radiation source by the "brightness" or "radiance" temperature. For a certain wavelength λ, the brightness temperature, $T_S(\lambda)$, is defined such that a blackbody at the brightness temperature, $T_S(\lambda)$, has the same "brightness" or spectral radiance, L^b_λ, as the spectral radiance, L_λ, of the investigated source at the temperature T and the same wavelength λ. Therefore, the definition of the brightness temperature is wavelength dependent, and, for a certain wavelength λ, $T_S(\lambda)$ is defined by

$$L_\lambda(T) = L^b_\lambda [T_S(\lambda)] \qquad (26)$$

This definition is illustrated in Figure 58.

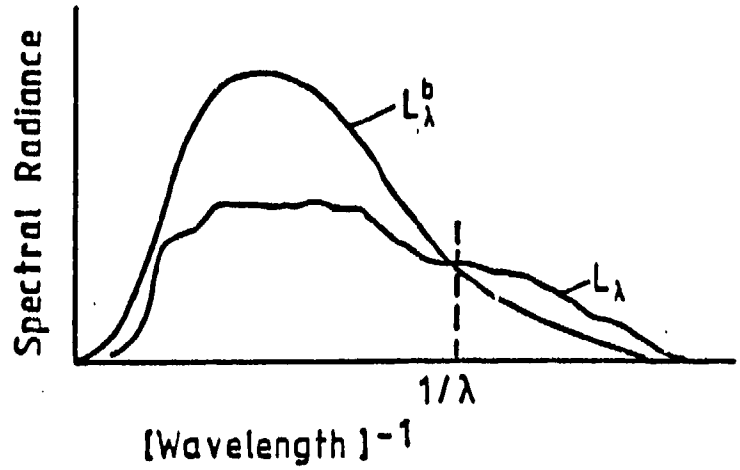

Fig. 58. Definition of brightness temperature ($L_\lambda^b = L_\lambda$ at $1/\lambda$)

By substituting Wien's equation (17) and Kirchhoff's equation (18) in equation (26), we get

$$a_\lambda(T)\ c_1/\lambda^5\ e^{-c_2/\lambda T} = c_1/\lambda^5\ e^{-c_2/\lambda\ T_S(\lambda)} \tag{27}$$

By taking the natural logarithm and regrouping we obtain

$$\frac{1}{T} = \frac{1}{T_S(\lambda)} + \frac{\lambda}{c_2} \ln a_\lambda(T) \tag{28}$$

which relates the gas temperature T of the radiation source to its brightness temperature $T_S(\lambda)$ and spectral absorptance $a_\lambda(T)$. Therefore, if $T_S(\lambda)$ and $a_\lambda(T)$ are measured, T can be evaluated.

In the measurements, the spectral radiance L_λ emitted by the source is related to that of a reference source or calibration lamp for which spectral radiance, L_λ^*, and brightness temperature, $T_S^*(\lambda)$, are known. The brightness temperatures $T_S(\lambda)$ and $T_S^*(\lambda)$ are defined by equation (26) or, using Wien's approximation for L_λ^b, are

$$\frac{1}{T_S(\lambda)} = \frac{\lambda}{c_2} [\ln c_1/\lambda^5\ L_\lambda(T)]^{-1} \tag{29}$$

$$\frac{1}{T_S^*(\lambda)} = \frac{\lambda}{c_2} [\ln c_1/\lambda^5\ L_\lambda^*(T)]^{-1} \tag{30}$$

It is easily shown that the combination of these two equations yields

$$\frac{1}{T_S(\lambda)} = \frac{1}{T_S^*(\lambda)} - \frac{\lambda}{c_2} \ln \left[\frac{L_\lambda(T)}{L_\lambda^*(T)} \right] \tag{31}$$

i.e., the relationship between $T_S(\lambda)$, $T_S^*(\lambda)$, $L_\lambda(T)$, and $L_\lambda^*(T)$. Optical pyrometers, which directly measure $T_S(\lambda)$, are based on this equation.

12.2.3 Temperature Evaluation

In the case of optical thick propellant flows, i.e., for $a_\lambda(T) \to 1$, equation (26) shows that the brightness temperature $T_S(\lambda)$ approximates the gas temperature T:

$$T_S(\lambda) \to T \tag{32}$$

For a given wavelength $\lambda = 589$ nm, Figure 59 shows, for example, the deviation of the brightness temperature $T_S(\lambda)$ from the gas temperature T = 2700 K as a function of the spectral absorptance $a_\lambda(T)$.

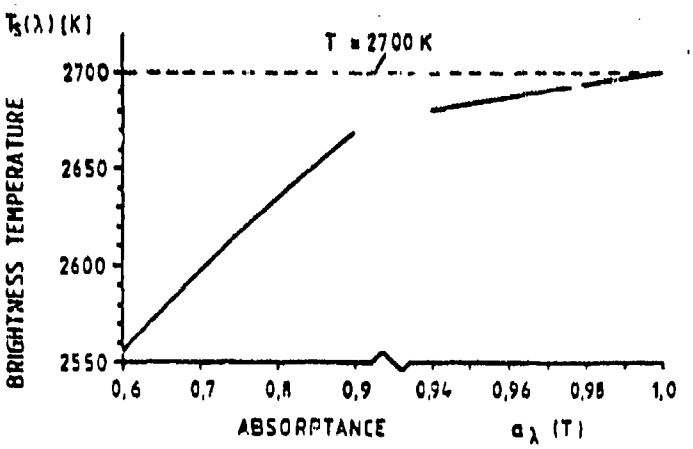

Fig. 59. Difference between $T_S(\lambda)$ and T = 2700 K versus $a_\lambda(T)$ at $\lambda = 589$ nm

The brightness temperature $T_S(\lambda)$ approaches the true gas temperature T as the absorptance $a_\lambda(T)$ increases. Since for the radiating 7.62-mm gun muzzle flow, an average spectral absorptance of $a_\lambda(T) \geq 0.7$ has been measured, the difference between $T_S(\lambda)$ and T in Figure 59 is of the order of 100 K, i.e., it stays within the error bounds of the measured temperature data.

Thus, an estimate of gas temperature can be obtained by measuring the local spectral radiance, $L_\lambda(T)$ versus t, emitted in the vicinity of the end surface of the intrusive temperature gauge. However, a calibration procedure is required in these data evaluations.

In the temperature gauge measurements, a tungsten ribbon lamp was used for calibration purposes, see Figure 60. The chopped beam of the tungsten lamp is focused on a scattering foil positioned at the entrance of the temperature gauge. The scattering device simulates the real test site conditions where the emitted light enters the light pipe bundle from all directions. The opening angle of the reference beam is adapted to the opening angle at the end surface of the emission probe in order to avoid calibration errors. The spectral radiance, L_λ^*, of the tungsten ribbon lamp is related to the spectral radiance, L_λ, of the source under investigation in terms of the photomultiplier currents. A micropyrometer measures the brightness temperature, T_S^*, at the scattering plastic foil as a function of the lamp current.

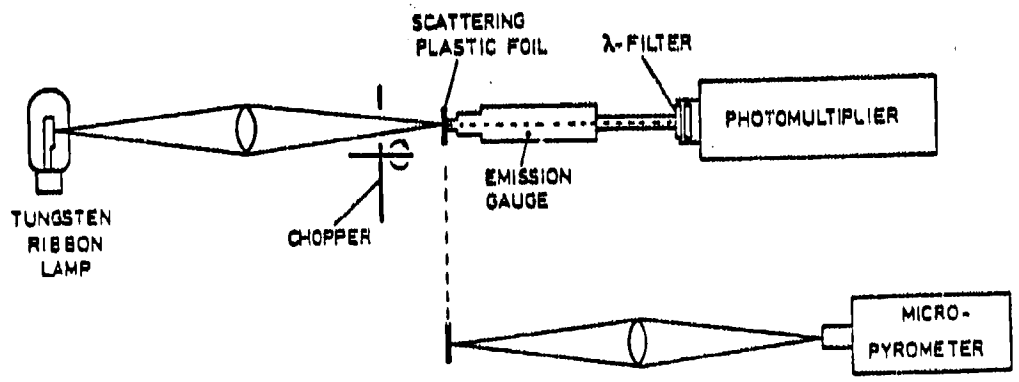

Fig. 60. Test setup used for the calibration of the temperature (emission) gauge measurements

12.2.4 Reversal Method

The determination of flame temperatures through the use of spectral line reversal measurements is well established and widely exploited [7,45]. Reversal measurements are not restricted to spectral lines, but can be also applied to band emission or continuous radiation. In principle, the reversal technique is nearly a null or balancing method. In its simplest form, the brightness temperature, $T_S(\lambda)$, of a background source, such as a tungsten ribbon lamp, is adjusted until the spectral radiance, L_λ, of the steady flame appears neither in absorption against the background source nor in emission superposed on the continuum emitted by the background source. It can be shown from Kirchhoff's law (equation 18) that at this reversal point the flame temper-

ature, T, is the same as the brightness temperature, $T_S(\lambda)$, of the background source. If we define L_λ^1 as the spectral radiance of the backlight source, L_λ^2 as the spectral radiance of the non-absorbed radiation of the backlight source after it has traversed the flame, and L_λ^3 as the spectral radiance emitted by the flame we obtain

$$L_\lambda^1 = L_\lambda^b [T_S(\lambda)] \tag{33}$$

$$L_\lambda^2 = [1 - a_\lambda(T)] \, L_\lambda^b[T_S(\lambda)] \tag{34}$$

$$L_\lambda^3 = a_\lambda(T) \, L_\lambda^b(T) \tag{35}$$

At the reversal point for a particular wavelength, λ, we obtain:

$$a_\lambda(T) \, L_\lambda^b(T) + [1 - a_\lambda(T)] \, L_\lambda^b[T_S(\lambda)] = L_\lambda^b[T_S(\lambda)] \tag{36}$$

and

$$a_\lambda(T) \, L_\lambda^b(T) = a_\lambda(T) \, L_\lambda^b[T_S(\lambda)]$$

or

$$L_\lambda^b(T) = L_\lambda^b[T_S(\lambda)] \tag{37}$$

i.e.,

$$T = T_S(\lambda) \tag{38}$$

Thus, the flame temperature is obtained by measuring the brightness temperature, $T_S(\lambda)$, of the backlight source at the reversal point with a pyrometer.

However, in transient flows, a modified reversal technique is required which permits an approximate determination of the reversal point. In this technique, the radiation flux with and without superimposed radiation of the background source is recorded photoelectrically, and the spectral radiances L_λ^2 and L_λ^3 are measured either simultaneously along parallel or vertical optical paths, or alternately by chopping the beam of the backlight source [7]. The spectral radiance of the comparison source, L_λ^1, is determined before of after the flow occurs. Then, we obtain:

$$\frac{L_\lambda^3}{L_\lambda^1 - L_\lambda^2} = \frac{L_\lambda^b(\lambda)}{L_\lambda^b[T_S(\lambda)]} = e^{-(c_2/\lambda)[1/T - 1/T_S(\lambda)]} \tag{39}$$

By taking the natural logarithm and regrouping, it follows that

$$\frac{1}{T} = \frac{1}{T_S(\lambda)} + \frac{\lambda}{c_2} \ln \left[\frac{L_\lambda^1 - L_\lambda^2}{L_\lambda^3} \right] \tag{40}$$

The spectral absorptance is given by the absorbed fraction of the incident beam, i.e.,

$$a_\lambda(T) = (1 - \frac{L_\lambda^2}{L_\lambda^1}) \tag{41}$$

The error of the modified reversal measurement is particularly dependent upon the difference between T and $T_S(\lambda)$ and the emitter concentration expressed in terms of $a_\lambda(T)$ [7]:

$$|\frac{\Delta T}{T}| \sim \frac{[1/T - 1/T_S(\lambda)]^{1/2}}{a_\lambda(T)} \tag{42}$$

The error is small, if the brightness temperature of the background source is well adjusted to the flame temperature, and high emitter concentrations are present in the flow.

Since the reversal method measures both the emission and absorption along a given optical path through the test volume it yields an average temperature along this path. The method tends to emphasize high temperature zones if cross-sectional temperature gradients are present in the flow. In this case an average value is determined which approximates the maximum gas temperature, but it may be 10 to 25 % below the real maximum. In general, however, the data evaluation presents difficulties if gradients in the emitter concentration and temperature are encountered. The method does, however, have the special advantage that it is a balancing method which, compared to other spectroscopic techniques, requires less sophisticated data acquisition procedures and analysis.

It has already been pointed out that the above equations are only valid if local thermal equilibrium prevails in the flow. For example, under non-equilibrium conditions the line-reversal gives only an effective electronic excitation temperature which is just a measure of the ratio of populations in the corresponding electronic states. Numerous measurements of the excitation temperatures of the internal degrees of freedom in flames have shown that quite often this temperature substantially exceeds the equilibrium values [7]. Non-equilibrium distribution in the rotational, vibrational, and electronic degrees of freedom have been detected. In reacting systems with heat release,

particles with a large reserve of vibrational energy may be formed and, in principle, the sodium atoms may be excited in collisions with these particles, so that the measured excitation is a reflection of the non-equilibrium conditions. Thus, the conditions in turbulent reacting gas-particle flows, such as in muzzle flashes, may significantly deviate from local thermal equilibrium.

12.2.5 Abel Inversion Techniques

As noted previously, Abel inversion of measurements along parallel lines-of-sight through the radiating flow has to be applied to overcome the difficulties of non-uniform temperature distributions. In this technique, the side-on distribution of the optical thickness, $D_\lambda(y)$, and the spectral radiance, $L_\lambda(y)$, is determined from emission and absorption measurements using the modified version of Kirchhoff's law. Since in the Abel inversion measurement, both the spectral emission and absorption coefficients are obtained in terms of the radial and axial coordinates R and x, the modified form of Kirchhoff's law in equation (20) is written as:

$$\left[\frac{\varepsilon^*_\lambda(R)}{a^*_\lambda(R)}\right]_x = L^b_\lambda[T(R)]_x \tag{43}$$

$\varepsilon^*_\lambda(R)$ and $a^*_\lambda(R)$ can be determined from the measured side-on distributions of $L_\lambda(y)$, and $D_\lambda(y)$ by applying inversion techniques.

The side-on distribution of $D_\lambda(y)$ from the center ($y = 0$) to the outer rim of the investigated gas volume ($y = R_a$) is given by the measured transmittance $\tau_\lambda(y,T)$, through equation (23).

In the axisymmetric case, we obtain:

$$D_\lambda(y) = \pi \int_{|y|}^{R_a} \frac{a^*_\lambda(R)\ R\ d\ R}{(R^2 - y^2)^{1/2}} \tag{44}$$

Equation (44) is an Abel integral equation and can be inverted to yield:

$$a^*_\lambda(R) = -\frac{1}{\pi} \int_{y=R}^{R_a} \frac{d\ D_\lambda(y)}{dy} \frac{dy}{(y^2 - R^2)^{1/2}} \tag{45}$$

For optically thin gases, the measured side-on distribution of $L_\lambda(T)$ yields analogously

$$L_\lambda(y) = \pi \int_{|y|}^{R_a} \frac{\varepsilon_\lambda^*(R)\ R\ d\ R}{(R^2 - y^2)^{1/2}} \tag{46}$$

and the inverted integral equation is

$$\varepsilon_\lambda^*(R) = -\frac{1}{\pi} \int_{|y|=R}^{R_a} \frac{d\ L_\lambda(y)}{dy} \frac{dy}{(y^2 - R^2)^{1/2}} \tag{47}$$

However, in gas flows with high absorptance, $a_\lambda^* > 3\ cm^{-1}$, the inversion $L_\lambda(y) \rightarrow \varepsilon_\lambda^*(R)$ must be performed by means of the equation [7]:

$$L_\lambda(y) = 2e^{-\frac{D_\lambda(y)}{2}} \int_y^{R_a} R\cosh\left[\int_y^R a_\lambda^*(R') \frac{R'\ d\ R'}{(R'^2 - y^2)^{1/2}} \frac{RdR}{(R^2 - y^2)^{1/2}}\right] \tag{48}$$

We cannot invert equation (48) in a similar fashion due to the dependence of the hyperbolic cosine. However, it can be solved by using a numerical solution given by Meiners [46].